The Effect of Precompression to Masonry Structures when Subject to Concentrated Loads

Kurt Ciantar

Dissertation submitted to the Faculty for the Built Environment, University of Malta in part fulfilment of the requirements for the attainment of the degree of Master of Engineering (Structural Engineering)

June 2023

L-Università ta' Malta

FACULTY/INSTITUTE/CENTRE/SCHOOL FACULTY FOR THE BUILT ENVIRONMENT

DECLARATIONS BY POSTGRADUATE STUDENTS

(a) Authenticity of Dissertation

I hereby declare that I am the legitimate author of this Dissertation and that it is my original work.

No portion of this work has been submitted in support of an application for another degree or qualification of this or any other university or institution of higher education.

I hold the University of Malta harmless against any third party claims with regard to copyright violation, breach of confidentiality, defamation and any other third party right infringement.

(b) Research Code of Practice and Ethics Review Procedures

I declare that I have abided by the University's Research Ethics Review Procedures. Research Ethics & Data Protection form code BEN-2023-00004.

As a Master's student, as per Regulation 77 of the General Regulations for University Postgraduate Awards 2021, I accept that should my dissertation be awarded a Grade A, it will be made publicly available on the University of Malta Institutional Repository.

Acknowledgements

I would like to thank everyone who contributed in some way or another and assisted me in completing this dissertation, without whom this study would not have been possible. In particular I would like to show my gratitude towards Prof. Alex Torpiano for being the supervisor of this dissertation and for his ongoing support, expert advice, and direction from the dissertation's inception to its completion.

A special thanks goes to Ballut Blocks Ltd. who at no cost, built, cast, and transported the wall specimens tested in this study, ensuring to complete the works within the imposed time-frames.

Additionally, I would like to express my gratitude to Mr. Nicholas Azzopardi and Mr. Alex Falzon, the Laboratory Technicians at the Faculty for the Built Environment. Their assistance throughout the testing program is greatly appreciated.

I am sincerely grateful to my father Samuel for our informal discussions about this study and for helping out on the steel works required for the test set-up.

Last but not least, my wholehearted appreciation goes to my family and my girlfriend Kelsey for their unconditional love and support throughout my studies.

I take full responsibility for any shortcomings in this dissertation.

Abstract

Unreinforced masonry (URM) has been the most predominant building type in the Maltese islands for a long period of time. The application of a concentrated load onto masonry walls is a very frequent case, and the ability to withstand a contact stress which is in excess of the wall's uniaxial compressive strength has been known and studied for quite a long time. Existing knowledge, however, lacks when it comes to factor into the effect of precompression to masonry structures in relation to the strength enhancement phenomenon when subject to concentrated loads.

An experimental programme was conducted to study this effect by representing masonry walls with scaled down homogenous concrete wall panels. This programme was split into 2 sets, implementing different loaded area ratios and design mixes. For each set, the precompressive stresses were varied in increments as a proportion of the previously found uniaxial compressive strength, and subsequently a central concentrated load was applied until failure.

Results indicate that contrary to the original hypothesis, for the smaller precompressive stress ratios, the strength enhancement effect is even more amplified, which seemed to peak and decline back at higher ratios. No representative data was tested and collected for the higher precompressive stresses; however, one can hypothesise that the enhancement effect neutralises when the precompression approaches the uniaxial compressive bearing strength.

Existing provisions given by masonry codes were also analysed and compared, highlighting possible future amendments to harmonise these codes by providing a holistic design equation including a modification factor to cater for the precompressive stresses.

Keywords: Masonry Walls, Concentrated Loads, Precompression, Lab Testing, Masonry Codes

Table of Contents

List of Figures

List of Tables

List of Equations

Symbols

a_1 The distance from the end of the wall to the nearer edge of the loaded area

A_b Loaded area

A_{eff} Effective area of bearing $(A_{eff} = L_{eff} \times t)$

b Width of specimen

b_p Width of bearing plate

e The eccentricity of the centroid of the loaded area from the longitudinal axis of the wall

E Young's Modulus

f_b Bearing strength under concentrated loading

f_o Bearing strength under uniform loading

$f_{o,1}$ Bearing strength under uniform loading for the first testing programme

$f_{o,2}$ Bearing strength under uniform loading for the second testing programme

f_d Design compressive strength of masonry

f_k Characteristic compressive strength of masonry

f_m Compressive strength of masonry mortar

f_p Precompressive stresses

F Force applied by the Loading jacks

F_b Concentrated force applied by the loading jack

F_o Cracking load

F_p Precompressive forces applied by the loading jacks

F_r Ratio of cracking load to ultimate load at failure

F_u Ultimate load at failure of the specimen

h Clear height of specimen

h_c Height of wall from base to the level of the load

l Length of the wall panel

l_{eff} Effective length of the wall panel

M Mass of the Specimen

R_f Flexural strength

t Thickness of a wall

v Volume of Specimen

α Wall aspect ratio $\left(\alpha = \frac{l}{h}\right)$

β Enhancement factor for concentrated loads

β_o Enhancement factor for concentrated loads for wall panels without precompression

γ_M Partial factor for materials

δ Precompressive stress ratio $\left(\delta = \frac{f_p}{f_o}\right)$

μ Poisson's Ratio

ξ Concentrated loading strength modifying factor

ρ Density of specimen

σ_x Stress in the x-direction

σ_y Stress in the y-direction

σ_z Stress in the z-direction

Φ Value for reduction factor for slenderness and eccentricity

Glossary

BSI	British Standard Institution
CL	Concentrated Load
EC6	Eurocode 6
FEA	Finite Element Analysis
GL	Globigerina Limestone
HCB	Hollow Concrete Blockwork
OPC	Ordinary Portland Cement
P.UDL	Partial Uniformly Distributed Load
UCS	Unconfined Compressive Strength
UDL	Uniformly Distributed Load
URM	Unreinforced Masonry

Chapter 1: Introduction

1.1 Background and Context

1.1.1 Introduction to Masonry

Masonry is an ancient construction technique involving the composite assembly of individual units such as stone, concrete blocks, or bricks, using mortar to create long-lasting robust structures. Throughout history, masonry has played a fundamental role in shaping the global architectural landscape, harnessing the natural properties of the available materials, standing as testament to human ingenuity and creativity. Masonry's stability and structural integrity have captivated the interest of engineers, architects and researchers for hundreds of years. However, the susceptibility to concentrated loads can result in localised stress concentrations and potential failure. Consequently, comprehending the behaviour of such structures under concentrated loads is crucial for ensuring structural safety and longevity.

1.1.2 Masonry in Malta

Unreinforced masonry (URM) has been the most common building technique in the Maltese islands for a long period of time, used to construct both monumental and traditional buildings. This building technique is one of the oldest used by mankind, having records dating back to the neolithic period. Monumental structures such as the Mnajdra Temples withstood the test of time to last over 5000 years, which is a proof on the level of understanding the masons had both on the structure itself and on the building materials. With practice and experience, masonry construction has evolved throughout the years, however, its current progress is being impacted by the introduction of new building materials such as steel and reinforced concrete (Bezzina, 2017).

Historically "Franka" was the main structural material used within our masonry structures, being one of our few resources available on the Maltese islands, outcropping mainly in the south-eastern part of Malta within the Lower Globigerina Limestone. The ability to cut and shape with ease, while having a fairly good load-bearing capacity, made this natural resource an ideal material to be used for masonry construction (Camilleri, 1988). Nowadays its popularity is being replaced with the use of the concrete Hollow Masonry Blocks (HCB), mainly because the latter is much lighter, more flexible in its structural use, and its strength and durability can be carefully controlled, reducing the uncertainties found within the "Franka" blocks (Vella, 2018). However, this does not imply that the quality of HCB is better than "Franka" blocks.

1.1.3 Advantages of Masonry Construction

Unlike steel or reinforced steel structures, the repetitive use of identical elements, along with its flexibility and simplicity, makes masonry construction one of the most popular construction techniques around the globe. Moreover, while masonry structures provide both structural stability and subdivision of spaces, it also has the ability to act as a thermal and acoustic break, a fire barrier and has the ability to protect the inside spaces from the outside weather conditions (Hendry, 1990). Both the mass and thickness of a typical masonry wall result into a high thermal capacity, increasing the energy performance of the building. This results into less cooling needed in the hot summer period, and less heating required during the cold seasons, reducing the energy required throughout the building's lifetime, and hence the carbon footprint (Curtin et al., 1997).

Although highly dependable on the workmanship, masonry structures can be very durable with minimal maintenance required, resulting into an overall cheaper structural solution when compared to cast in-situ concrete (Curtin et al., 1997).

On the other hand, one of the main disadvantages of masonry structures is its weak tensile strength. Most often, this is the limiting factor even when compressed vertically due to the lateral tensile stresses generated by Poisson's effect. As a result of the unequal transverse strains between the masonry units and the mortar layers, the friction between them will generate tensile stresses in the masonry blocks accompanied by compressive stresses in the mortar layer. Hence failure can occur either by compressive failure of the latter, or else by vertical tensile splitting through the former (Torpiano, 1988). This also means that barely any bending can be withstood. Unlike steel or reinforced concrete structures, it is very difficult to achieve large uninterrupted spans without making use of a substantial volume of material, generating a line of pure compression thrust through which loads can propagate without inducing any bending.

1.2 Motivation Behind Research

1.2.1 Existing Problem and Literature Gap

Over the lifespan of masonry buildings, change in use and layout can lead to alterations, changing the load path and possibly introducing concentrated stresses. Within the past years, following changes of the Local Policy plans, an increase in demand and property prices, and the desire of modernising existing traditional layouts, structural engineers in Malta have been frequently encountering the challenge of removing a dividing wall within the existing levels while building additional floors above. Modernisation of the typical traditional masonry terraced house consists of a change in the internal layout from the traditionally separate kitchen, dining and living room, into a one whole open-plan space. Moreover, frequently, this development is accompanied by the construction of additional floors, dividing the original single terraced house into a number of dwelling units. This involves structural alterations

within the internal layout, where a beam has to be introduced to transfer the loads of the upper floor levels in order to generate an open-plan at the existing ground and/or first floor level. This structural intervention would alter the simpler load path, generating a concentrated load due to the transfer beam acting on a wall, which is uniformly precompressed from the existing and/or additional floors above.

Masonry design codes allow for an increase in stresses just beneath the concentrated load such that 2 checks are required; one just under the applied load, and the other at the midspan of the wall's height, having the concentrated load dispersed into a larger area. For just under the contact area, the design codes provide an enhancement factor which is induced by the unloaded and hence unconfined adjacent masonry units. However, in the majority of the cases, the walls onto which a concentrated load is applied, are most often already loaded from the upper floors. This is a very frequent case which the structural engineers have to face. There are no existing design codes which can be used to allow for the modification in the enhancement factor, when the walls onto which a concentrated load is applied, are subject to precompressive stresses. Applying the recommended enhancement factor can lead to an overestimation of the masonry's wall capacity. On the other hand, by conservatively excluding the phenomenon of strength enhancement, this can lead to the need of reinforcing and hence overdesigning, which reduces the intervention's efficiency.

1.3 Scope and Objectives

This study continues on the works by Farrugia (1990) and other researchers both in the local and global context, with Farrugia confirming that the strength enhancement phenomenon on the local globigerina limestone blocks is fairly comparable to the results obtained abroad.

The main scope of this dissertation is to investigate the effect of precompression onto the strength enhancement factor of masonry wall panels when subject to concentrated loads. An experimental programme is performed to analyse the original hypothesis formulated within the previous limited studies. Also, a modification factor is proposed to factor into the effect of precompression as it varies from zero to the uniaxial compressive strength.

Moreover, this study compares and contrasts between the major masonry design codes, seeing how these correlate to each other, and how a better formula could be used to group up all the variables into a single equation, modelling the effects of concentrated loads more accurately and hence less conservatively.

Further issues which are discussed and investigated is whether the use of concrete homogenous walls is able to model accurately the behaviour of concentrated loads on the non-homogenous composite masonry walls, consisting of both masonry units and mortar layers.

1.4 Layout of Dissertation

In addition to the introduction, the structure and a chapter-by-chapter summary of this dissertation is provided below:

Chapter 2: Literature Review

Literature review of the previous studies and investigations performed to analyse the effect of concentrated loads on masonry structures, along with the existing design rules provided by the different masonry codes. This chapter also includes a stress distribution analysis, the failure mechanisms, and the use of finite element to represent a typical situation.

Chapter 3: Experimental Methodology

The experimental investigation to study the effect of precompression on walls when subject to concentrated loads; including the construction and transportation of the wall panels, the setting up of the testing rig and the testing procedure.

Chapter 4: Test Results

The test results of the experimental programme, including graphs, tables, photo records and failure modes. These provide the basis upon which discussions and conclusions are formulated.

Chapter 5: Analysis of Results

The validity and variables of the experimental programme are highlighted and analysed. Also, the test results are studied and compared to the original hypothesis, providing a new theoretical framework.

Chapter 6: Comments and Conclusions

The overall general summary and conclusions along with recommendations for further research.

Chapter 2: Literature Review

2.1 Introduction

There are multiple scenarios where masonry walls are subject to concentrated loads, example loadings from beam bearing, lintels and prestressing anchorage blocks. In the majority of the cases, such loading conditions are applied locally, accompanied by precompressive stresses due to loads coming from the floors above. Some examples of such typical load scenarios are shown in the below Fig. 2.1 (Malek, Mohammad H., 1987).

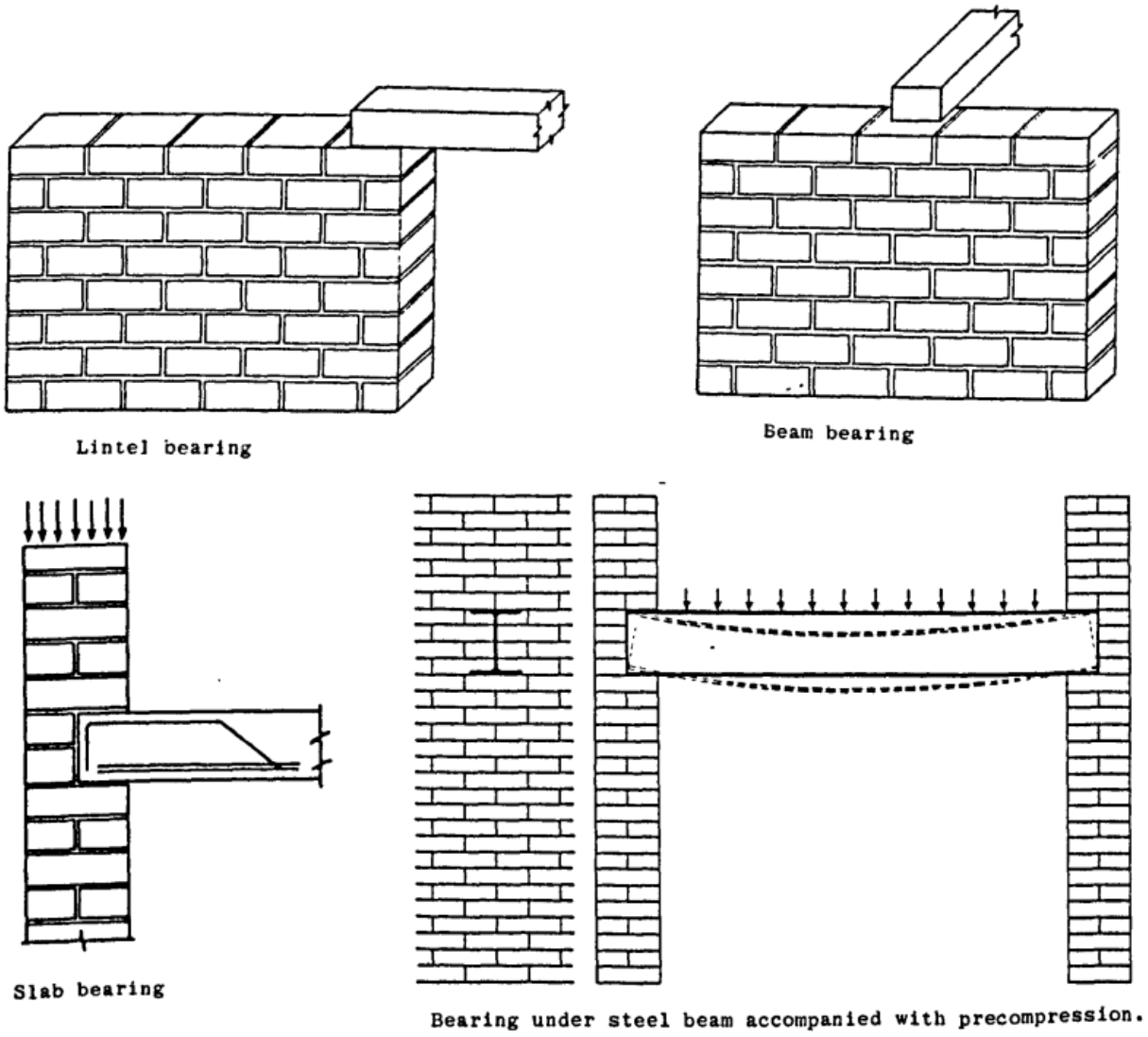

Figure 2.1 – Typical concentrated loading scenarios in masonry structures (Malek, Mohammad H., 1987)

It has been a known fact for quite a long time that the masonry elements just under the concentrated loads are able to withstand larger stresses when compared to the failure stresses at uniaxial loading conditions. This strength enhancement is due to the confinement provided by the lightly stressed material within the stress influenced zone, restraining the stressed material from expanding laterally due to the Poisson's effect (Farrugia, 1990).

The magnitude of such strength enhancement is affected by a large number of factors and variables which are to be dealt with in the following sections. Also, this chapter deals onto how these factors are adopted by the different masonry codes, which are altered when comparing one code to another. This results to a change in the strength enhancement factors adopted by different countries abiding to different codes, leading to considerable differences when comparing particular design codes (Asteris et al., 2005).

Moreover, this section deals with the stress distribution under concentrated loading, studied using different analysis techniques. Reference is also made to the accuracy of using a homogenous wall to represent the behaviour of the non-homogenous masonry wall panels.

The works carried out by previous researchers is reviewed and analysed, using their conclusions and recommendations as basis for further study within this dissertation.

2.2 Concentrated Loads Theory

2.2.1 Factors Affecting the Strength Enhancement

The phenomenon of strength enhancement when loading wall panels with a concentrated load is caused due to:

A. the restraint generated by the adjacent less confined material. This material restrains the confined stressed area from expanding laterally by Poisson's effect, generating confinement and a 3-D compressive stress state.
B. the load being dispersed onto a larger area, hence relieving the stresses from the strip of loaded material beneath the load, to the adjacent unconfined areas (Farrugia, 1990).

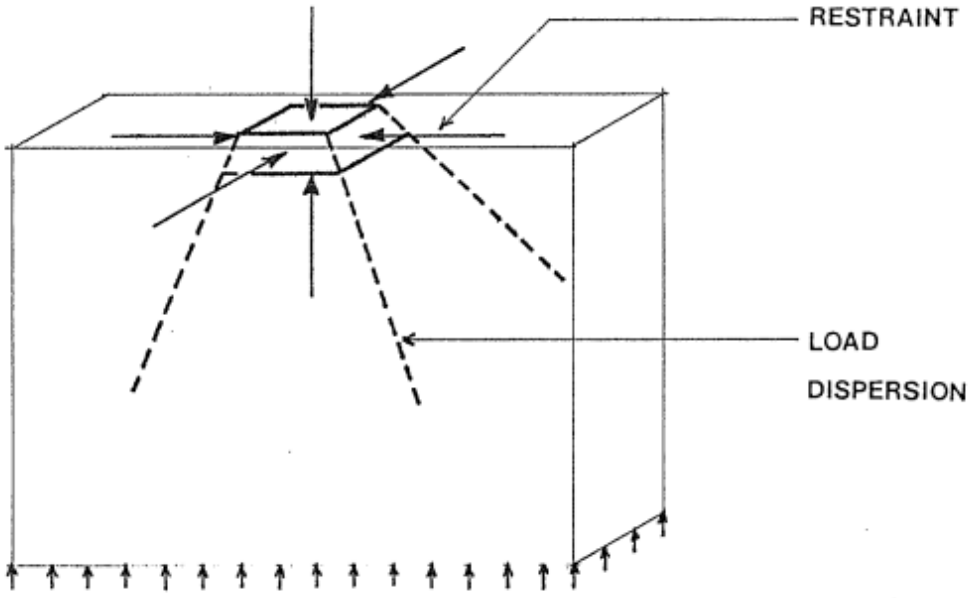

Figure 2.2 – Mechanisms causing strength enhancement to concentrated loads (Farrugia, 1990)

The factors and variables which influence the magnitude of such strength enhancement are (Page & Hendry, 1988):

A. The loaded area ratio $\left(\frac{A_b}{A_{eff}}\right)$;
B. The position along the wall and its eccentricity $\left(\frac{a_1}{l}\ and\ \frac{e}{t}\right)$;
C. The type of loading, i.e., patch or strip loading;
D. The strength and type of the masonry wall configuration;
E. The wall panel ratio $\left(\frac{l}{H}\right)$;
F. The application of parallel loads;
G. The use of spreader beams;
H. The degree of rigidity/flexibility of the loading plate;
I. Precompressive stresses from the above floors;

Throughout the experiments and investigations performed, variables from the above factors have usually been omitted, resulting into a large scatter and inconsistent results when comparing one test programme to another. However, the 2 most important factors that have been heavily studied are the loaded area ratio and the position of the concentrated load along the wall. As a general rule, the strength enhancement increases as the loaded area ratio decreases (Asteris et al., 2005; Page & Hendry, 1988).

Gunkler and Dashkuu also shown that as the distance between the end of the wall and the nearest edge of loading (a_1) decreases, the enhancement factor decreases. Also, they concluded that as $a_1 = 0$, i.e., the concentrated load is at the edge, in some particular cases the enhancement factor can actually become a reduction factor, hence having a value which is less than 1.0 (Gunkler & Dashkhuu, 2014).

2.2.2 Stress Distribution and Failure Mechanisms

When subject to a uniformly distributed load, masonry walls fail by vertical splitting which is induced by Poisson's ratio effect, i.e., the development of lateral tension within the masonry blocks, known as bursting stresses. For a stack-bonded prism, since the masonry blocks and the mortar layers have different lateral strains, this will lead to the generation of a biaxial tensile stress within the masonry blocks, accompanied by the vertical compressive stresses. As a consequence, the mortar layer is always in a state of tri-axial compression, as shown in Fig. 2.3. This theoretical approach cannot be directly applied to masonry panels due to the presence of the vertical bed joints, which can be either in a state of tri-axial compression or else in axial compression accompanied by bi-lateral tension. As a result of the weak tensile bond strength of a typical masonry configuration, a crack would form along the vertical bed joint, which propagates into the masonry blocks when its transverse tensile strength is reached, leading to failure (Malek, Mohammad H., 1987; Page & Hendry, 1988).

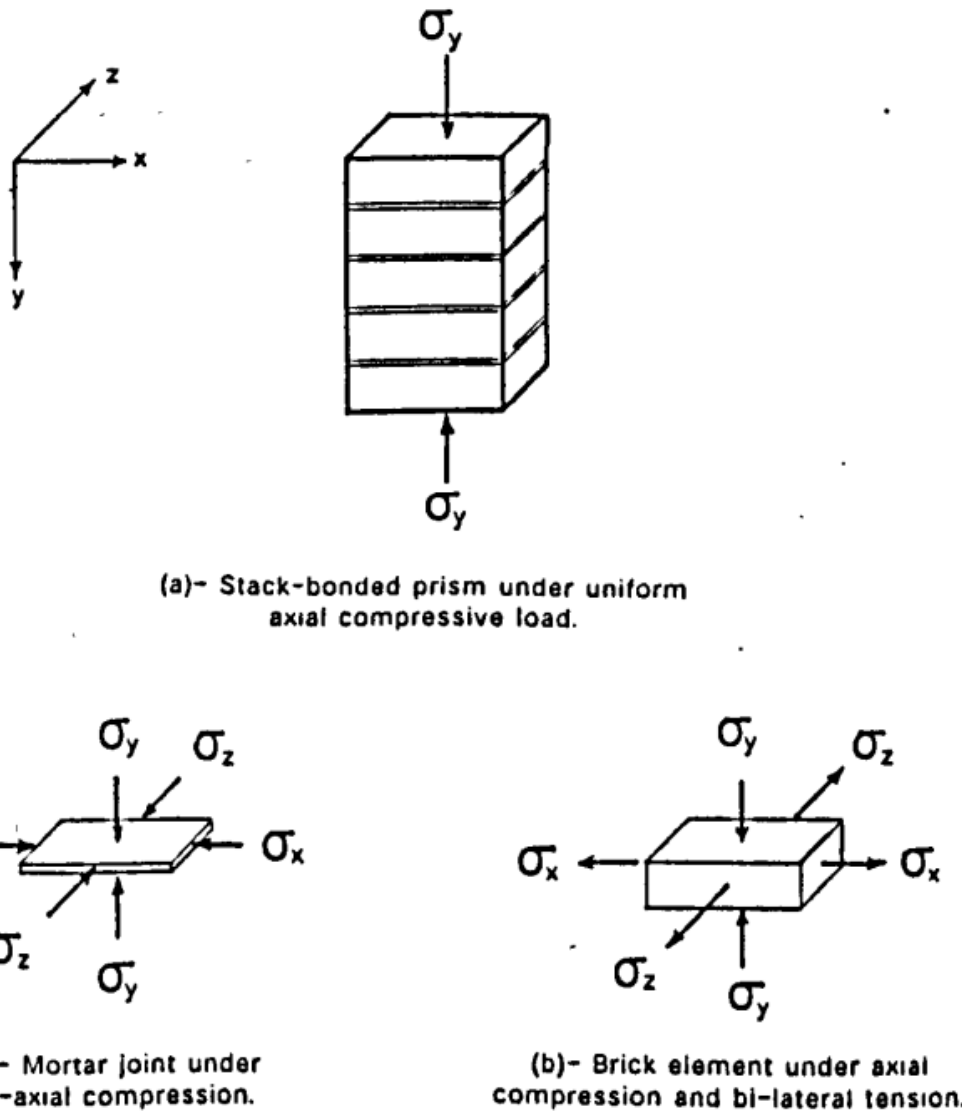

Figure 2.3 – The state of stress of masonry configuration under uniform axial compression (Malek, Mohammad H., 1987)

Applying the same theoretical framework to a masonry wall panel subject to concentrated loads, would lead to a tri-axial compressive stress state within the masonry block just under loading. As the load disperses, the stress state changes to one of axial compression and biaxial tension, showing a similar stress behaviour to a masonry wall panel subject to uniform compressive loading. This results in a shift from a 3D compressive stress state to a bi-axial tensile stress state along the horizontal plane as shown in Fig. 2.4 (Malek, Mohammad H., 1987).

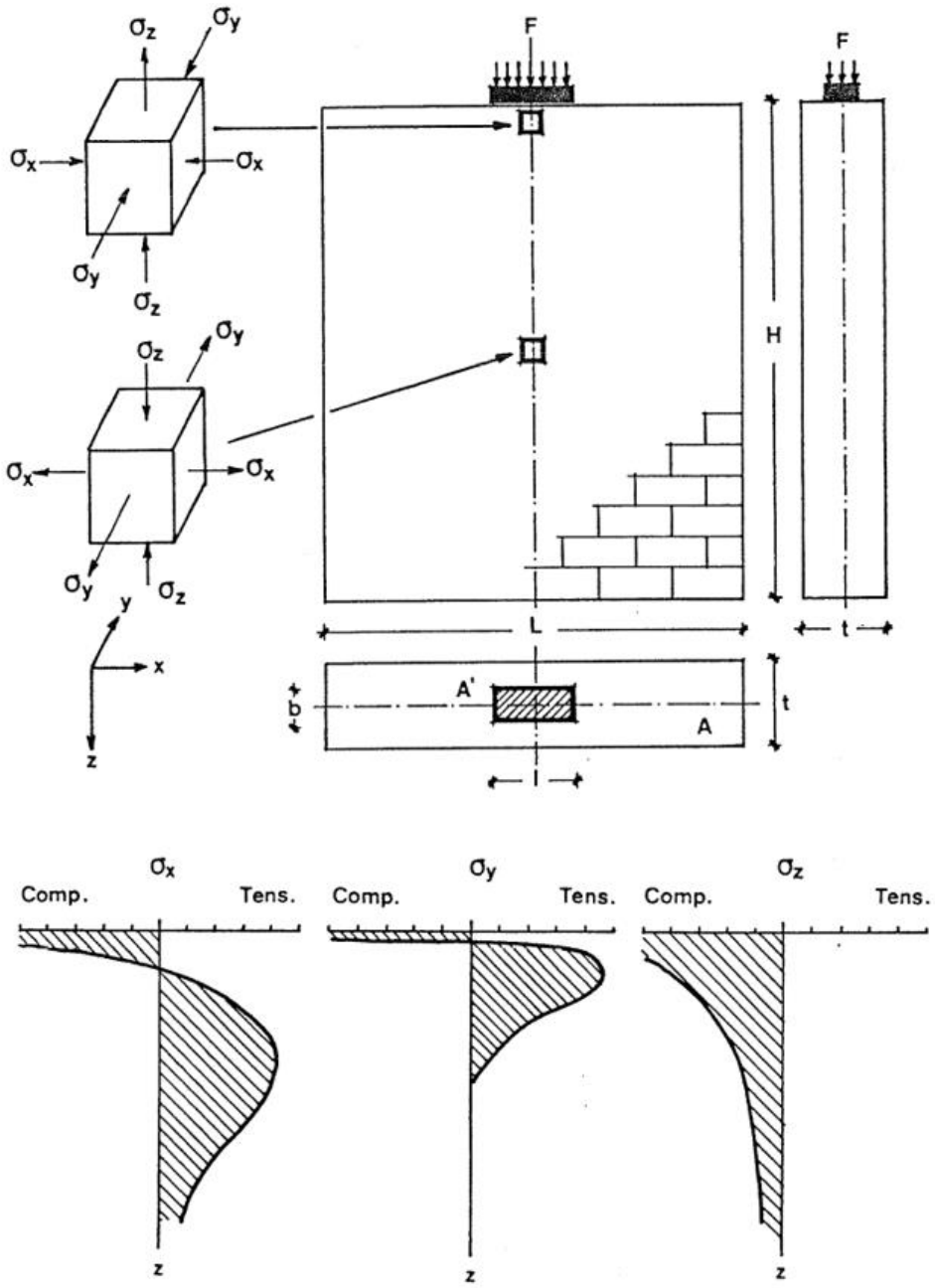

Figure 2.4 – State of stress in masonry element and its stress distribution along the centre line when subject to concentrated loading (Malek, Mohammad H., 1987)

Also, as the loaded area ratio (A_b/A_{eff}) increases, the maximum horizontal tensile cracking stress decreases. As shown in Fig. 2.5, when loaded area ratio is equal to 1, i.e., full width loading, then the maximum horizontal tensile cracking stress is 0, and maximum when the loaded area ratio approaches 0 (Mann & Pfeifer, 1985).

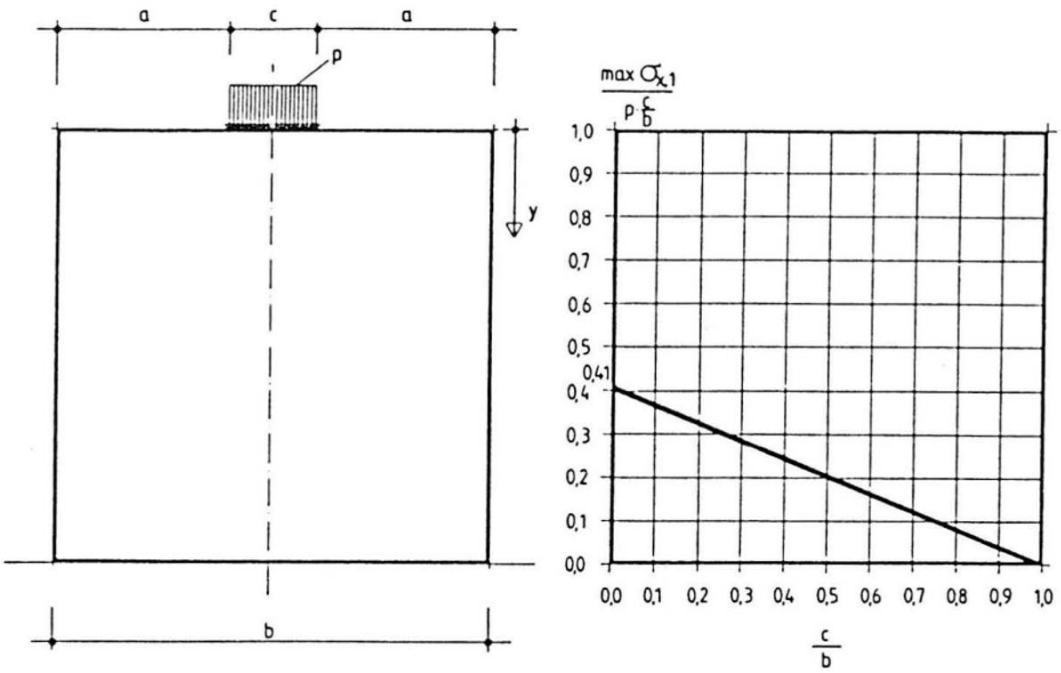

Figure 2.5 – Maximum tensile cracking stress vs loaded area ratio for a homogenous wall (Mann & Pfeifer, 1985)

The spreading of the concentrated load, which results into the tensile cracking forces, is only transferred via the masonry units, and not the vertical joints. Since the mortar layers cannot induce tensile forces, the tensile cracking stresses are not able to run continuously over the full wall height. This results that, along the length of the vertical joints, the tensile cracking forces within the masonry units must be doubled as the units only exist at every second course. This is represented by Fig. 2.6, where along section I, the horizontal tensile cracking stress ($\sigma_{x,1}$) is twice that along section II, which however, is accompanied by an additional horizontal tensile stress ($\sigma_{x,0}$) due to the transverse strain difference between the mortar and masonry blocks. For section I, $\sigma_{x,0}$ is neglected because the vertical stress (σ_y) along the vertical butt joint is very small, hence the transverse strain difference can be considered negligible, as represented by Fig. 2.7 (Mann & Pfeifer, 1985).

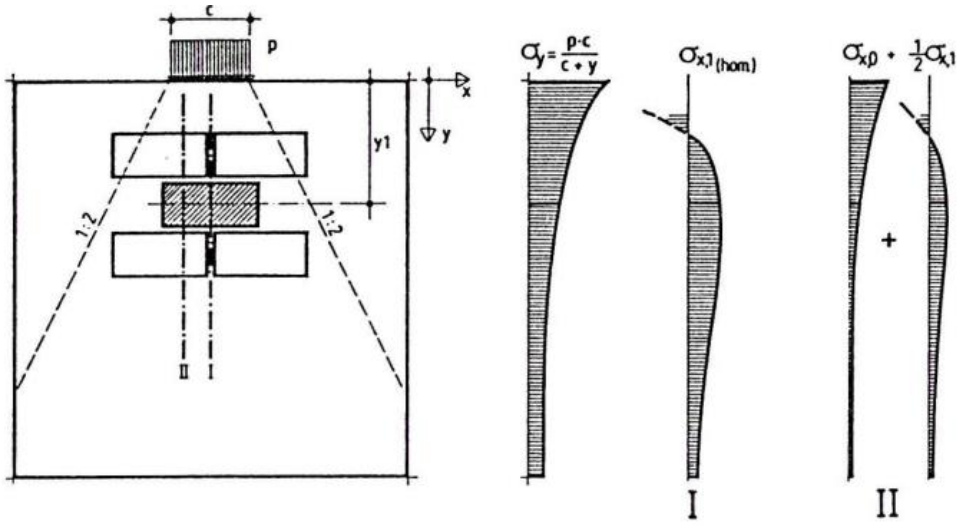

Figure 2.6 – Stresses along different sections within a masonry wall panel (Mann & Pfeifer, 1985)

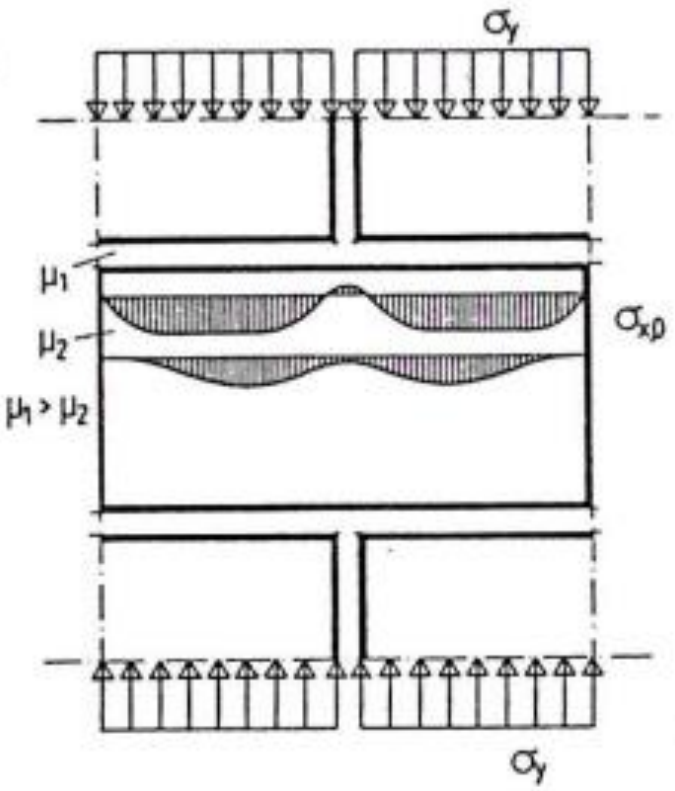

Figure 2.7 – Horizontal tensile stresses from transverse strain difference (Mann & Pfeifer, 1985)

Failure is usually induced by vertical and/or diagonal cracks, and, in some of the cases, this is accompanied by local failure in the bearing zone area. Moreover, the failure mechanism changes as the strength of the masonry units decreases, forming a wedge under the loaded area, moving downwards and splitting the masonry element apart (Page & Hendry, 1988). Moreover, in the cases where the load is located along the edge of the wall, the crack is generated under the inner edge of the bearing plate and propagates to the free edge of the wall, as shown in Fig. 2.8.

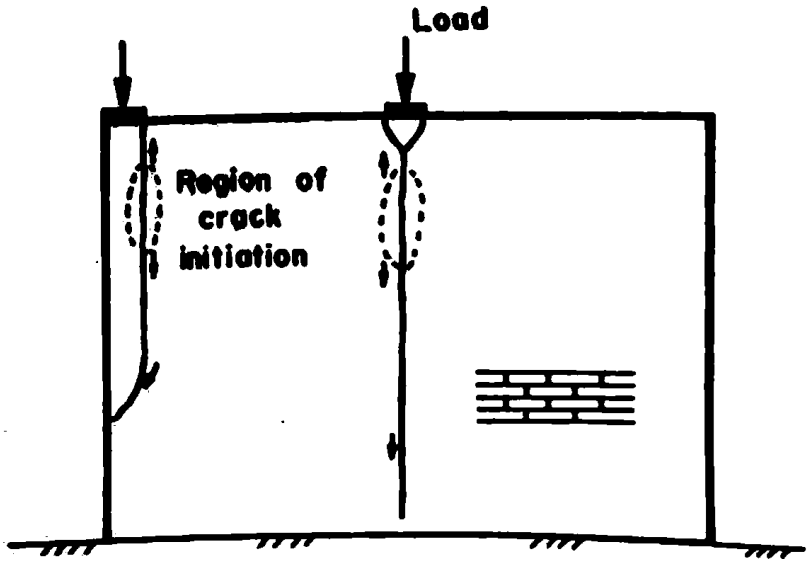

Figure 2.8 – Failure mechanisms of masonry wall subject to concentrated loads (Page & Hendry, 1988)

Ali and Page also noted the shift of the location of the crack formation. As the loaded area increases, the crack shifts from the centre of the loading plate to its edge due to the effect of the shear stresses on the bond strength of the vertical mortar joints (Ali & Page, 1988).

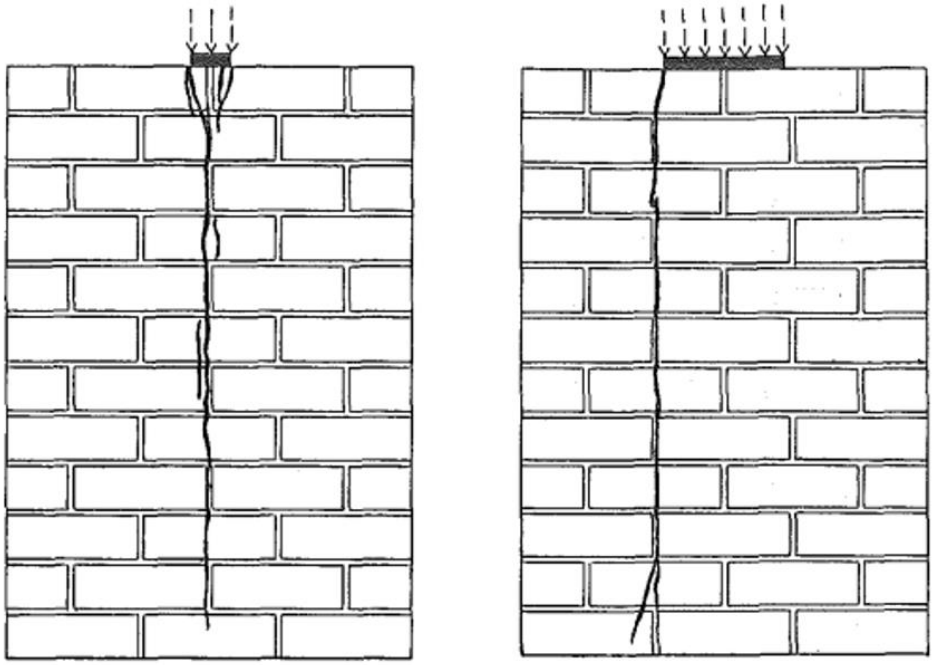

Figure 2.9 – The shift in the crack propogation when increasing the bearing plate (Ali & Page, 1988)

The masonry wall panel does not fail upon the appearance of the first crack (F_o). The loaded area ratio will heavily influence the ratio between the cracking load and the ultimate failure load (F_u). As the loaded area ratio increases, F_r (which is the ratio F_o to F_u) decreases, resulting in failure taking place at a large time interval between the appearance of the first crack and the ultimate load at failure. For smaller loaded area ratios, failure is instant and close to the load at cracking, resulting in a larger F_r ratio (Farrugia, 1990; Mann & Pfeifer, 1985). Mann & Pfeifer et al. came up with the following equation, relating F_r to the loaded area ratio;

$$F_r = 0.8 - 0.3 \times \frac{A_b}{A_{eff}}$$

Equation 2.1 – The relationship between the ratio of cracking load to ultimate failure load, to the loaded area ratio (Mann & Pfeifer, 1985)

This equation states that as the loaded area ratio is 1, i.e., full width loading, then F_r = 0.5, meaning that the masonry wall panel has double the capacity reached upon the initiation of the first crack.

Moreover, Gunkler and Dashkuu concluded that the effect of the type of mortar and masonry group onto the stress distribution of masonry walls can be considered negligible (Gunkler & Dashkhuu, 2014).

2.3 Analytical Techniques and Experimental Research

2.3.1 Finite Element Modelling

The solution to the stress distribution within masonry panels when subject to concentrated loads is not an easy one, especially due to the non-homogenous behaviour of the masonry configuration and its anisotropic structure. When applying finite elements to represent the behaviour of masonry structures, there are 2 main types which were incorporated throughout the years (Asteris et al., 2005);

A. Macromodelling – Considering masonry as a homogeneous continuum, ignoring the distinction between the joints and the masonry units, being represented as a one-phase material.
B. Micromodelling – Considering masonry as a multiphase material, modelling separately the joints and masonry units which leads to a more detailed stress analysis. This technique is compromised by the large computational effort needed, hence simplified techniques have been adopted to overcome this issue (Asteris et al., 2005).

For long periods of time, the effect of concentrated loads on masonry walls was predicted by applying a linear elastic finite element analysis, implementing the theory of elasticity on solid, isotropic, and homogenous wall. Since the masonry units and mortar layers have different deformational properties, this will influence the horizontal strain distribution throughout the composite material. The mortar joints act as weak planes, having no tensile and shear bond strength. Therefore, one can question the validity of the results obtained by using the theory of elasticity, which underestimates the developed tensile stresses. However, this type of analysis still provides useful guidance as the stress trajectories are fairly similar, as shown in Fig. 2.10 (Ali & Page, 1988; Asteris et al., 2005; Malek, Mohammad H., 1987).

Comparing a homogenous wall to a masonry wall, one must consider that for the latter, the tensile cracking forces are interrupted by the vertical joints, while additional tensile stresses are generated due to the difference in transverse strain between the masonry unit and the mortar layers. This results that the tensile forces from homogenous modelling cannot be directly applied to masonry walls. This can be shown by comparing Fig. 2.5 with Fig. 2.11, where the maximum horizontal tensile cracking stresses are larger within the masonry walls when compared to the homogenous walls (Mann & Pfeifer, 1985).

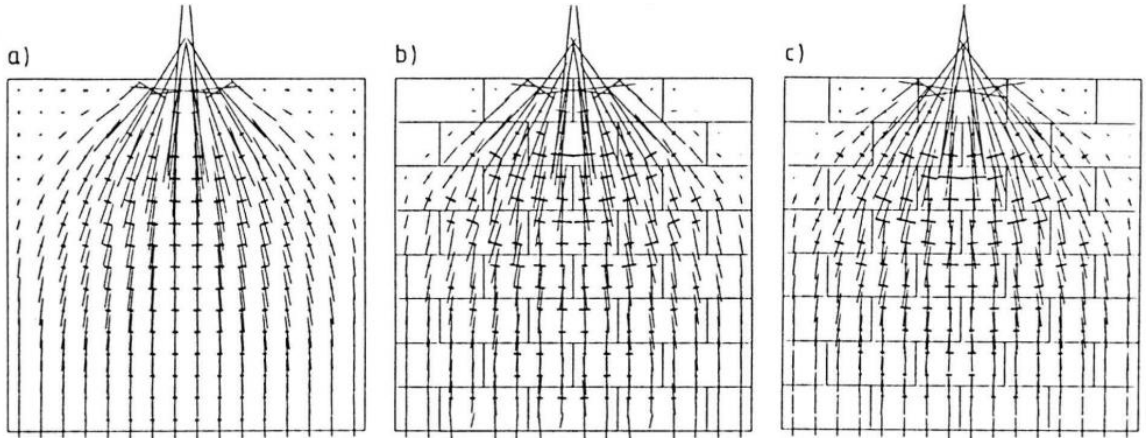

Figure 2.10 – Stress trajectories for a) homogenous wall, b) & c) masonry walls with different brick sizes (Mann & Pfeifer, 1985)

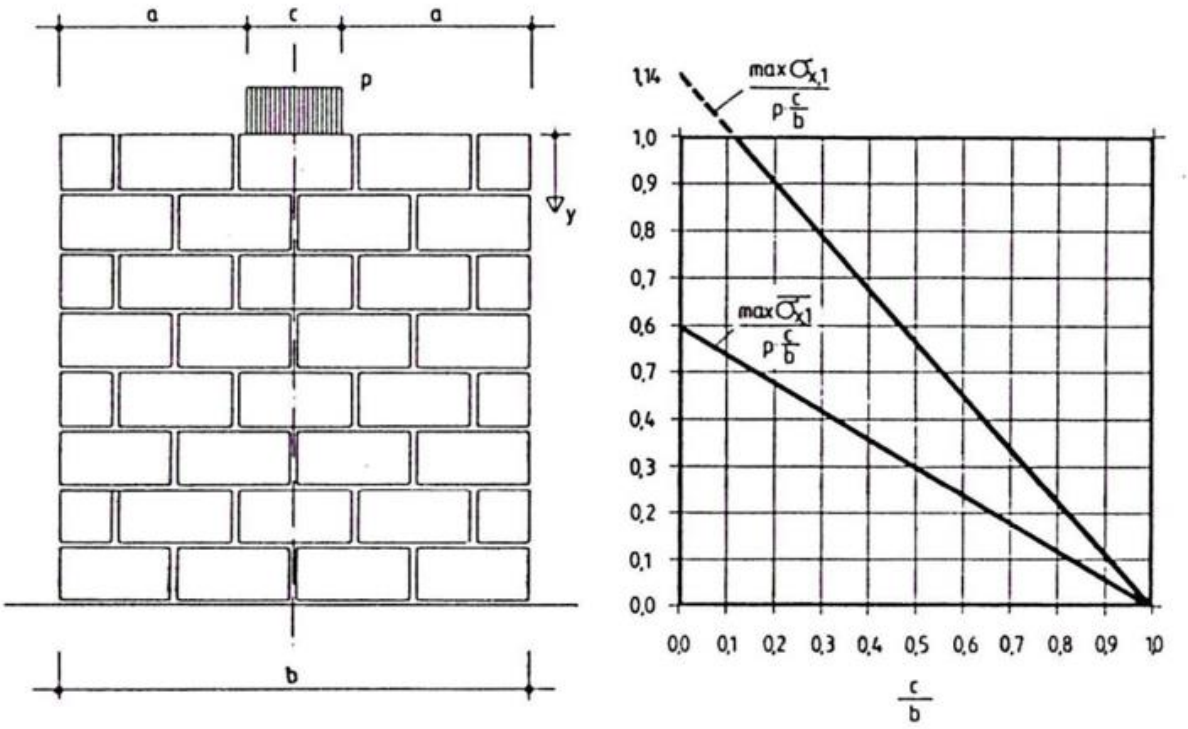

Figure 2.11 – Maximum tensile cracking stress vs loaded area ratio for a masonry wall (Mann & Pfeifer, 1985)

As concluded by Asteris et al., by considering masonry as an isotropic elastic homogenous continuum, i.e., macromodelling, can be ideal to analyse stress distribution within large masonry structures. However, for detailed stress analysis of small masonry panels, this technique might omit some failure mechanisms because it fails to address the planes of weakness (Asteris et al., 2005).

Moreover, the majority of the experimental tests reviewed loaded the wall along its full thickness in order to treat the situation as a two-dimensional parameter, keeping the experiment simpler by reducing variables. However, equations have been proposed in order to describe the transition from a 2D to a 3D stress condition as the eccentricity (e) increases

(Gunkler & Dashkhuu, 2014). 2D analysis can be applied as long as the loading covers at least ¾ of the wall's thickness. One must also note that such analysis assume that the stress underneath the loading plate is uniform. In the case of having beams spanning at right angles to the wall panel, the displacement and stresses underneath the bearing plate is not uniform, hence such assumption is not completely representative of the actual loading scenario (Farrugia, 1990).

Asteris et al. used parametric analysis in order to come up with a more holistic and representative equation, modelling the nonlinear anisotropic behaviour of masonry as a one-phase material, averaging the properties of the masonry units and mortar joint layers. This technique concluded that a coarse finite element mesh could be adopted, limiting the computational effort required. Moreover, for areas with high stress gradients, i.e., below the loaded area, a finer mesh as shown in Fig. 2.12, would enhance the accuracy of the finite element model.

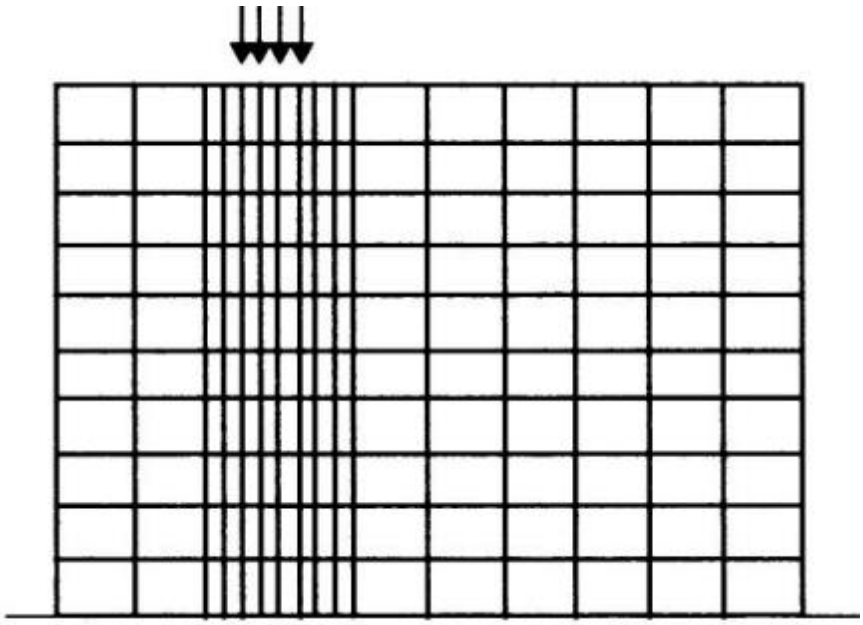

Figure 2.12 – Typical finite element mesh (Asteris et al., 2005)

Previous literature, including tests performed by A.W. Page, has been reviewed in order to model accurately the particular masonry properties to which the parametric analysis was compared to. The sophisticated developed model was validated by Asteris et al., comparing the stress distribution with existing experimental tests. Adopting inelastic analysis presented a strong agreement with the lab experimental results, as opposed to elastic analysis, hence proving the inelastic behaviour of masonry, as shown in Fig. 2.13 (Asteris et al., 2005).

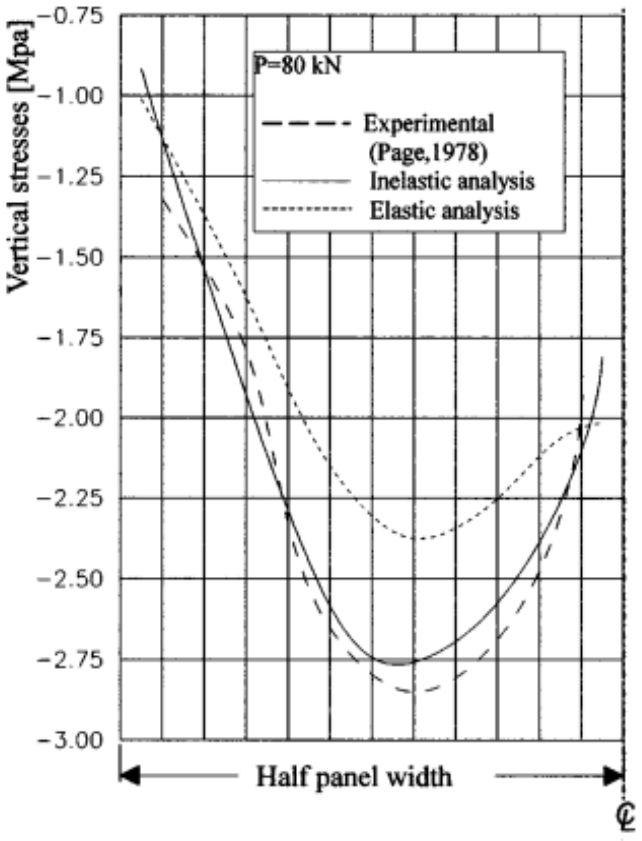

Figure 2.13 – Vertical stress distribution in masonry (Asteris et al., 2005)

Asteris et al. reinforced the possibility of having a strength enhancement load factor which is less than 1, in accordance with (Arora, 1988) and (Gunkler & Dashkhuu, 2014). A design equation was proposed which is more holistic, taking into account this phenomenon, along with the effects from the loaded area ratio, the position of the load, and the panel's aspect ratio (α);

$$\beta = \theta \left(1.00 + \frac{2}{\alpha} \frac{\left(1 - \frac{A_b}{A_{eff}}\right)}{\left(1 + 3\frac{A_b}{A_{eff}}\right)^4} \right)$$

Where;

$$\theta = 1.00 \text{ for the case of } 0.20 \leq \frac{a_1}{l} \leq 0.50$$

$$\theta = 1.00 - 12\left(0.20 - \frac{a_1}{l}\right)^2 \text{ for } 0.00 \leq \frac{a_1}{l} \leq 0.20$$

Equation 2.2 – Strength enhancement factor β, as proposed by (Asteris et al., 2005)

Although it could be quite accurate, to average the properties of the brick and mortar, this would smear the effect of local failure within each of these elements. This can be limiting, especially when it comes to study the local effects in detail, such as the area underneath the concentrated loads, having high stress gradients (Ali & Page, 1988).

For finite element modelling, Ali and Page went one step forward, by modelling separately both the masonry units and mortar layers, hence being able to model these local effects more accurately. This adopted model allowed for the observation of progressive local failure by applying the load incrementally, hence simulating the crack behaviour of the masonry wall, which is the leading cause for masonry's nonlinearity. 4-noded quadrilateral elements were adopted, and a mesh refinement scheme was applied near the loaded area, as shown in Fig. 2.14 (Ali & Page, 1988).

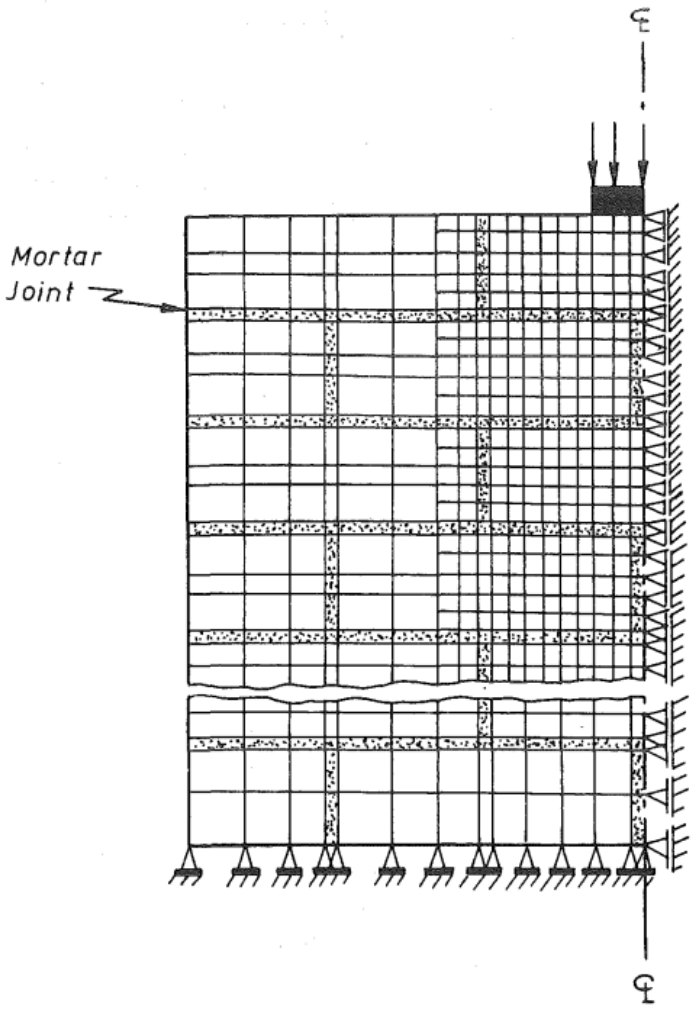

Figure 2.14 – Finite element mesh as proposed by Ali and Page (Ali & Page, 1988)

To improve the post-cracking behaviour of the model, a linear tension strain softening model was applied to replace the brittle collapse model, as shown in Fig. 2.15. The gradient of the descent is dependent on the parameter defined as 'n', which was calibrated by Ali and Page as shown in Fig. 2.16. This led to a better agreement between the analytical model and the experimental results, concluding that the rate of stress release in the cracked region is a vital parameter in such analysis (Ali & Page, 1988). Having found the material properties, the adopted model by Ali and Page could represent accurately the failure mechanism and behaviour of masonry wall panels subject to concentrated loads, and hence could be an ideal research tool for parametric analysis.

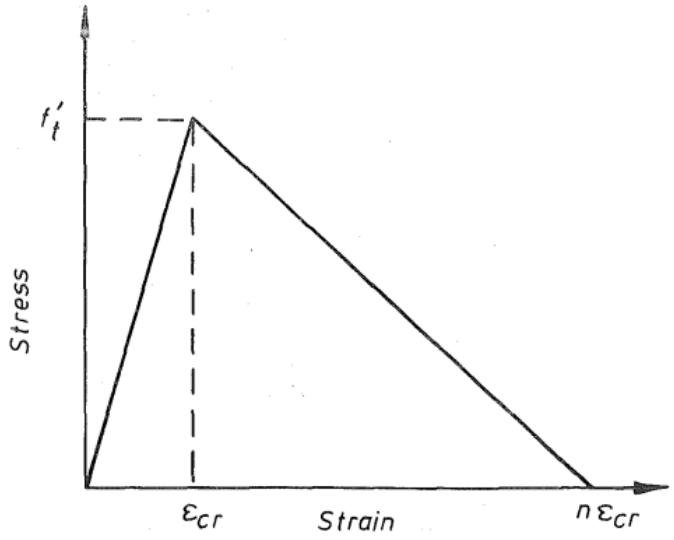

Figure 2.15 – Strain softening representation (Ali & Page, 1988)

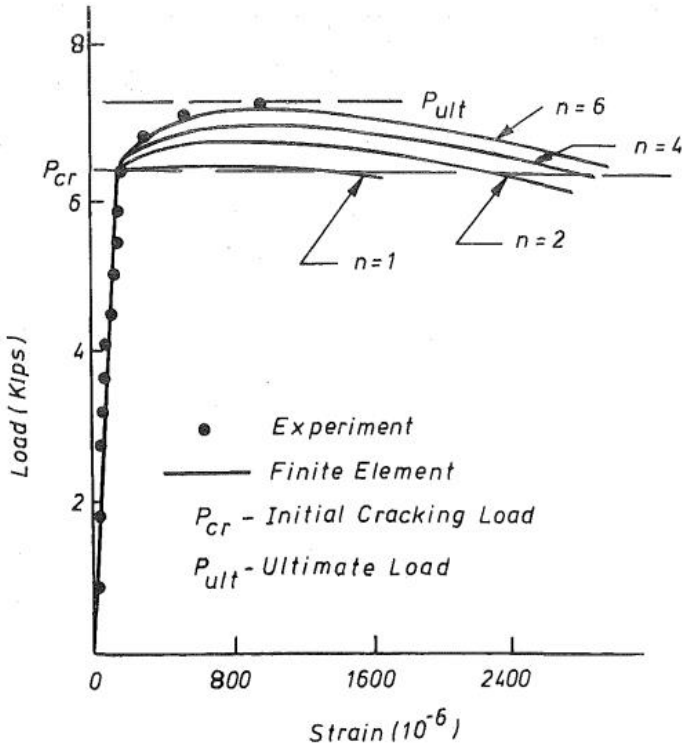

Figure 2.16 – Calibration of parameter 'n', showing load against strain (Ali & Page, 1988)

2.3.2 Experimental Research

Comparing the experimental work by different researchers can get quite tricky, because the results vary drastically, since they are sensitive to a large number of variables, including the material properties, procedure and interpretation. Considering also the scale of panel testing, most times the situation is scaled down, hence the wall would not represent the behaviour of storey-height walls, ending up with an overestimation of the uniaxial strength, hence underestimating the strength enhancement factor (Page & Hendry, 1988).

Experimental tests performed by S.K. Arora challenged the conventional load dispersion model from the British Standard, which assumes that the load is dispersed at 45 degrees, and terminates at 0.4 h from the loading position. Arora measured the angle of the line joining the points of 0 vertical stresses. This study proved that the 45-degree dispersion is unconservative, hence the stresses at the dispersed position in the middle are larger than that calculated by the conventional dispersion model. A safer criterion has been proposed where it was recommended to implement a dispersion of 60 degrees from the horizontal for loaded area ratios which are less than 0.1, terminating at half the height. For a loaded area ratio of 0.5, this angle changes to 80 degrees, allowing interpolation between both values (Arora, 1988). The angle of dispersion is also dependent on the position of the concentrated loads, which, as also confirmed by Gunkler and Dashkuu, is even steeper when the loading is applied at the wall ends, as shown in Fig. 2.17.

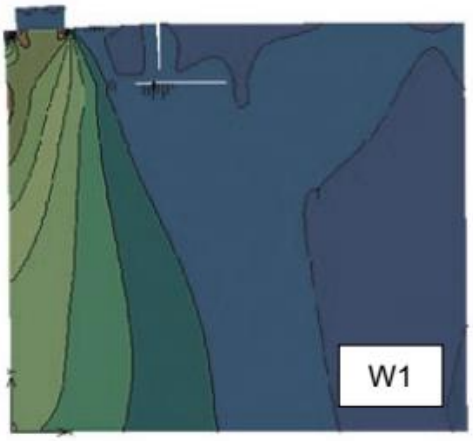

Figure 2.17 – Finite element model representing the distribution of vertical stresses σ_y (Gunkler & Dashkhuu, 2014)

Malek and Hendry's experimental research concluded that the dominant effect onto the strength enhancement factor is the loaded area ratio. Moreover, it was found that type of masonry and type, and/or thickness of mortar used did not affect this enhancement factor; however, the strength of masonry unit itself did affect it. They concluded that the weaker the masonry units were, the larger the strength enhancement factor was. Given the degree of scatter of their experimental results, and in order to incorporate the effect of each parameter which affect the strength enhancement, a lower bound approach was used to come up with a simpler relationship as represented by equation 2.3 (Malek, M. H. & Hendry, 1988);

For Central loads: $$\beta = 0.701\left(\frac{A_{eff}}{A_b}\right)^{0.462}$$

For Intermediate loads: $$\beta = 0.806\left(\frac{A_{eff}}{A_b}\right)^{0.393}$$

For End loads: $$\beta = 0.856\left(\frac{A_{eff}}{A_b}\right)^{0.266}$$

Equation 2.3 – Enhancement factor relationship as proposed by Malek and Hendry (Malek, M. H. & Hendry, 1988)

A lower bound approach would lead to a simpler design formula that can be used to predict the strength enhancement factor; however, this would often underestimate the strength of the panel, leading to overdesigning. Taking a similar approach, Page and Hendry also came up with an equation which provided the possibility to interpolate, and to factor in more accurately the position of the load. The following equation was based on all the previous experimental and analytical data by different researchers;

$$\beta = 1.00 \leq \frac{0.55}{\left(\frac{A_b}{A_{eff}}\right)^{0.33}}\left(1 + \frac{a_1}{l}\right) \leq \left(1.50 + \frac{a_1}{l}\right)$$

Equation 2.4 – Enhancement factor relationship as proposed by Page and Hendry (Page & Hendry, 1988)

Farrugia, in 1990, performed a small scaled test programme on local masonry, and compared the results to Malek and Hendry's work, as presented in Table 2.1. Farrugia's test confirmed the presence of strength enhancement on local masonry, which are fairly comparable to the results obtained abroad. Also, a correlation was found between the initial cracking load and the failure load, which is in accordance with the outcome predicted by Mann & Pfeifer.

Wall No.	$\frac{A^{eff}}{A^{b}}$	Strength Enhancement β	
		Malek and Hendry $\beta = 0.701\left(\frac{A_{eff}}{A_b}\right)^{0.462}$	Farrugia $\beta = 0.57\left(\frac{A_{eff}}{A_b}\right)^{0.643}$
3	8	1.83	2.17
4	12	2.21	2.82
5	16	2.52	3.39
6	20	2.82	3.91
7	24	3.04	4.40

Table 2.1 – Comparison of equations (Farrugia, 1990)

2.4 Current Design Guides

The design rules presented in masonry codes differ between one another, which can indicate the lack of a comprehensive equation which takes into account all the variables influencing the enhancement factor. The codes which exclude the critical parameters can be non-conservative, especially in the case when the concentrated load is close to the edge (Malek, Mohammad H., 1987). On the other hand, the majority of the current design codes underestimates the strength of the masonry wall panels, leading to conservative design approaches.

The provisions given by Eurocode 6 (EC6) are based onto the works of Page and Hendry (Gunkler & Dashkhuu, 2014), recommending a stress distribution at an angle of 60 degrees to the horizontal as shown in Fig. 2.18 and providing the following equation for the strength enhancement represented by factor β;

$$\beta = \left(1 + 0.3\frac{a_1}{h_c}\right)\left(1.50 - 1.1\frac{A_b}{A_{eff}}\right) \leq \text{minimum of } 1.5 \text{ or } 1.25 + \frac{a_1}{2h_c}$$

where $\frac{A_b}{A_{eff}} \leq 0.45$ and $e \leq \frac{t}{6}$

Equation 2.5 – Enhancement factor by EC6 (European Committee for Standardization, 2013)

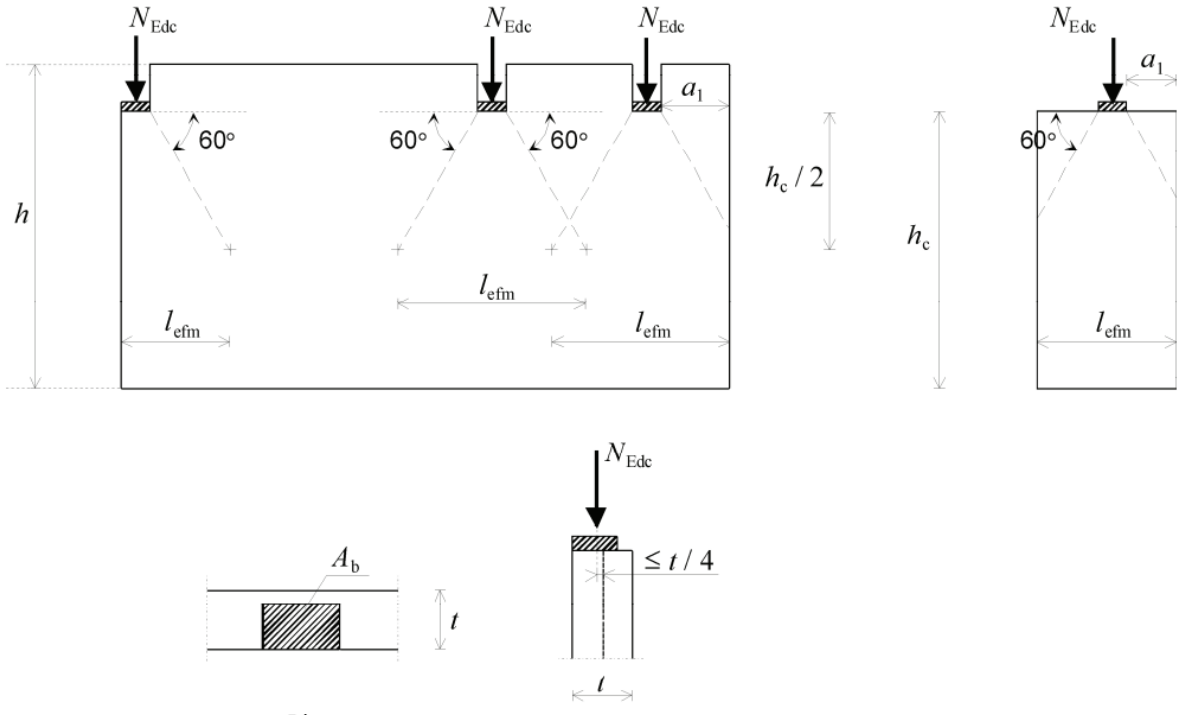

Figure 2.18 – Stress distribution and allowable ecentricity given by EC6 (European Committee for Standardization, 2013)

The British Standards Institution (BSI) groups up the loading scenarios into 3 bearing types, giving an increase in strength of 25%, 50% and 100% respectively as shown in Fig. 2.19 and Fig. 2.20. Moreover, the dispersion is assumed to be at an angle of 45 degrees, and recommends that checks are to be performed just underneath the bearing and at a height of 0.4h from the loaded area, as shown in Fig. 2.21 (British Standards Institution, 2005). The provisions given by the BSI are based on work related to concrete specimens, and hence do not comply accurately with the experimental work performed on masonry specimens (Malek, Mohammad H., 1987).

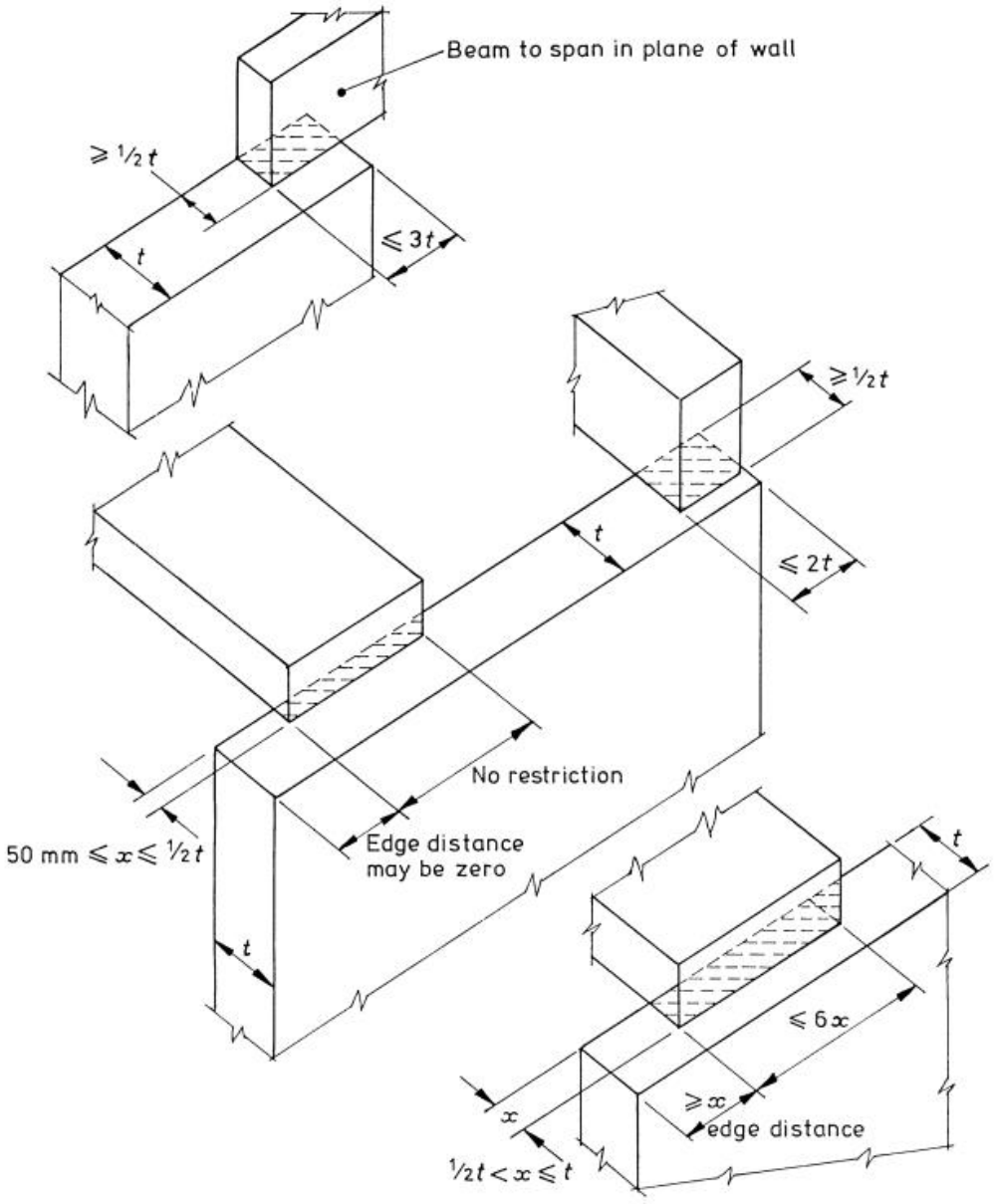

Local design strength $\frac{1.25f_k}{\gamma_m}$

(a) Bearing type 1

Figure 2.19 – Bearing type 1 as recommended by BS 5628 (British Standards Institution, 2005)

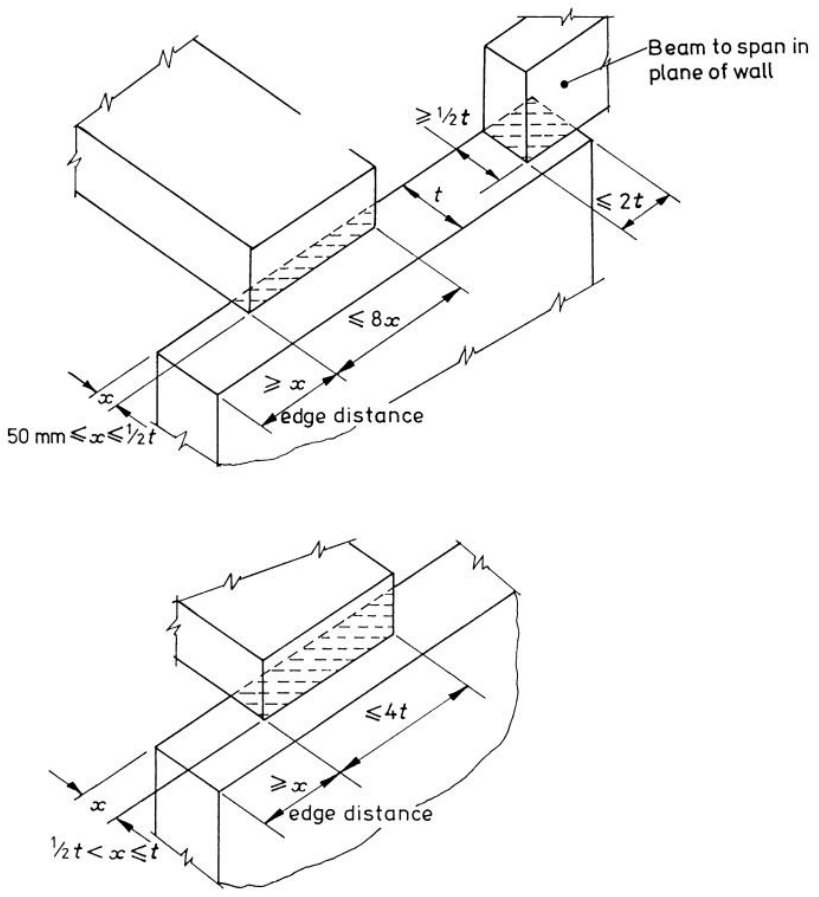

Local design strength $\frac{1.5f_k}{\gamma_m}$

(b) Bearing type 2

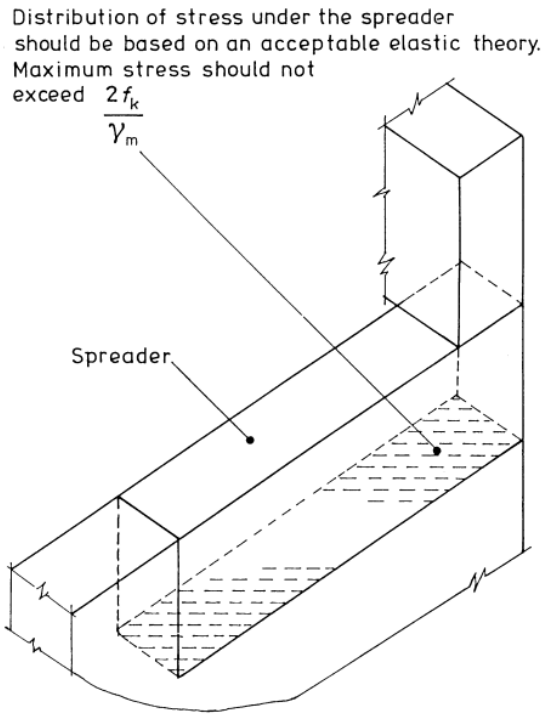

(c) Bearing type 3

Figure 2.20 – Bearing type 2 and 3 as recommended by BS 5628 (British Standards Institution, 2005)

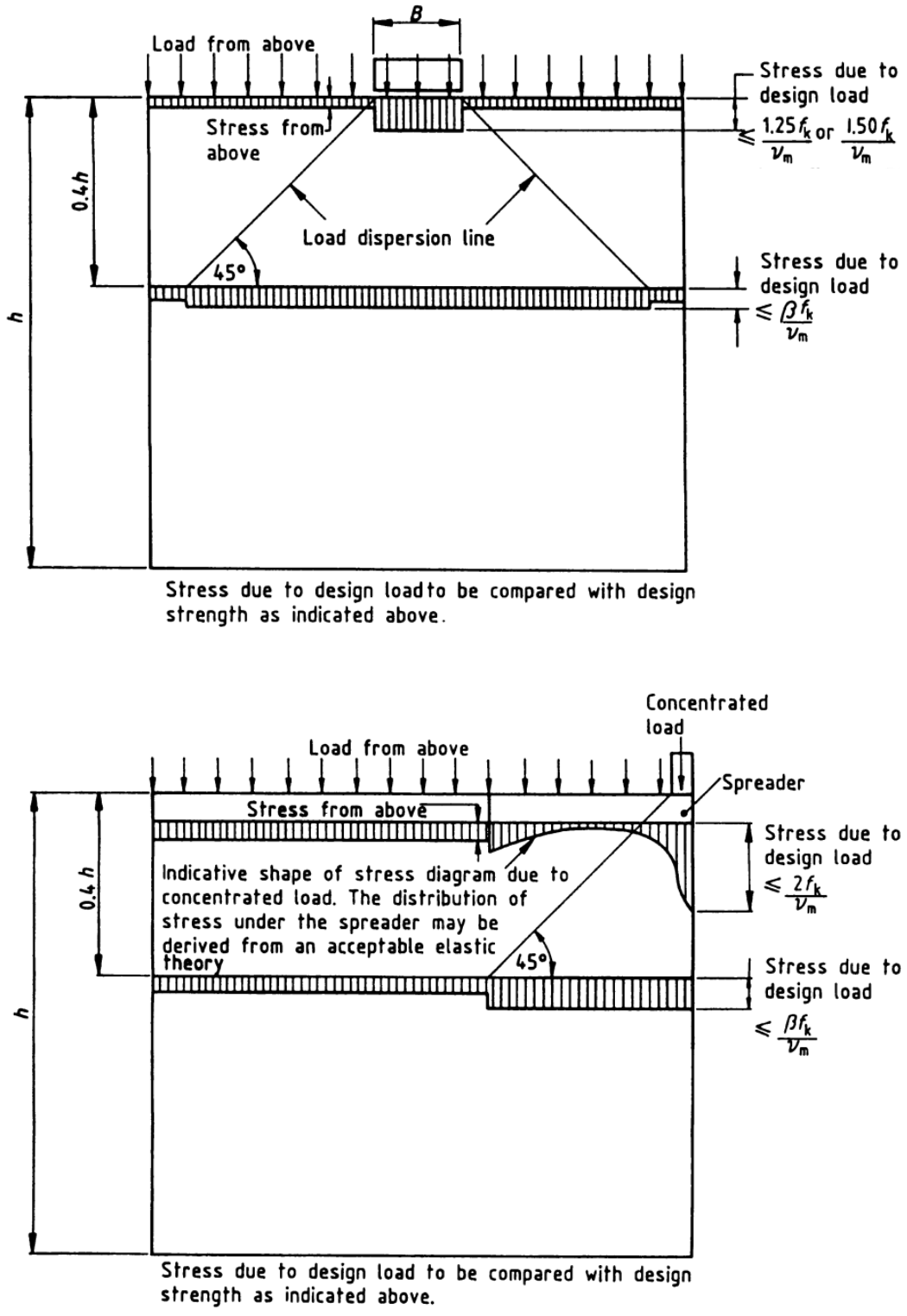

Figure 2.21 – Distribution of stresses for the 3 bearing types as recommedned by BS 5628 (British Standards Institution, 2005)

The Canadian code (S304.1-04) recommends a load dispersion angle of 45 degrees and takes into account the stress distribution by the bearing plate onto the masonry wall, applying an additional factor of 0.5 in the case of having a triangular stress distribution. The recommended strength enhancement factor is;

$$\beta = 0.55\frac{\left(1+0.5\frac{a_1}{l_2}\right)}{\left(\frac{A_b}{A_{eff}}\right)^{0.3}} \quad \text{or} \quad \beta = 1.5 + \frac{a_1}{l_2}$$

whichever is less, where l_2 = "the length of the wall between ends and/or movement joints" (CSA, 2004).

Equation 2.6 – Enhancement factor by the Canadian Code, S304.1-04 (CSA,2004)

Bright and Roberts compared the similarities and differences between the Eurocode (EN1996-1-1), the British Standard (BS5628) and the Canadian code (S304.1-04), making reference also to the findings of Page and Hendry. The strength enhancement factor and design spread for a particular case were compared by taking 2 different loading scenarios as shown in Fig. 2.22 and 2.23. The results are listed in Table 2.2.

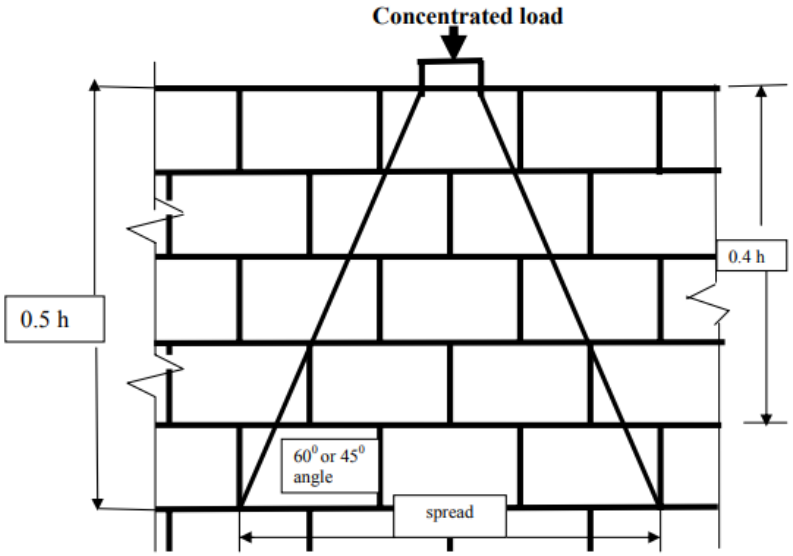

Figure 2.22 – Load Case A (Bright & Roberts, 2005)

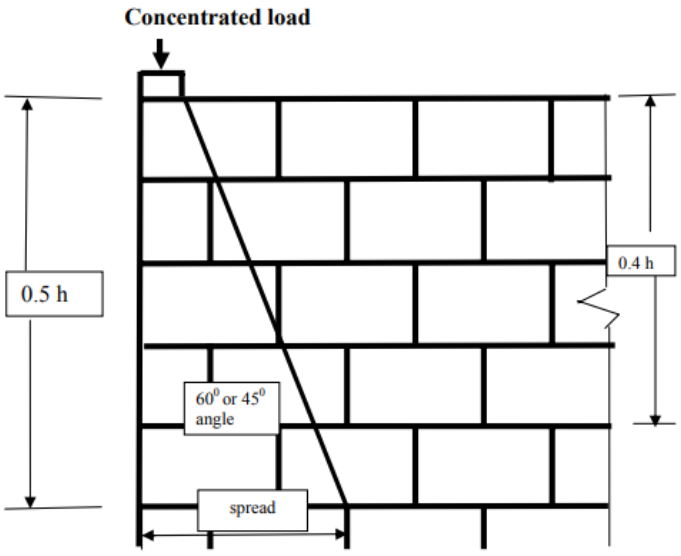

Figure 2.23 – Load Case B (Bright & Roberts, 2005)

	Load Case A		Load Case B	
Code	Enhancement factor under load	Design length in masonry (spread) In m	Enhancement factor under load	Design length in masonry (spread) In m
EC6	1.5	1.5	1.3	0.8
BS5628	1.5	2.1	1.5	1.1
S304*	1.0	2.6	1.0	1.4
S304**	2.0	2.6	1.3	1.4

Table 2.2 – Masonry design code comparison (Bright & Roberts, 2005)

* Assuming bearing plate will impose a triangular stress distribution

** Assuming bearing plate will impose a rectangular stress distribution

The Australian code, on the other hand is fairly similar to the Canadian standard, and suggests an identical equation for the strength enhancement factor, while recommending also the same load dispersion angle. This code also suggests that the use of the enhancement factor should not be considered in the case of having hollow masonry units, and, unlike the Canadian standard, does not distinguish between the different bearing stress distributions (Australian Standard, 2011).

As it currently stands, there is no design code which provide wholly satisfactory results. This was concluded after analysing the different codes, obtaining different enhancement factors and stress distributions. The difference between these codes is not negligible. Also, neither code takes into consideration the effect of having precompression applied to these walls, which is almost present in every real-life scenario. Moreover, neither gives provision for the possibility of having a factor which is less than 1.

2.5 The Effect of Precompression

The study of the effect of precompression is still in its early stages, and existing literature is very limited to a few small scaled tests. Moreover, the masonry design codes exclude the effect of precompressive stresses, besides the fact that this is a very frequent occurrence.

From previous studies, one can conclude that the unconfined material is one of the main factors contributing to the strength enhancement phenomenon of walls subject to concentrated loads. In the case of having a wall which is uniformly loaded from loads above, the surrounding material is now no longer unloaded. Hence one can hypothesise that as the precompression increases, the bearing strength underneath the concentrated load would reduce, such that as the precompressive loads approach the ultimate uniform load bearing strength, the enhancement effect reduces to 1.0 (Hendry, 1981).

Hendry and Malek studied briefly this effect, by first finding the failure stress at which the wall panels failed under uniform loading, and then varied the precompressive stresses, recording the changes within the enhancement factor beneath the concentrated loading. Accurate

conclusions could not be made on such a limited number of tests; however, Hendry, in a separate experimental programme, concluded that the enhancement factor was still present, and that the effect of precompression could be neglected for loads below 30% of the ultimate failure load (Hendry, 1981).

A simulated chart as shown in Fig. 2.6 has been developed, from which a reduction factor was drawn out to take into account the effect of precompression. However, a proper design chart is still to be developed based onto a sufficient number of tests (Malek, Mohammad H., 1987).

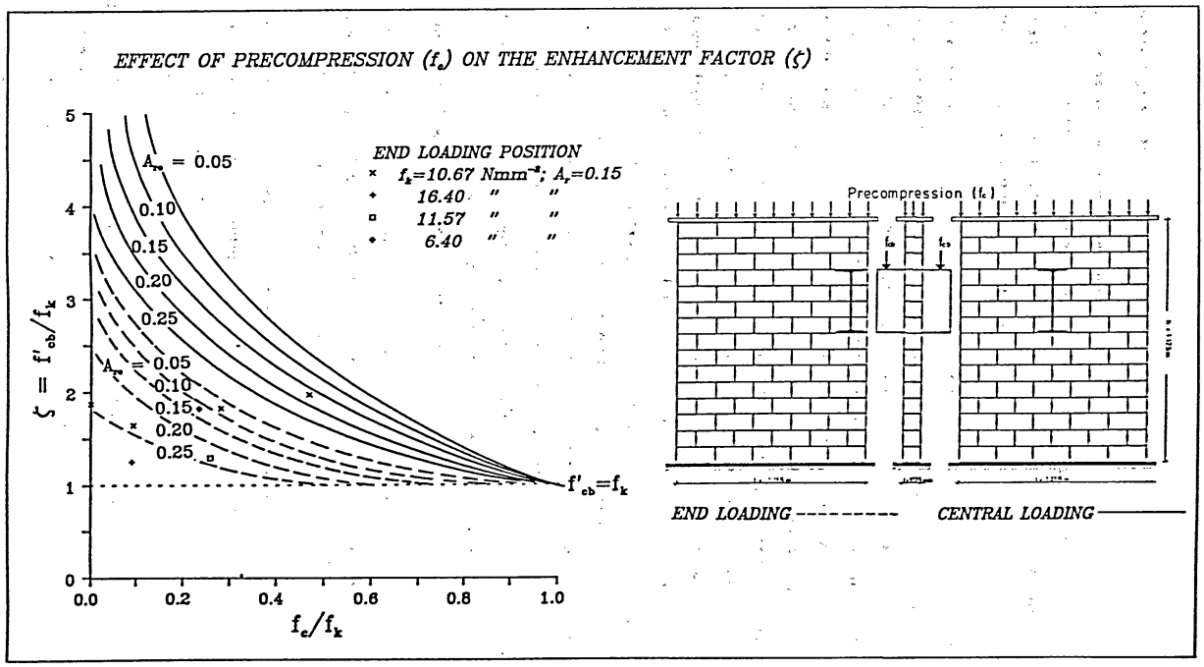

Figure 2.24 – A simulated chart predicting the reduction effect of precompression on the enhancement factor (Malek, Mohammad H., 1987)

Chapter 3: Experimental Methodology

3.1 Introduction

In general, in order to be able to investigate masonry structures, this would require ample time, effort and resources. Although the work involved in this study is only moderately complex, it could serve as the foundation for future, more in-depth research. Scaled down tests were performed on concrete homogenous wallets, representing the effect of precompressive stresses onto the behaviour of masonry walls when subject to concentrated loads. This chapter documents the provisions taken to represent and scale down masonry wall panels, the construction, preparation and transportation of the test specimens, the setting up of the testing rig, and the loading procedures.

3.2 Testing Objectives

3.2.1 General Aims

In this testing programme, the general aim was to study the effect of precompression onto the strength enhancement factor when walls are subject to concentrated loadings. Being a preliminary test programme, the majority of the variables were kept constant, however the loaded area ratio was varied to observe whether there is the same correlation in the changes to the enhancement factor when compared to unloaded masonry wall panels.

3.2.2 Experimental Programme

By definition, the strength enhancement factor (β) is the ratio of the bearing strength under the concentrated load (f_b) to the compressive strength of the wall panel (f_o);

$$\beta = \frac{f_b}{f_o}$$

Equation 3.1 – Strength enhancement factor definition

Throughout this testing programme, the levels of precompressive stresses were varied relative to the compressive strength of the wall panels. This implies that preliminary tests were essential in order to determine the baseline f_o. As specified by the British Standard Institution, at least 2 tests should have been performed in order to obtain the averaged value of f_o (Farrugia, 1990). A third test was performed in the case of having a large margin of difference between the first 2 tests in order to be able to estimate more accurately the compressive strength of the wall panel, onto which all of the succeeding tests were to be based on. The increments of the precompressive stresses should have ranged from a ratio of $\frac{f_p}{f_o} = 0 \; to \; 0.9$.

The wall panels were split into two batches both due to logistic reasons, and to be able to use preliminary information from the first batch in order to refine the design mix of the second batch. As two concrete wall batches were cast, f_o for each batch had to be found separately.

Apart from the 2 or 3 wall panels to determine f_o, additional 10 panels were cast per each batch to study the variation in the enhancement factor with changes in precompressive stresses. This resulted that in total, 25 wall panels were to be cast and tested, split into 2 batches, testing different loaded area ratios for each set. A schematic view of the testing programme is shown in Fig. 3.1, where in (a), a beam is used to distribute the applied load until failure, and in (b), 2 secondary load jacks are used to pre-set the precompressive distributed stresses, and the main central jack is then used to load the wall until failure.

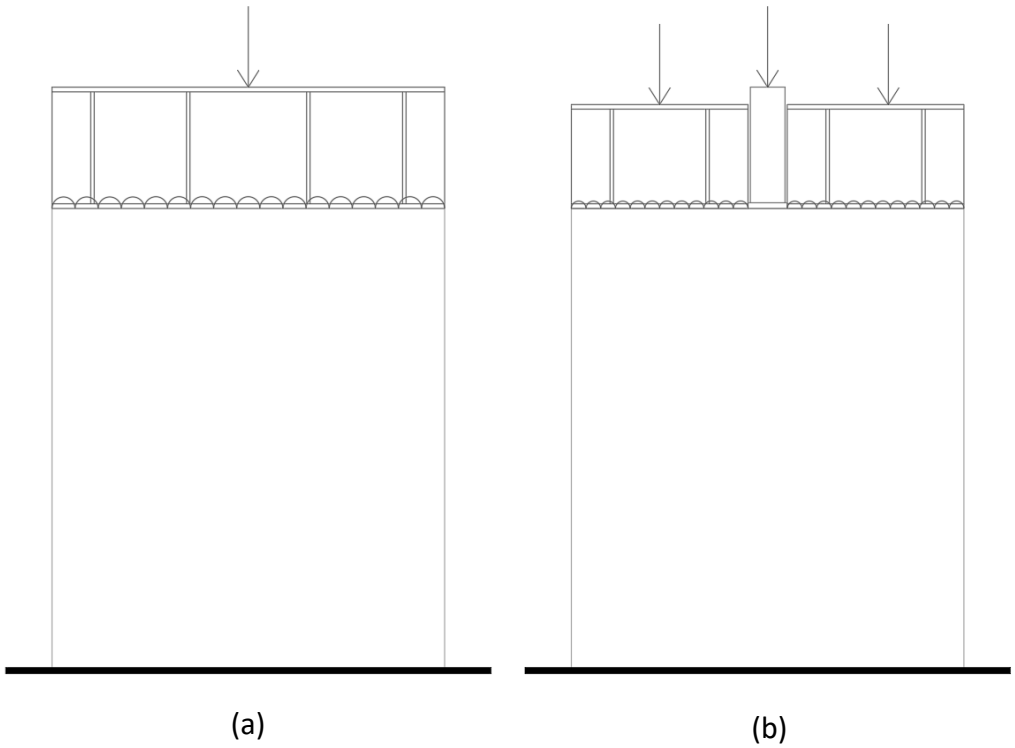

Figure 3.1 – Schematic Loading Diagram for; a). Finding f_o; b). Finding the modified enhancement factor due to the effects of precompressive stresses

Throughout all the testing programme, the concentrated loads were to be distributed over the whole wall thickness using stiff bearing plates, opting for the strip loading approach as opposed to patch loading, treating the situation as a 2D parameter. This is a similar approach to the majority of the previous small scaled experimental studies.

Also, being modest in scale, a system was adopted to make the most out of the limited number of tests. Rather than following the traditional approach, that of testing multiple walls with identical boundary conditions and averaging their results, single tests were performed while varying more frequently the increments between the ratio of the precompressive stresses. This approach could be adopted as long as the wall's variables and testing procedures are heavily controlled. As a result of this small incremental change, in the case of having defective tests, these could be highlighted when compared to the overall result scenario. Moreover, this

approach provided a clearer picture on the behaviour of the strength enhancement factor against changes in the level of precompressive stresses, which was this study's main aim.

Between the different batches, the loaded area ratio (A_b/A_{eff}) was altered such that more conclusions and patterns could be based on different boundary conditions. This also helped in calibrating the results with masonry wall panels by comparing the test results without any precompression to the existing literature for masonry structures. The forecasted testing programme is tabulated below;

Wall No.	Batch No.	Loading Type	$\frac{A_b}{A_{eff}}$	Plate Size (mm)	Precompressive stresses $\left(\delta = \frac{f_p}{f_o}\right)$
1	2	UDL	1	/	/
2	2	UDL	1	/	/
3	2	UDL	1	/	/
4	2	CL	0.1	68 x 82	0.0
5	2	P.UDL + CL	0.1	68 x 82	0.1
6	2	P.UDL + CL	0.1	68 x 82	0.2
7	2	P.UDL + CL	0.1	68 x 82	0.3
8	2	P.UDL + CL	0.1	68 x 82	0.4
9	2	P.UDL + CL	0.1	68 x 82	0.5
10	2	P.UDL + CL	0.1	68 x 82	0.6
11	2	P.UDL + CL	0.1	68 x 82	0.7
12	2	P.UDL + CL	0.1	68 x 82	0.8
13	2	P.UDL + CL	0.1	68 x 82	0.9
14	1	UDL	1	/	/
15	1	UDL	1	/	/
16	1	CL	0.2	136 x 82	0.0
17	1	P.UDL + CL	0.2	136 x 82	0.1
18	1	P.UDL + CL	0.2	136 x 82	0.2
19	1	P.UDL + CL	0.2	136 x 82	0.3
20	1	P.UDL + CL	0.2	136 x 82	0.4
21	1	P.UDL + CL	0.2	136 x 82	0.5
22	1	P.UDL + CL	0.2	136 x 82	0.6
23	1	P.UDL + CL	0.2	136 x 82	0.7
24	1	P.UDL + CL	0.2	136 x 82	0.8
25	1	P.UDL + CL	0.2	136 x 82	0.9

Table 3.1 – Testing programme

Where; UDL = Uniformly Distributed Load

P.UDL = Partial Uniformly Distributed Load

CL = Concentrated Load

3.2.3 Additional Tests Performed

Additional tests were carried out to determine the mechanical properties of the materials used, providing preliminary information to aid further works and to predict the expected wall panels' failure loads. The main additional tests performed were the unconfined compression strength (UCS) tests on both the concrete cubes and grout samples.

3.3 Wall Panel Considerations

3.3.1 The use of Homogenous Concrete Walls

In this testing programme, concrete homogenous walls were used to replicate the effect of precompression to masonry structures when subject to concentrated loads. In order to assess solely this property, considering the modest scale of these tests, it was vital to reduce the variabilities between one wall and another. Moreover, the use of solid concrete wall panels implies that a larger number of tests could be performed in a shorter period of time, as these are less labour intensive to cast, resulting into conclusions being formulated onto a larger sample.

Ali and Page used solid concrete masonry wall panels in order to compare between the experimental evidence and the predicted finite element theory, proving that the enhancement behaviour of solid concrete masonry is still evident and comparable to typical masonry structures (Ali & Page, 1988). The effect of strength enhancement under concentrated load is also applicable to solid concrete structures (Mann & Pfeifer, 1985), and as proved by Hawkins, Au and Baird back in the 1960's, the failure mechanism for solid masonry wall panels subject to concentrated loads are correspondent to homogenous panels as is concrete (Yi & Shrive, 2003). Also, the current design codes are mostly based on theories which were formulated on the assumptions that masonry walls behave as homogenous and isotropic walls (Malek, Mohammad H., 1987). Hence the use of concrete wall panels can be a great starting point to analyse the pattern and the overall expected behaviour.

3.3.2 Concrete Wall Panels Design Mix and Dimensions

The strength of the concrete's design mix and the wall panel's size were restrained by the testing rig's and apparatus' limitations. The initial target strength for the first batch was that of 10 N/mm^2 cube strength. This should provide enough strength to withstand the loads during handling, transportation and setting up of the equipment, while excluding the possibility of failure or cracking prior testing.

The dimensions of the wall panel were dependent on both the dimensions of testing rig, along with the maximum allowable load that could be applied by the loading jacks. The use of a full-scale model, as per appendix A, was impossible both because of the testing rig's size, and also to optimise material handling and efficiency. Having set the design strength, the size of the

wall panel had to be limited in order to generate enough stress by the available loading jacks, which the testing rig could withstand without failure. The final chosen dimensions of the wall panels are as shown in Fig. 3.2.

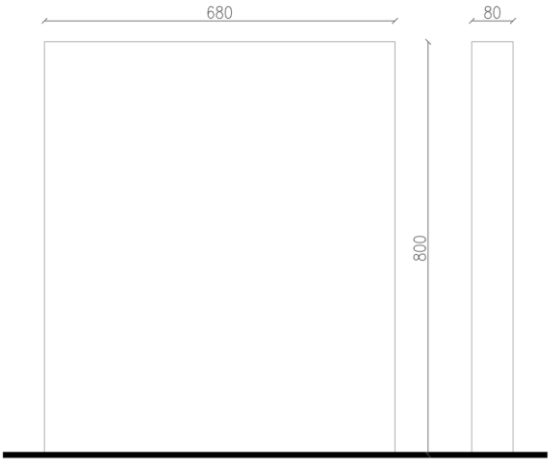

Figure 3.2 – Wall Panel Finalised dimensions (in mm)

The height of the panel was limited in proportion to its thickness, in order to reduce the effect of slenderness, which is just under the slenderness ratio of a contemporary 230mm masonry wall. Having set a target ratio (h/t) of 10, the ideal thickness and height of a typical wall panel would be that of 80mm and 800mm respectively. This panel would easily fit within the testing rig, allowing enough space for the beams to distribute the loads. Moreover, a thickness of 80mm would limit the gross cross-sectional area, reducing the required load to fail the wall.

Additionally, enough width had to be provided to allow for the strength enhancement phenomenon, generated by the less confined material. However, this had to be restricted to limit the load needed to generate the precompressive stresses (as shown in Fig. 3.1), while ensuring that the load had distributed enough to safely assume that the panel's whole width (l) could be considered as the effective width (l_{eff}), as shown in Fig.3.3. Since the wall panels were made out of concrete, a load dispersion angle of 45° was assumed.

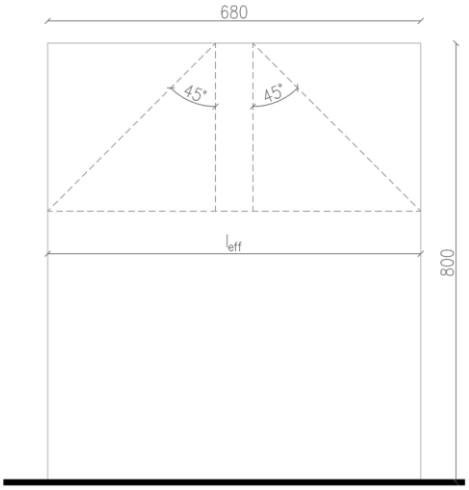

Figure 3.3 – Concentrated Load dispersion for $\frac{A_b}{A_{eff}} = 0.1$

3.4 Construction of Concrete Walls

3.4.1 Casting Set-up

The concrete wall panels were cast by Ballut Blocks Ltd., at their manufacturing plant in Naxxar, Malta. The thickness of the wall panels was slightly altered from the designed 80mm to 82mm, in order to use the readily available wooden beams as the main formwork. Perpendicular wooden strips were used to subdivide the whole length into separate walls, cast on appropriately flat ground over wooden boards, as shown in Fig. 3.4. The dimensions and angles were double checked to ensure the casting of identical concrete panels.

Figure 3.4 – Formwork setup before casting

3.4.2 Casting Procedure

The wall panels were cast in 2 batches, using 2 different design mixes as tabulated in table 3.2 and 3.3. The second design mix was altered as per the results obtained in appendix D. Each batch was cast using a homogenous mix, and the formwork was filled up partially and sequentially in order to ensure similar properties between the different walls. Before casting, appropriate lubrication was used to be able to extract the formwork upon hardening. The panels were then slightly vibrated and covered with sheeting for plastic curing. After 4 days, the plastic sheets were removed, to allow the wall panel to cure at ambient conditions and at the 7th day from casting, the formworks were removed. Moreover, for each cast, a number of cube samples were taken as per MSA EN 12390-2:2009. Results are recorded in appendix D.

Concrete Strength C10: UOM – Mix per 1 cu.yard			
Material	**Type**	**Amount**	**Unit**
CEM II/A. LL 42.5R	OPC	150	Kgs
Fine Aggregate	0/4	873	Kgs
Coarse Aggregate	4/10	715	kgs
Water	H2O	150	Lts
	Average per 1 cu.yd:	1887	Kgs

Table 3.2 – Concrete Mix Design for the first batch (by Ballut)

Concrete Strength C8: UOM – Mix per 1.5 cu.yard			
Material	**Type**	**Amount**	**Unit**
CEM II/A. LL 42.5R	OPC	120	Kgs
Fine Aggregate	0/4	820	Kgs
Coarse Aggregate	4/10	759	kgs
Water	H_2O	120	Lts
	Average per 1 cu.yd:	1213	Kgs

Table 3.3 – Concrete Mix Design for the second batch (by Ballut)

3.4.3 Grouting and Grinding of the Concrete Walls

For the weaker batch, during handling and transportation the surfaces onto which the wall had to be tested ended up not being consistently flat, resulting in the need for capping. Considering a thickness of 82mm, a slight surface imperfection would lead to immediate instability and test failure. This was confirmed by the first preliminary test, where an ungrouted sand capping layer was used to level the wall surfaces, which ended up in unsatisfactory results as shown in section 4.2.1 (wall 1). As a result, each concrete wall had to be resurfaced with a grouting capping layer. Perfectly aligned and surfaced wooden formworks were built, and the short edged parallel surfaces were grouted using SikaGrout 212, as shown in Fig. 3.5.

For the stronger concrete batch, the wall panels' surfaces did not crumble during handling, which meant that grinding of the casting imperfections could eliminate the need to grout each and every wall. However, after inconsistent results as per section 4.3.2, the rest of the wall panels of the stronger concrete batch were also grouted, maintaining uniformity throughout the whole testing programme.

Figure 3.5 – L*eft*, formwork for grouting; *right*, grouted Wall Panel

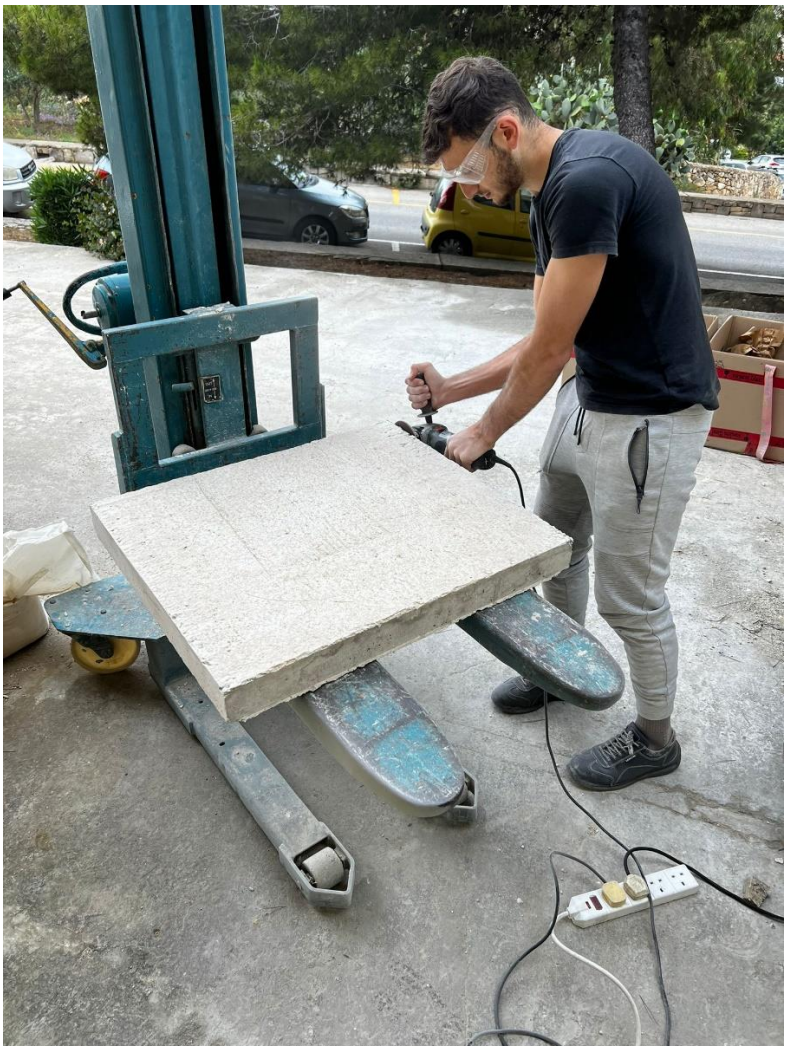

Figure 3.6 – Grinding off the surfaces' imperfections

3.4.4 Testing Performed During Casting

Apart from wall testing, it was deemed important to keep account on the strengths of the concrete mix and grout used.

Unconfined compression Strength (UCS) tests were performed on 150x150x150mm cubes as per BS EN 12390-3:2009. Ballut Blocks Ltd. performed the 7-day tests, and the rest of the samples were then tested at the laboratory. Loading rates were altered to get a more representative prediction for the concrete wall's compressive failure load. Results are presented in appendix D.

Also, to ensure that the grout layer did not fail prior wall failure, grouting prism samples with the dimensions of 160x40x40mm were taken as shown in Fig. 3.7 to test its flexural and compressive strength. Tests were performed as per BS EN 196-1:2016, at different days depending on the period between grout casting and testing of the wall panels. Results are tabulated in appendix E.

Figure 3.7 – Typical Grouting Samples

3.5 Apparatus Setup

3.5.1 Testing Rig Used

The testing rig consisted of a closed box bolted system made out of 4 stiffened UB 533x210x122 sections, with an internal dimension of 1790mm x 1790mm. This internal space had to accommodate the wall specimens together with the hydraulic jacks, beams and/or plates to distribute the vertical loads. As described schematically in section 3.2.2, a total of 3 vertical jacks were used. The middle Holmatro double acting hydraulic jack, having a load capacity of 60t, was lined up centrally within the rig and above the wall specimens, which was used mainly to apply the central concentrated loads (f_b). The other 2 single acting Holmatro hydraulic jacks with a maximum load capacity of 100t, were aligned symmetrically around the main jack, positioned to act centrally over the 2 stiffened IPN 180 beams, used to apply the precompressive stresses, as shown in Fig. 3.8. For finding the UDL failure load (f_o), a stiffened IPN 280 beam was used to distribute the loads from the hydraulic jacks, as shown in Fig. 3.9. Also, although a grouting layer was cast along the loaded faces, a neoprene rubber layer was placed between the wall and the beams to ensure flush contact over the loaded area.

The 3 jacks had load cells attached to be able to monitor and record the loadings via a data logger. The central load cell had a capacity to read 500kN, while the other 2 load cells had a capacity to read 1000kN. Prior testing these were calibrated to ensure accuracy in the results.

Also, as represented in Fig. 3.10 and 3.11, the position of the 100t jacks was shifted between the 2 testing batches, depending on the loaded area ratio, ensuring that the load is applied centrally over the distributing IPN beam.

As shown in Fig. 3.12, 2 wooden strips along each face of the concrete wall specimen were clamped with the testing rig, used to hold the wall into position and restrain the wall from crumbling down upon failure. Also, when finding f_o, an angle section along each façade was clamped with the rig at the foot of the wall, acting as additional supports to restrain lateral movement. Additionally, safety straps were used to hold the beams from falling upon failure, as shown in Fig. 3.13.

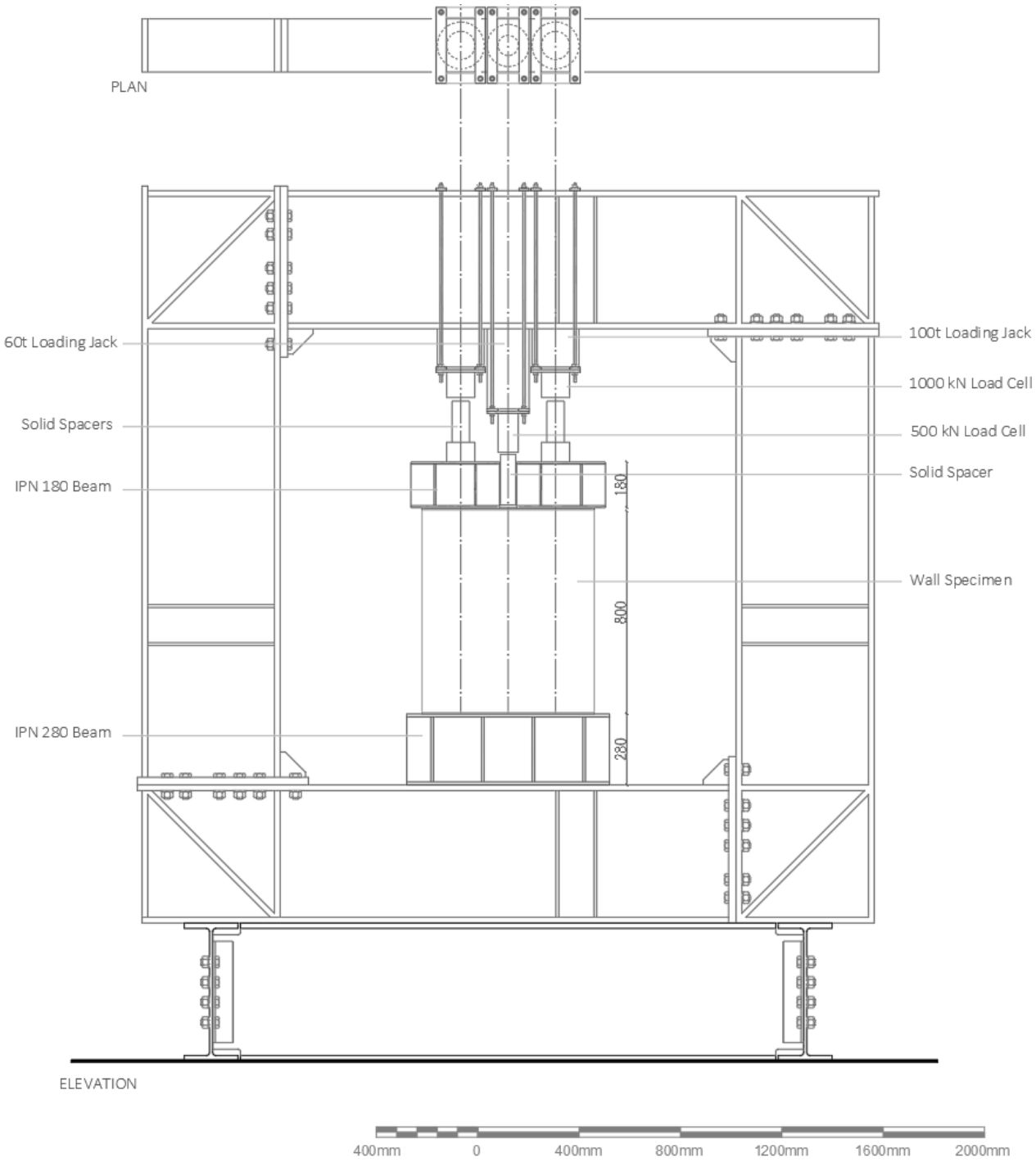

Figure 3.8 – Testing rig setup for precompression and concentrated load tests

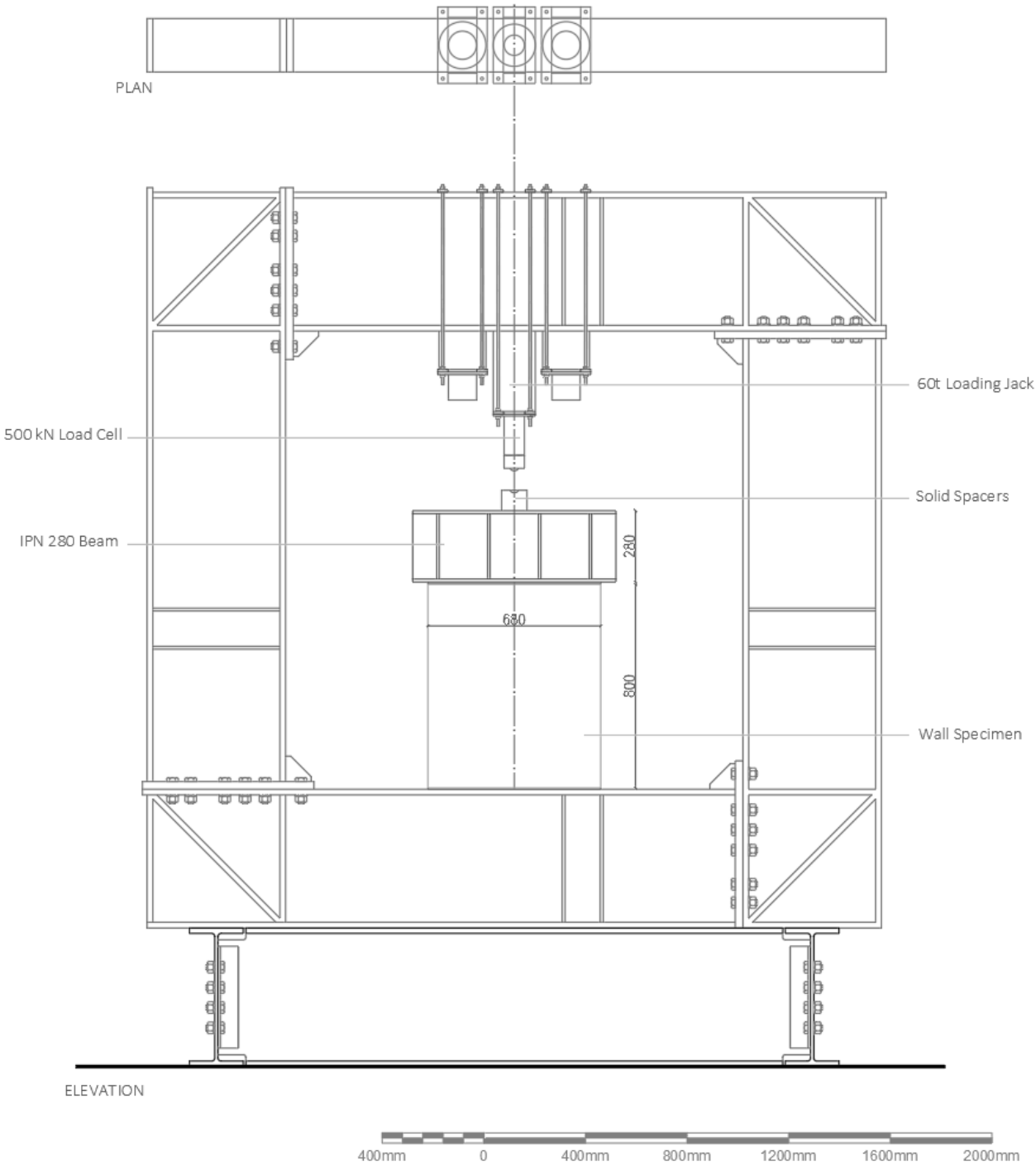

Figure 3.9 – Testing rig setup for UDL loading

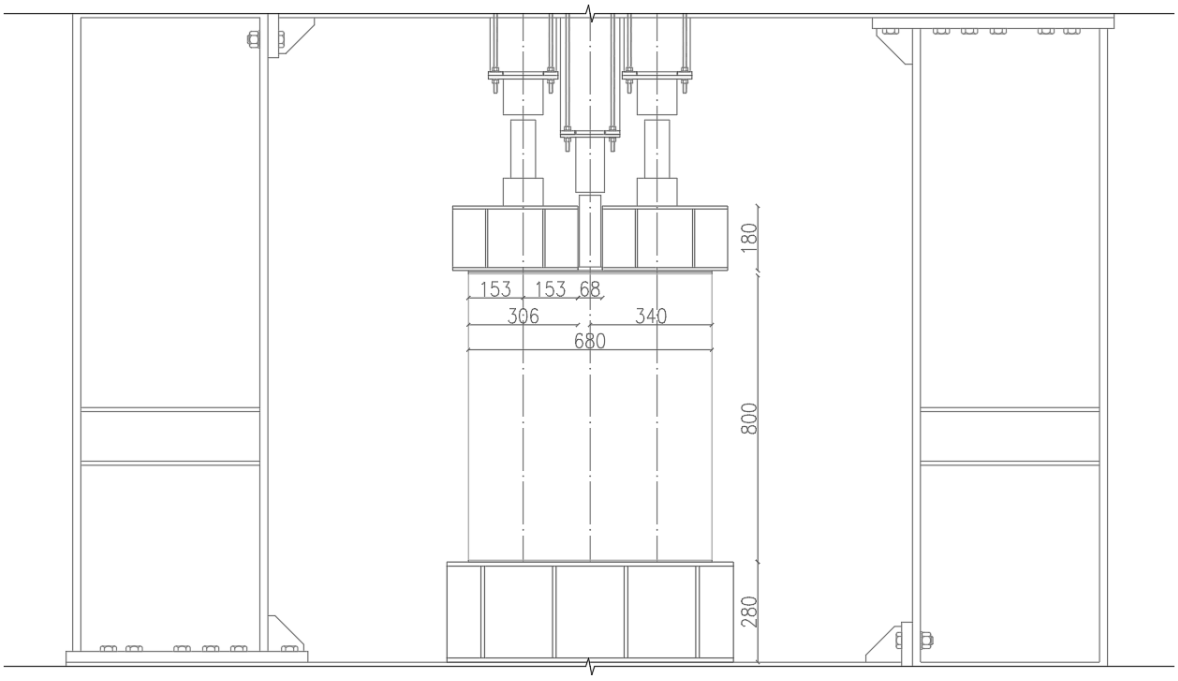

Figure 3.10 – Testing rig setup dimensions for Ab/Aeff = 0.1 (concrete batch 2)

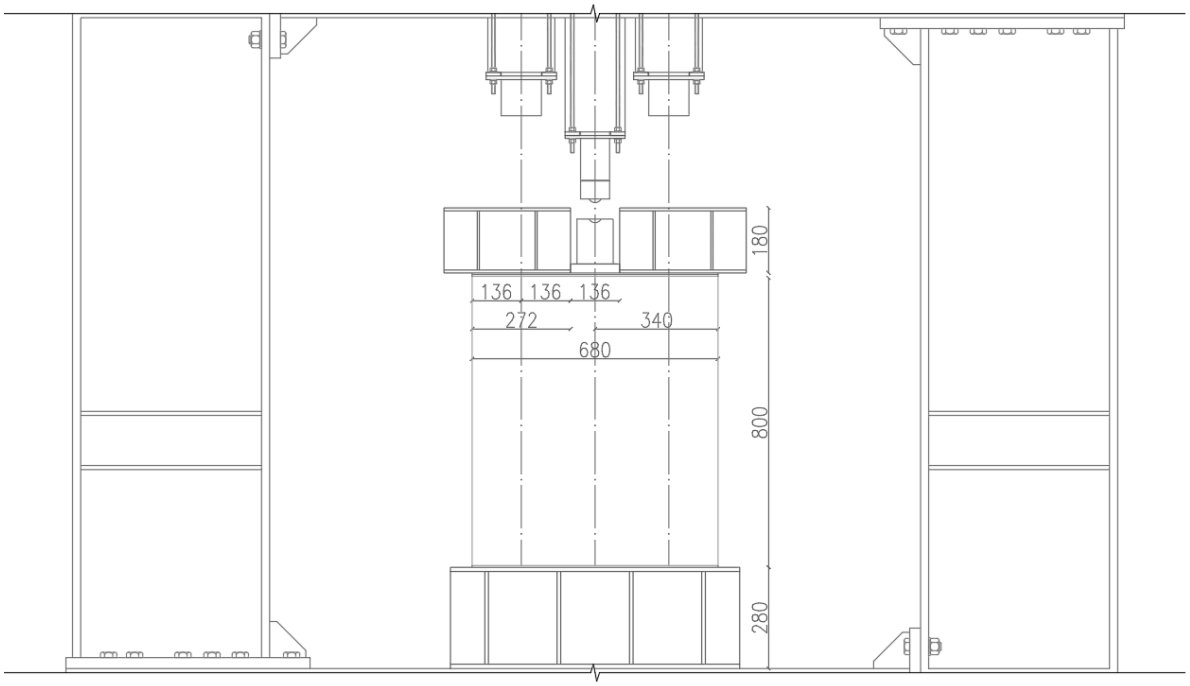

Figure 3.11 – Testing rig setup dimensions for Ab/Aeff = 0.2 (concrete batch 1)

Figure 3.12 – Typical test performed, including both the precompression and concentrated loads

Figure 3.13 – Typical test performed with failure under UDL

3.6 Wall Testing Procedure

3.6.1 Transportation and Placing of the Wall Specimens:

At Ballut Blocks Ltd. manufacturing plant, the wall panels were transferred from their casting location onto pallets using a mechanical scissors lifting clamp and were stacked over each other with separators in between. Each batch was transported from the plant to the laboratory using a small high up crane. The walls were then stored outside of the laboratory as shown in Fig. 3.14.

Figure 3.14 –Concrete wall panels outside the laboratory

Handling of the walls at the laboratory was not the easiest of tasks, especially during the transportation of the second cast concrete batch which resulted to be severely fragile. As the laboratory was not equipped with a mechanical scissors lifting clamp, each wall was slid over a forklift, as shown in Fig. 3.15 and lowered down on a flat surface for the grouting process. Once ready for testing, the wall panels were cautiously levered from the side edges and a strap was then inserted to tighten the walls. A strategic technique as shown in Fig. 3.16 was adopted such that each wall could be lowered down into position and the strap can be easily detached, keeping the horizontal surfaces intact.

The overhead crane was used to carefully manoeuvre the wall through the laboratory, down into the testing rig. Hauling of the walls within the testing rig was quite challenging because of the frictional forces generated by the wall's gravitational weight. Hence it was imperative to mark the wall's centre prior lifting such that it can be lowered down perfectly into position.

Figure 3.15 – Moving the wall from outside the laboratory using a forklift

Figure 3.16 – Transportation of a typical wall within the lab using the overhead crane

3.6.2 Wall checks and Alignment

Once in position, a spirit level was used to ensure each wall's verticality and that the loading surface is perfectly horizontal. In most of the cases, due to the capping layer, the walls were found to be exactly plumb resulting into a perfect horizontal surface. For the few exceptions, the out-of-plumb was very minimal, always less than 3mm. In such cases, the wooden supports along both façades were used to provide lateral support and reduce the possibility of premature failure.

Figure 3.17 – Ensuring the loading surface is perfectly aligned using a spirit leveler

Moreover, the position of the jacks was adjusted slightly before each test such that the load is applied axially to the centre of the wall's thickness, since a small eccentricity can induce secondary effects and premature failure.

3.6.3 Loading

As the walls and jacks were properly aligned, the loading was initiated at a particular rate. Following on the works of Farrugia, the same loading rate of 1N/mm^2 per minute was to be adopted. However, for the first testing programme, the walls showed themselves to be much weaker than predicted, meaning that using such a loading rate would have led to failure within the first 2 to 3 minutes of loading.

As a result, a different loading rate was adopted for this weaker batch. For the first 3 tests, when finding f_o, a loading rate of 25kN per minute was adopted. This loading rate corresponds to a stress of around 0.45 N/mm^2 per minute, as per appendix C.

When it comes to the concentrated loads, considering a loaded area ratio of 0.1, a load of 2.5kN/minute would result into the equivalent 0.45N/mm^2 per minute. Moreover, the precompressive stresses were also applied using the same rate, which is equivalent to approximately a load of 11.5kN/minute, as shown in table 3.4.

Wall No.	**Loading Type**	**Precompressive stresses** $\left(\frac{f_p}{f_o}\right)$	**Loading Rate (Middle sack) kN/min**	**Loading Rate (Each side jack) kN/min**
1	UDL	/	25	/
2	UDL	/	25	/
3	UDL	/	25	/
4	CL	0.0	2.5	/
5	P.UDL + CL	0.1	2.5	11.5
6	P.UDL + CL	0.2	2.5	11.5

Wall No.	Loading Type	Precompressive stresses $\left(\frac{f_p}{f_o}\right)$	Loading Rate (Middle sack) kN/min	Loading Rate (Each side jack) kN/min
7	P.UDL + CL	0.3	2.5	11.5
8	P.UDL + CL	0.4	2.5	11.5
9	P.UDL + CL	0.5	2.5	11.5
10	P.UDL + CL	0.6	2.5	11.5
11	P.UDL + CL	0.7	2.5	11.5
12	P.UDL + CL	0.8	2.5	11.5
13	P.UDL + CL	0.9	2.5	11.5

Table 3.4 – Loading rates for the first testing programme, equivalent to 0.45N/mm^2 per minute

Where; UDL = Uniformly Distributed Load

P.UDL = Partial Uniformly Distributed Load

CL = Concentrated Load

When it came to test the stronger concrete batch, using the rate of 1N/mm^2 per minute, and considering the expected strength enhancement, these panels could have sustained a continuous loading period of 1 hour. Hence, a faster loading rate was adopted, applying a load of 100kN/minute for finding f_o, equivalent to 1.79N/mm^2 per minute. Considering that the middle jack's maximum load capacity of 597.8kN is not sufficient to find f_o, instead the side jacks were used and were loaded simultaneously with a load of 50kN/minute each. Applying the same stress rate to both the concentrated load and the precompressive stresses resulted into the loading rates of 20kN/minute and 40kN/minute respectively. Calculations for these load rate conversions are presented in appendix C, and the results are tabulated in the below table 3.5.

Wall No.	Loading Type	Precompressive stresses $\left(\frac{f_p}{f_o}\right)$	Loading Rate (Middle sack) kN/min	Loading Rate (Each side jack) kN/min
14	UDL	/	/	50
15	UDL	/	/	50
16	UDL	/	/	50
17	CL	0.0	20	/
18	P.UDL + CL	0.1	20	40
19	P.UDL + CL	0.2	20	40
20	P.UDL + CL	0.3	20	40
21	P.UDL + CL	0.4	20	40
22	P.UDL + CL	0.5	20	40
23	P.UDL + CL	0.6	20	40
24	P.UDL + CL	0.7	20	40
25	P.UDL + CL	0.8	20	40
26	P.UDL + CL	0.9	20	40

Table 3.5 – Loading rates for the second testing programme, equivalent to 1.79N/mm^2 per minute

Chapter 4: Test Results

4.1 Introduction

In this chapter the experimental test results are presented, showing graphs representing the progression of the applied loads with time for each tested wall. Moreover, comments, observations and failure modes are presented which will be analysed and commented upon in Chapter 5 and 6.

The preliminary concrete cubes and grout prisms strength tests are presented in appendix D and E respectively. Moreover, a time-history, indicating the relative time period for curing and testing with respect to the date of casting is presented in appendix F. This appendix also includes additional photos representing the failure modes and testing apparatus used throughout this testing programme.

4.2 First Testing Programme

For this experimental work, the first testing programme was performed on the second and weaker batch. Results from the UCS tests, as presented in Appendix D, gave a good prediction on the failure load required to test the wall panels. For the stronger batch, this load can approximate the failure limit of the testing rig, resulting into a small factor of safety. As a result, the second cast batch was initially tested to at least obtain representative results onto which conclusions could be drawn. Although this batch was cast at a later stage compared to the first batch, prior to the first wall test, 44 days have passed, resulting that the strength difference between the first and the last tested wall could be considered negligible.

4.2.1 UDL Tests

The initial 3 tests were loaded with a uniformly distributed load, finding the average bearing strength (f_o) under uniform loading. The typical setup used is as shown in section 3.5.1. The failure mode of these tests consisted of diagonal cracking generated from the middle top surface down to the bottom side corner. Prior failure, crushing and crumbling of concrete pieces was observed at around 80% of the wall's capacity, followed by instant diagonal cracking failure.

Wall 1

Wall No.	Setup No.	Days from casting	h	b (average)	t (average)	F	f_o
			mm	mm	mm	kN	N/mm^2
1	1	39	800	680	82.5	80.57	1.43
1	2	44	820	680	82.5	148.9997	2.66

Table 4.1 – Failure stress under UDL for wall 1

The first wall had to be tested twice as the initial setup, as presented in appendix F, was found to be incorrect and some amendments had to be performed. For this setup, the wall's surfaces were levelled using fine sands, and the beam used to distribute the load was relatively wide compared to the wall's thickness.

Upon loading, the wall did not fail by crushing, but, because of the instability of the wall's surface, the beam tilted and led to premature failure as shown in Fig. 4.2.

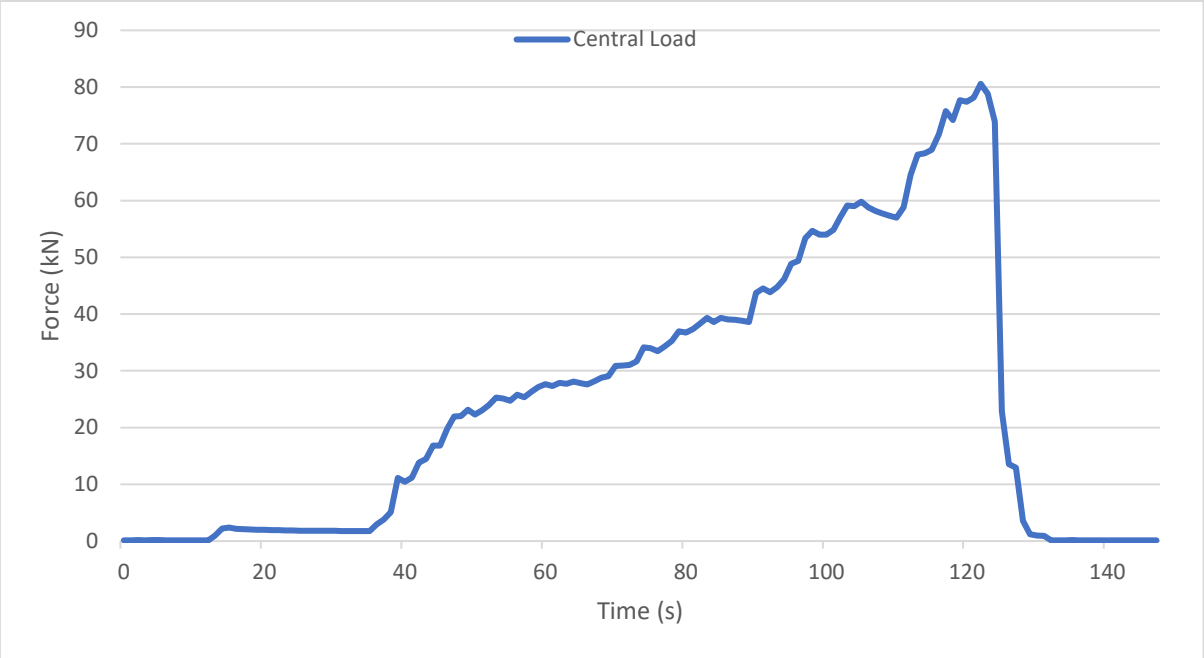

Figure 4.1 – Force vs time graph for wall 1, setup 1

Figure 4.2 – Premature failure of wall 1, setup 1

Given the limit on the number of samples available for testing, and considering that the wall did not fail in compression, the same wall was grouted as described in section 3.4.3, and a new beam was used to distribute the loading, as shown in the typical setup, represented by Fig. 3.13. The wall was then retested and loaded until failure, as shown below.

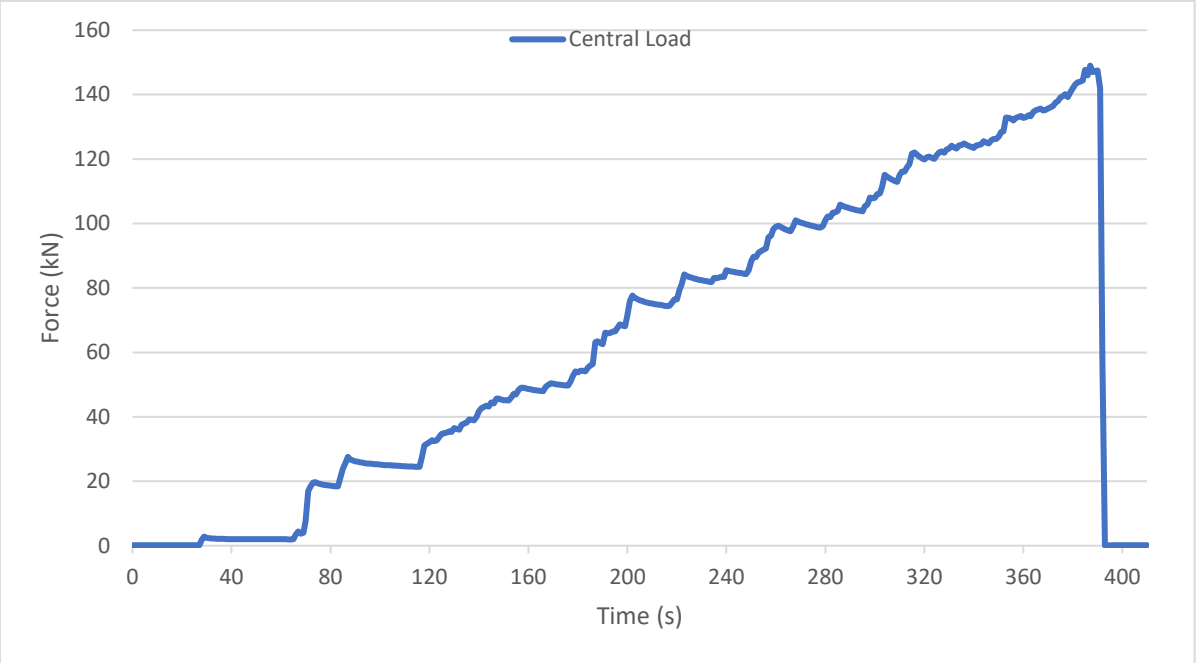

Figure 4.3 – Force vs time graph for wall 1, setup 2

Figure 4.4 – *Left*, failure mode front elevation; *right*, failure mode back elevation

Wall 2

Wall No.	Days from casting	h	b (average)	t (average)	F	f_o
		mm	mm	mm	kN	N/mm^2
2	46	820	682	84	217.7437	3.80

Table 4.2 – Failure stress under UDL for wall 2

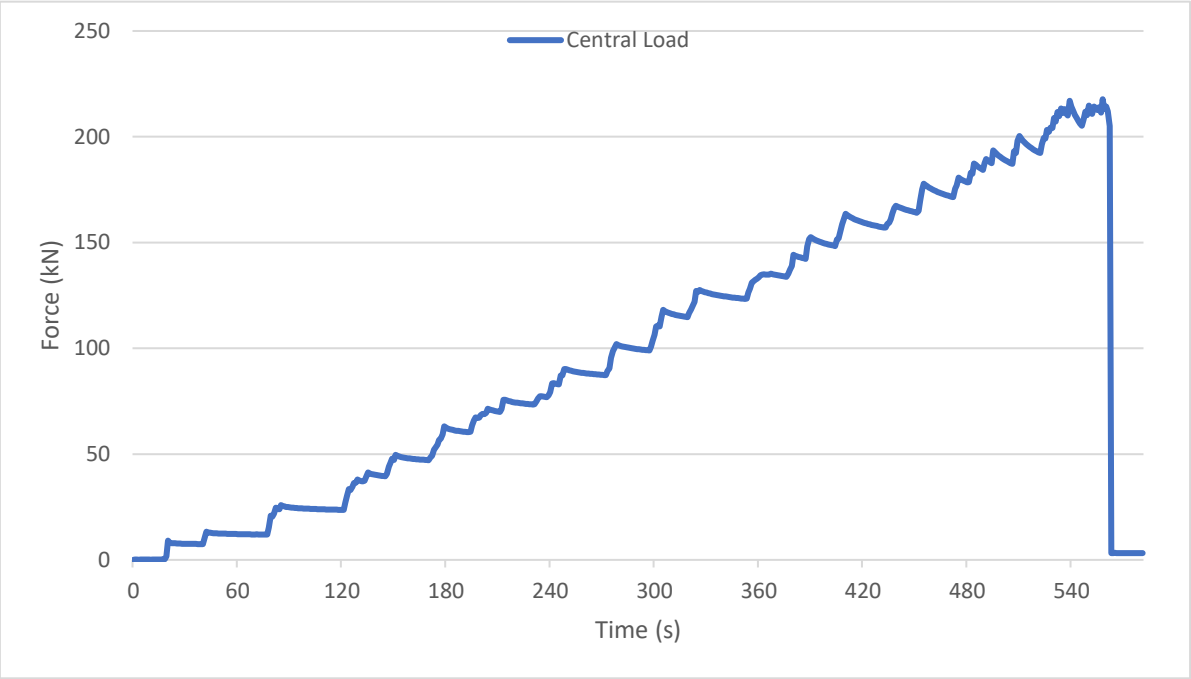

Figure 4.5 – Force vs time graph for wall 2

Figure 4.6 – Failure mode front elevation

Wall 3

Wall No.	Days from casting	h	b (average)	t (average)	F	f_o
		mm	mm	mm	kN	N/mm^2
3	49	820	682	83.5	206.2047	3.62

Table 4.3 – Failure stress under UDL for wall 3

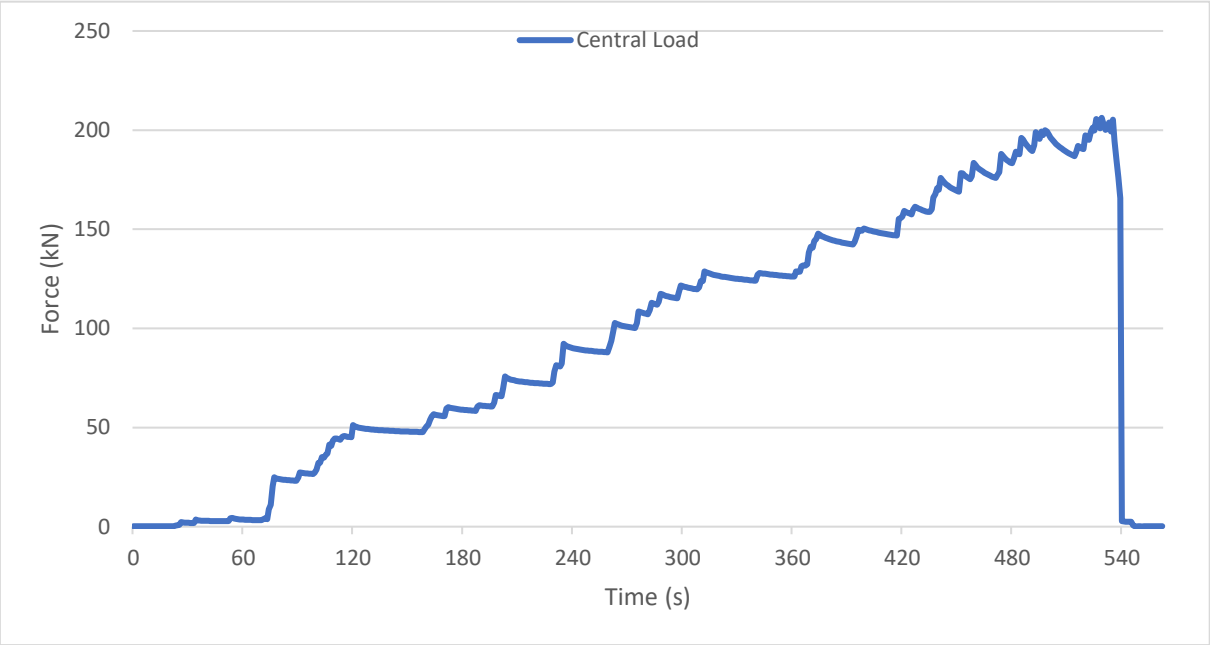

Figure 4.7 – Force vs time graph for wall 3

Figure 4.8 – Failure mode front elevation

Figure 4.9 – *Left*; failure mode back elevation; *right*, diagonal cracking through the top surface

The results of the first three tests are summarised below in table 4.4, including the average uniform bearing strength ($f_{o,1}$) to be used as a baseline for the following concentrated load tests.

Wall No.	Days from casting	h	b (average)	t (average)	F	f_o
		mm	mm	mm	kN	N/mm^2
1	44	820	680	82.5	148.9997	2.66
2	46	820	682	84	217.7437	3.80
3	49	820	682	83.5	206.2047	3.62
					$f_{o,1}$ average =	3.36

Table 4.4 – Failure stress under UDL for the first 3 walls

4.2.2 Concentrated Load Tests

For this testing programme, a loaded area ratio (A_b/A_{eff}) of 0.1 was maintained constant throughout all the tests, using a stiff bearing pad with a width (b_p) of 68mm. Also, precompressive stresses were varied as per section 3.6.3, relative to $f_{o,1}$. The typical setup adopted is as shown in section 3.5.1. In general, the failure mode consisted of a cone failure along with an axial compressive crack just underneath the concentrated load, propagating down through the centre of the specimen. As the ratio of the precompressive stresses increased, the crushing of the material underneath the bearing pad also increased and the main vertical crack was observed to be less prominent and consistent throughout the height of the specimen.

Wall 4

Wall No.	Days from casting	a_1	b_p	t	F_p (Avg.)	f_p	$\frac{f_p}{f_{o,1}}$	F_b	f_b	β
		mm	mm	mm	kN	N/mm²		kN	N/mm²	
4	52	306	68	83	/	/	/	49.58	8.87	2.61

Table 4.5 – Failure stress and strength enhancement factor for wall 4

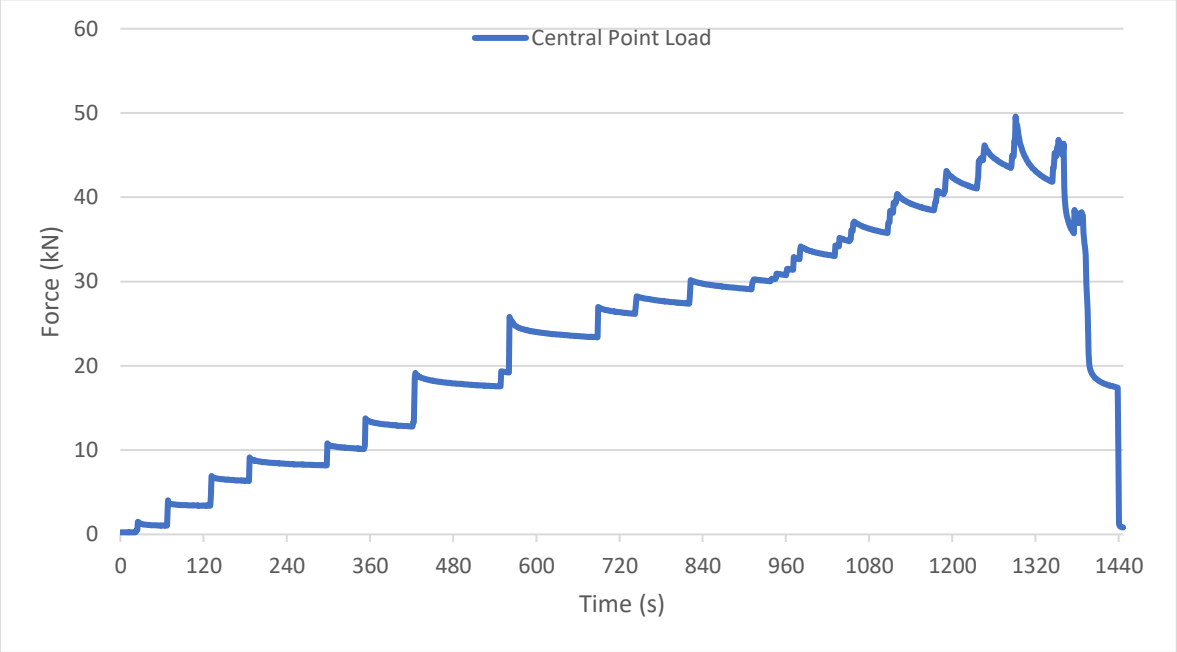

Figure 4.10 – Force vs time graph for wall 4

Figure 4.11 – Failure mode front elevation

Wall 5

Wall No.	Days from casting	a_1	b_p	t	F_p (Avg.)	f_p	$\frac{f_p}{f_{o,1}}$	F_b	f_b	β
		mm	mm	mm	kN	N/mm^2		kN	N/mm^2	
5	53	306	68	83.1	6.4	0.252	0.075	50.03	8.85	2.63

Table 4.6 – Precompressive stresses and strength enhancement factor for wall 5

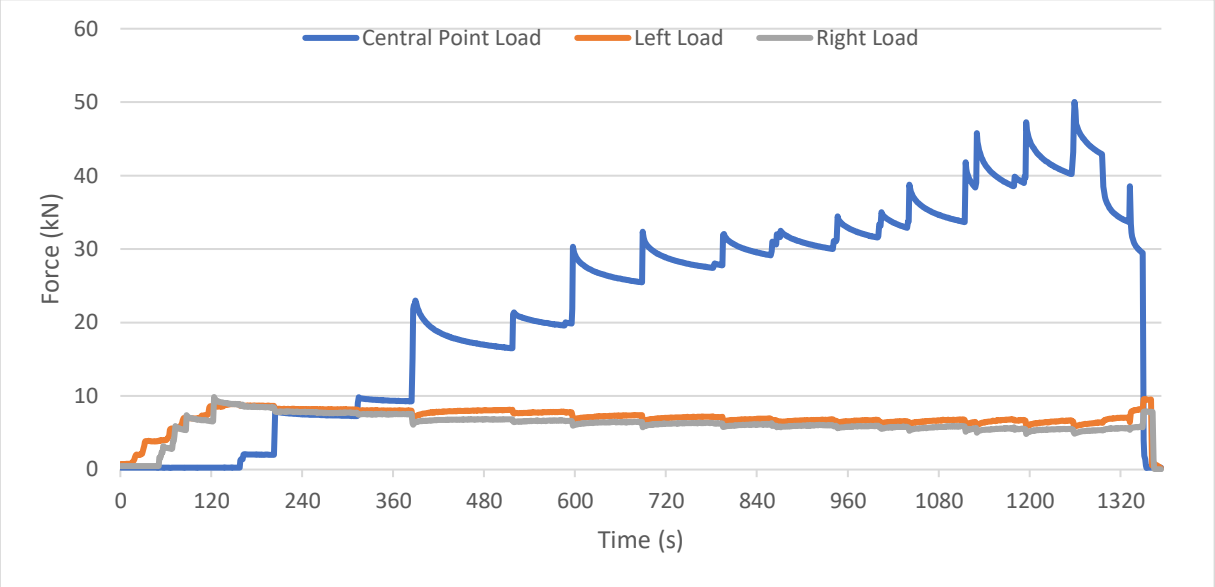

Figure 4.12 – Force vs time graph for wall 5

Figure 4.13 – *Left*, failure mode front elevation; *right*, failure mode back elevation

Throughout this test, as the central point load was increasing, the load cells responded with a decrease in loading. Upon failure, the precompressive forces were at an average of 6.40kN, corresponding to a stress of 0.252N/mm^2, having the ratio $f_p/f_{o,1}$ of 0.075. For the following tests, these stresses were sequentially increased along the application of the central point load to maintain the desired precompressive stresses constant throughout the whole tests.

Wall 6

Wall No.	Days from casting	a_1	b_p	t	F_p (Avg.)	f_p	$\frac{f_p}{f_{o,1}}$	F_b	f_b	β
		mm	mm	mm	kN	N/mm^2		kN	N/mm^2	
6	56	306	68	82.8	17.1	0.675	0.201	54.12	9.613	2.86

Table 4.7 – Precompressive stresses and strength enhancement factor for wall 6

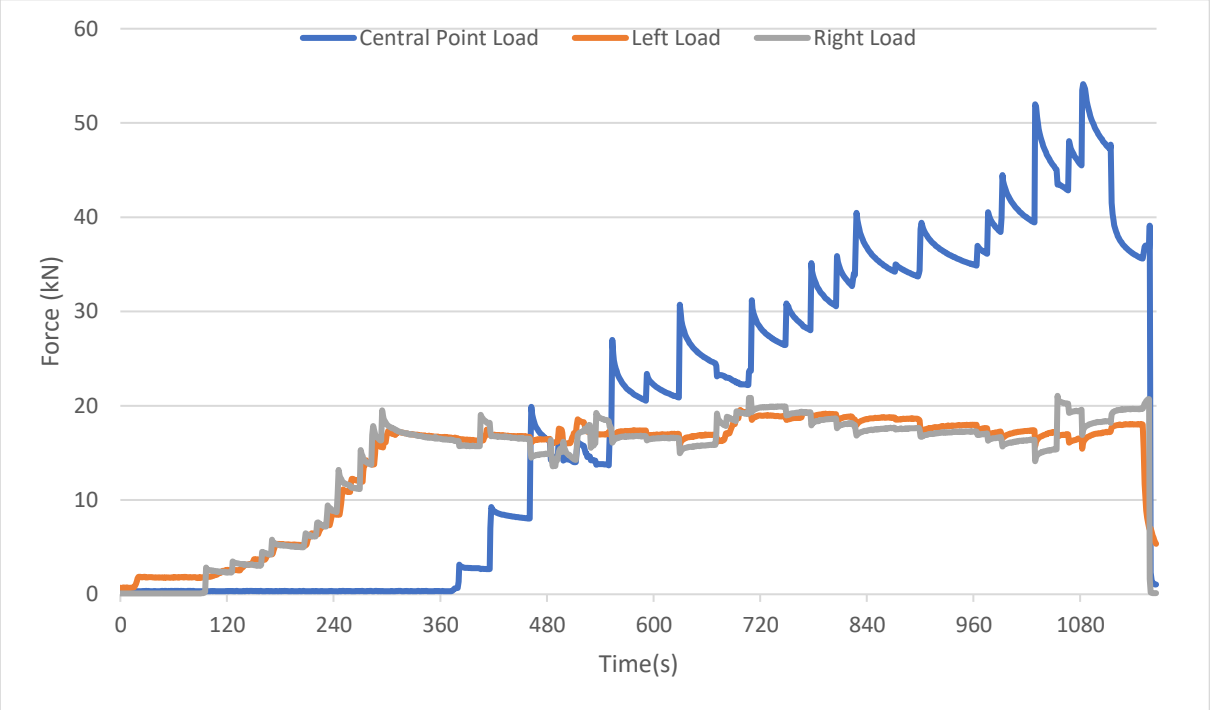

Figure 4.14 – Force vs time graph for wall 6

Figure 4.15 – *Left*, failure mode front elevation; *right*, failure mode back elevation

Wall 7

Wall No.	Days from casting	a_1	b_p	t	F_p (Avg.)	f_p	$\frac{f_p}{f_{o,1}}$	F_b	f_b	β
		mm	mm	mm	kN	N/mm^2		kN	N/mm^2	
7	57	306	68	82.3	25.2	1.00	0.298	55.34	9.90	2.94

Table 4.8 – Precompressive stresses and strength enhancement factor for wall 7

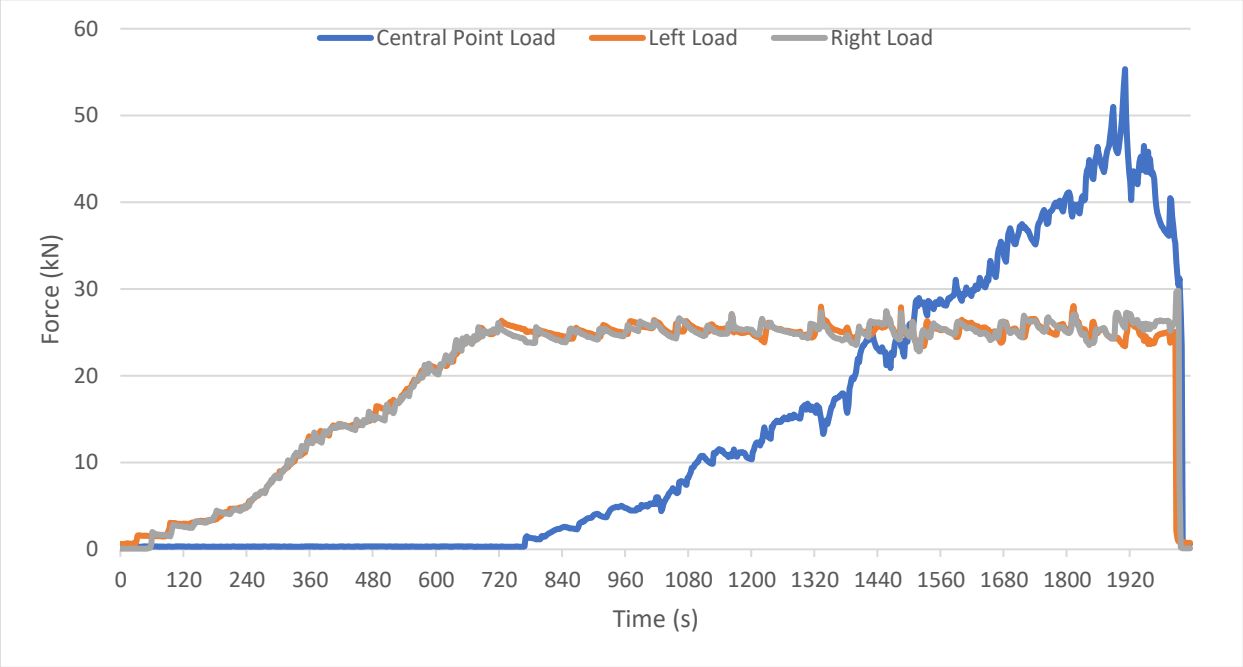

Figure 4.16 – Force vs time graph for wall 7

Figure 4.17 – *Left*, failure mode front elevation; *right*, failure mode back elevation

Wall 8

Wall No.	Days from casting	a_1	b_p	t	F_p (Avg.)	f_p	$\frac{f_p}{f_{o,1}}$	F_b	f_b	β
		mm	mm	mm	kN	N/mm²		kN	N/mm²	
8	57	306	68	83.9	33.9	1.32	0.393	61.33	10.75	3.20

Table 4.9 – Precompressive stresses and strength enhancement factor for wall 8

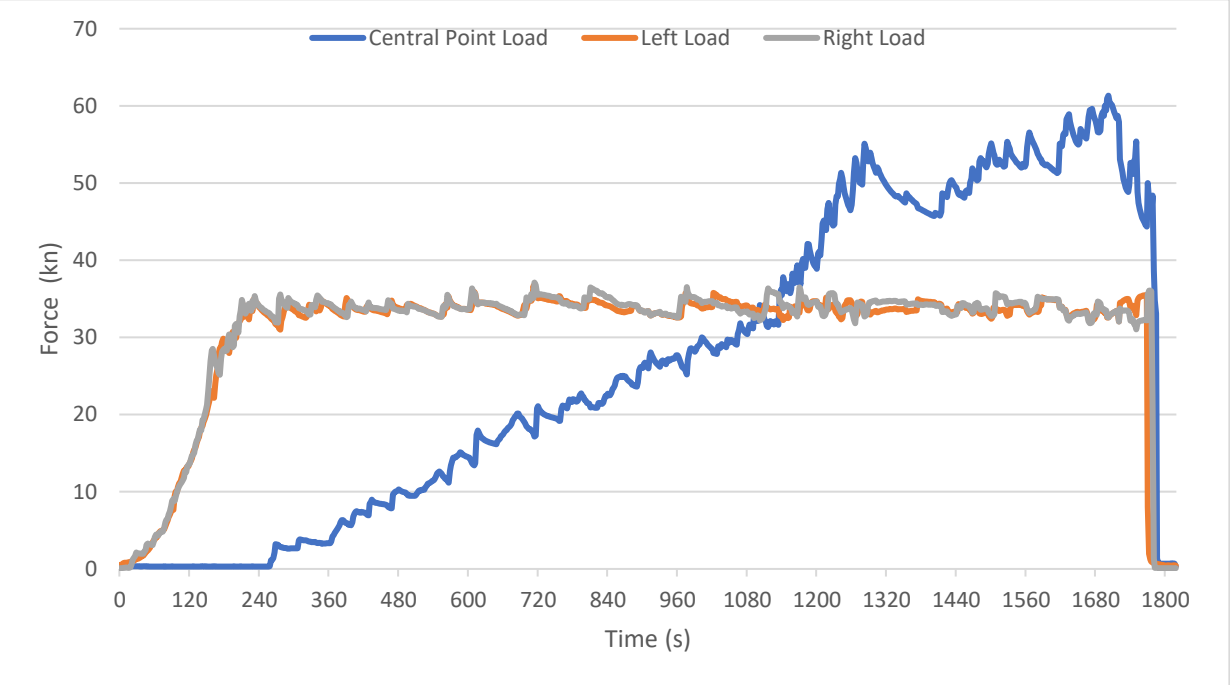

Figure 4.18 – Force vs time graph for wall 8

Figure 4.19 – *Left*, failure mode front elevation; *right*, failure mode back elevation

Wall 9

Wall No.	Days from casting	a_1	b_p	t	F_p (Avg.)	f_p	$\frac{f_p}{f_{o,1}}$	F_b	f_b	β
		mm	mm	mm	kN	N/mm^2		kN	N/mm^2	
9	58	306	68	82.0	42.8	1.71	0.508	56.29	10.10	3.00

Table 4.10 – Precompressive stresses and strength enhancement factor for wall 9

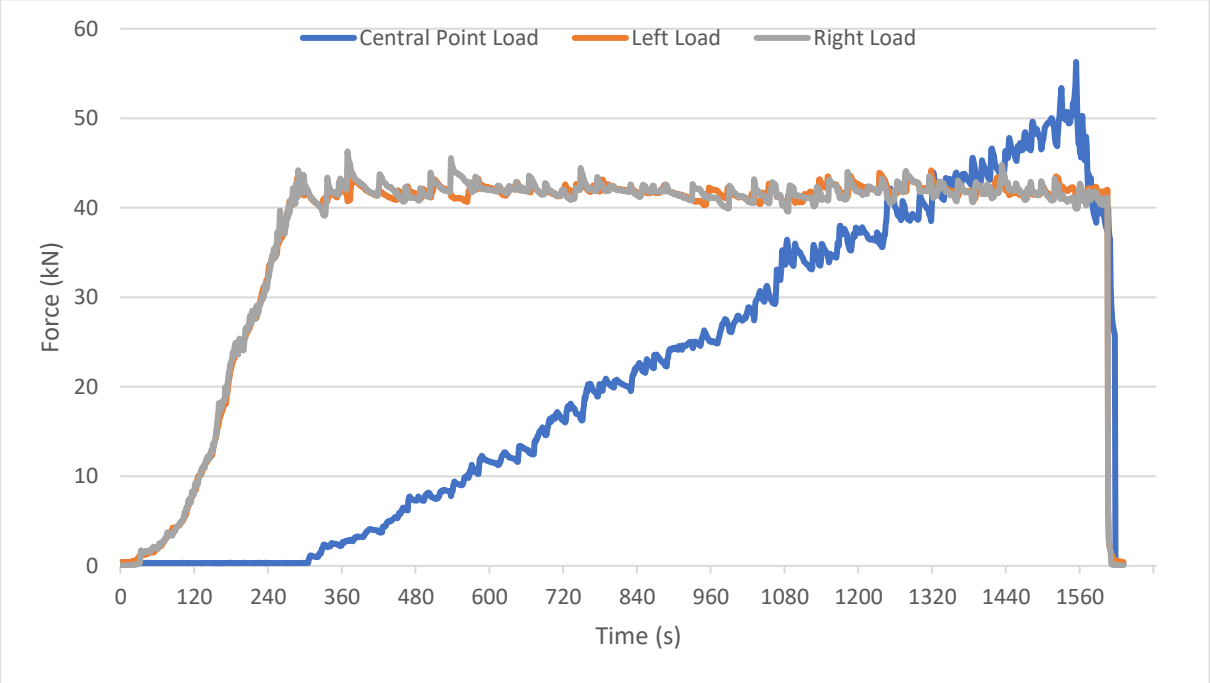

Figure 4.20 – Force vs time graph for wall 9

Figure 4.21 – *Left*, failure mode front elevation; *right*, failure mode back elevation

Wall 10

Wall No.	Days from casting	a_1	b_p	t	F_p (Avg.)	f_p	$\frac{f_p}{f_{o,1}}$	F_b	f_b	β
		mm	mm	mm	kN	N/mm²		kN	N/mm²	
10	58	306	68	83.2	51.15	2.01	0.597	55.87	9.88	2.94

Table 4.11 – Precompressive stresses and strength enhancement factor for wall 10

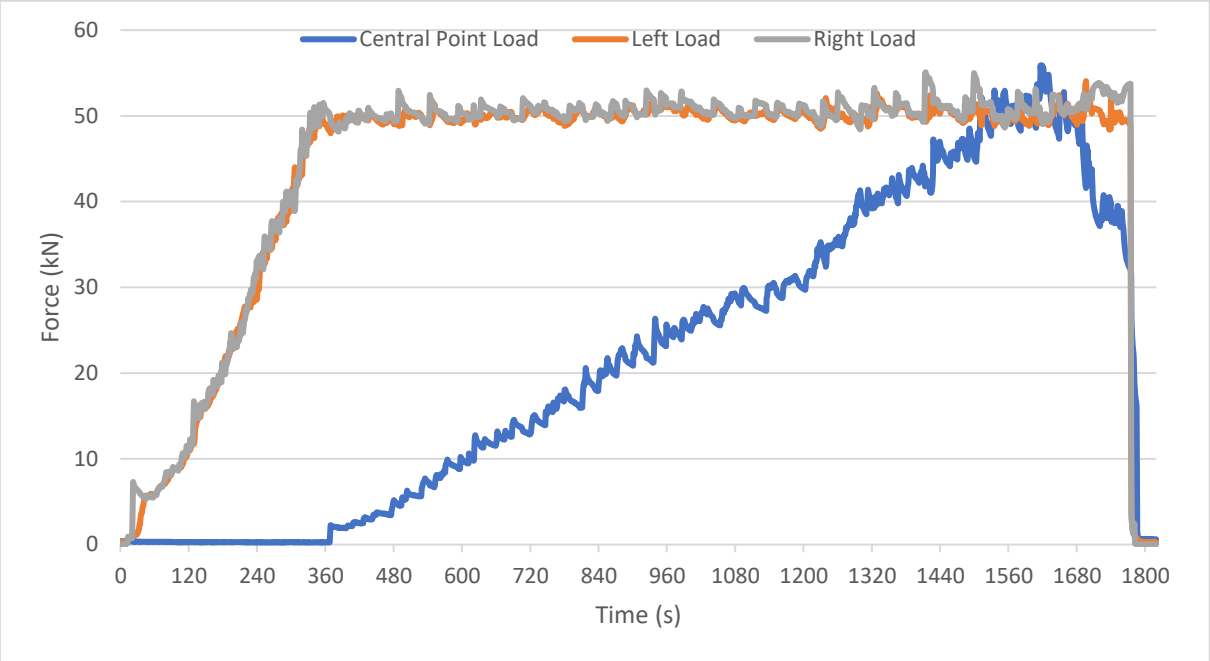

Figure 4.22 – Force vs time graph for wall 10

Figure 4.23 – *Left*, failure mode front elevation; *right*, failure mode back elevation

Wall 11

Wall No.	Days from casting	a_1	b_p	t	F_p (Avg.)	f_p	$\frac{f_p}{f_{o,1}}$	F_b	f_b	β
		mm	mm	mm	kN	N/mm^2		kN	N/mm^2	
11	59	306	68	81.9	59.05	2.36	0.701	47.31	8.50	2.53

Table 4.12 – Precompressive stresses and strength enhancement factor for wall 11

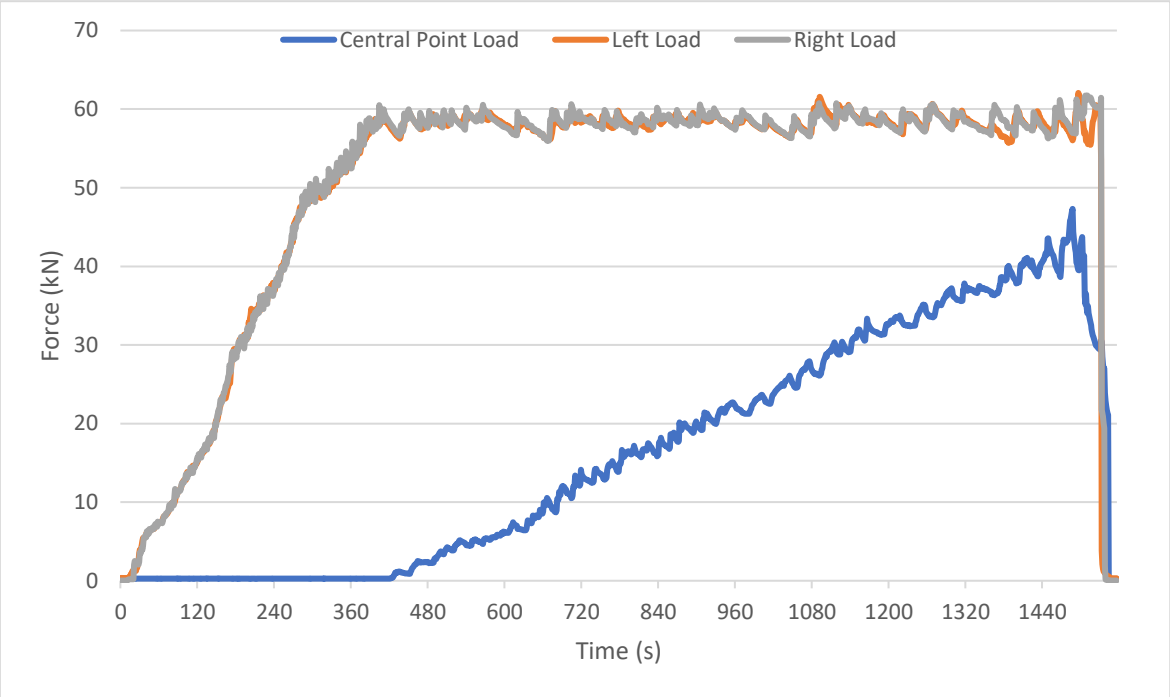

Figure 4.24 – Force vs time graph for wall 11

Figure 4.25 – *Left*, failure mode front elevation; *right*, failure mode back elevation

Wall 12

Wall No.	Days from casting	a_1	b_p	t	F_p (Avg.)	f_p	$\frac{f_p}{f_{o,1}}$	F_b	f_b	β
		mm	mm	mm	kN	N/mm^2		kN	N/mm^2	
12	59	306	68	83.0	53.0	2.087	0.621	27.33	4.84	1.44

Table 4.13 – Precompressive stresses and strength enhancement factor for wall 12

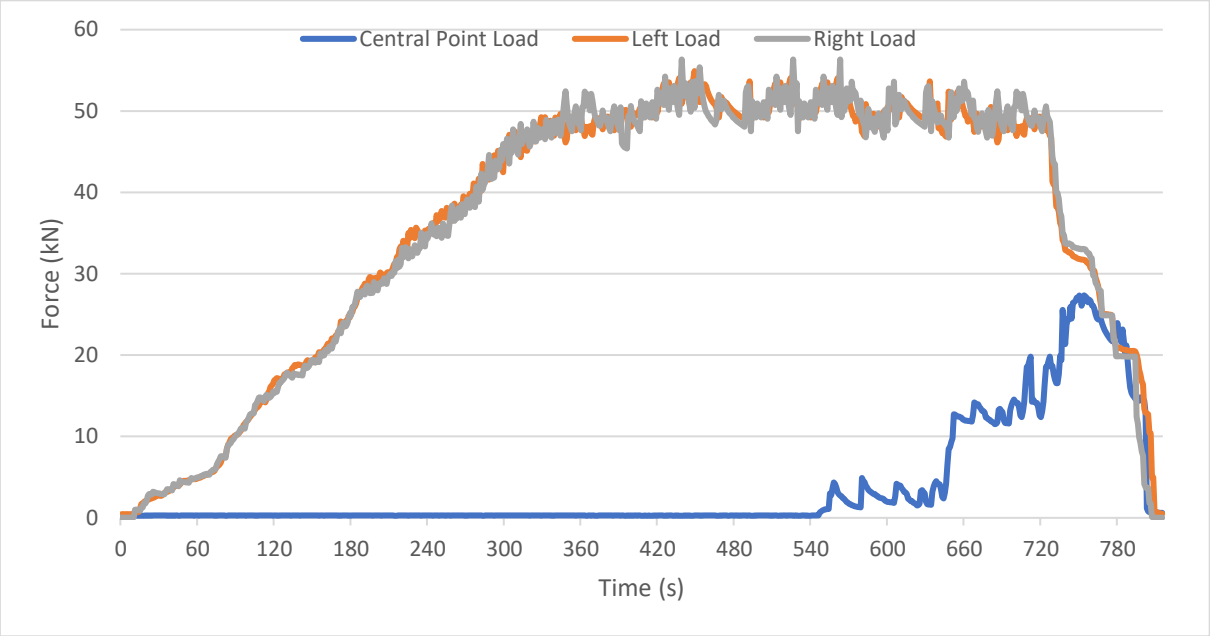

Figure 4.26 – Force vs time graph for wall 12

The original planned testing programme had to be amended since 2 of the wall specimens were found to be cracked, as shown in Fig. 4.27. The only available wall had already been slightly loaded and damaged through handling, hence grouting was used to repair the damaged surface, as shown in Fig. 4.28.

During loading, the expected prestressing load could not be reached as the wall started to show premature failure, resulting in the application of the central point load at a lower precompressive stresses than the one originally desired.

Figure 4.27 – Cracked walls which had to be abandonded

Figure 4.28 – *Left*; damaged wall pre-grouting; *right*, repaired wall setup

Figure 4.29 – *Left*, failure mode front elevation; *right*, failure mode back elevation

The concentrated load test results of the first experimental programme are summarised in table 4.14.

Wall No.	Days from casting	a_1	b_p	t	F_p		f_p	f_o	$\delta = \frac{f_p}{f_{o,1}}$	F_b	f_b	β
					Left	Right						
		mm	mm	mm	kN	kN	N/mm^2	N/mm^2		kN	N/mm^2	
4	52	306	68	83.0	/	/	/	3.36	/	49.5792	8.784	2.614
5	53	306	68	83.1	6.6	6.2	0.252	3.36	0.075	50.0324	8.854	2.635
6	56	306	68	82.8	16.8	17.4	0.675	3.36	0.201	54.1243	9.613	2.861
7	57	306	68	82.3	25.5	24.9	1.001	3.36	0.298	55.3454	9.889	2.943
8	57	306	68	83.9	34.1	33.7	1.320	3.36	0.393	61.3268	10.749	3.199
9	58	306	68	82.0	42.5	43.1	1.706	3.36	0.508	56.2901	10.095	3.004
10	58	306	68	83.2	50.9	51.4	2.009	3.36	0.597	55.8661	9.875	2.939
11	59	306	68	81.9	59.4	58.7	2.356	3.36	0.701	47.3086	8.495	2.528
12	59	306	68	83.0	53.2	52.8	2.087	3.36	0.621	27.3271	4.842	1.441

Table 4.14 – Summary of precompressive stresses, failure stress and strength enhancement factor for the first experimental programme

4.3 Second Testing Programme

A similar procedure was adopted for the testing of the second and stronger set. Loading was performed more cautiously and attention was given to observe how the rig was responding to the applied loads. Also, for the UDL tests to find $f_{o,2}$, the side jacks were loaded simultaneously as shown in Fig. 4.30 as the central jack's maximum load capacity was not sufficient.

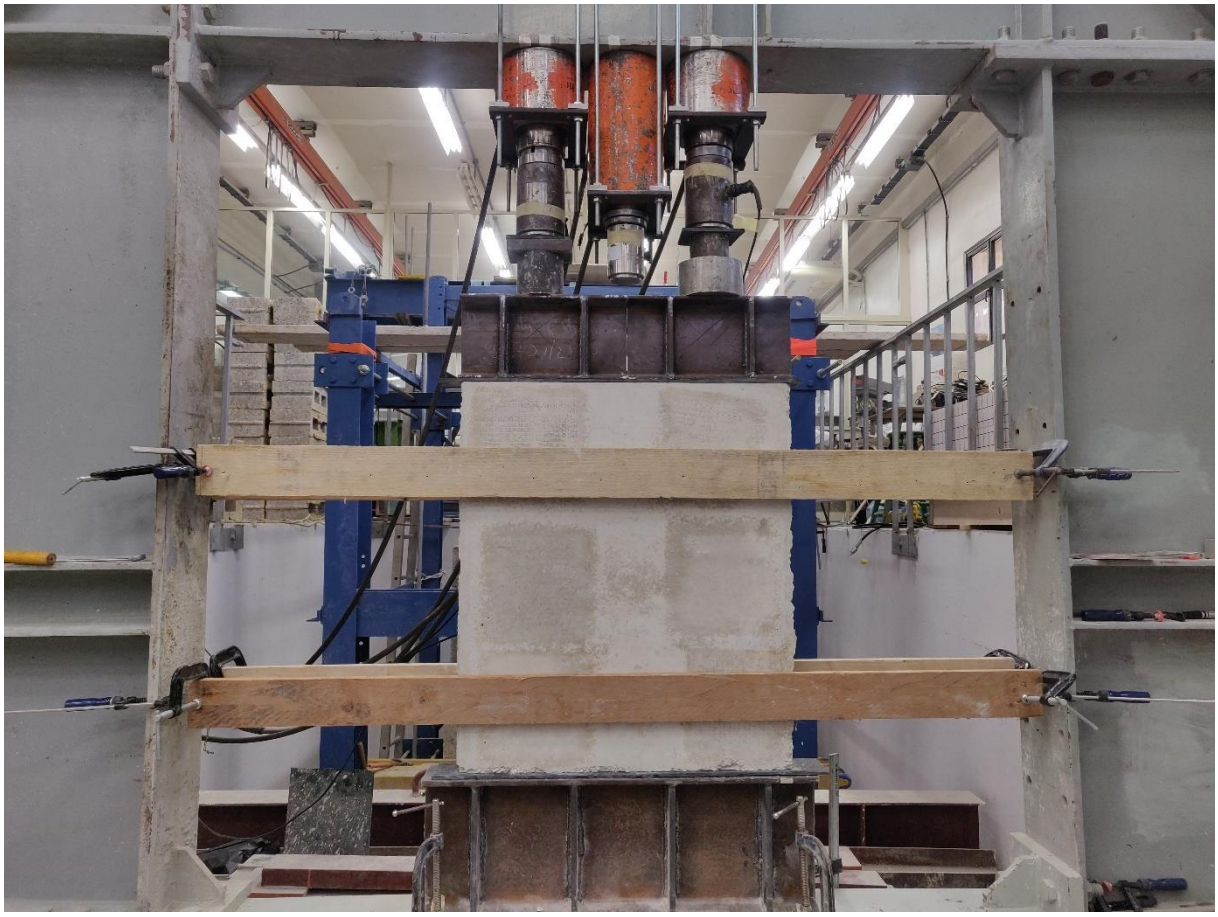

Figure 4.30 – UDL Loading setup for the second test programme

4.3.1 Ungrouted Wall Panels

Being much stronger than the first testing set, the walls' surfaces were less prone to crumble during handling, hence the first few walls were tested ungrouted. The surfaces were grinded to level out any imperfections, as per section 3.4.3. As these wall panels were much stronger than the walls of the first testing programme, failure was usually more explosive, in particular wall 13. Also, for all the cases failure occurred primarily along the unsmoothed face, preceded by rotational failure, leading to concentration of stresses along the edge of rotation. Besides the eccentricity effects, this might be the result of strength variation along the walls' thickness, generated during the horizontal casting and curing of the wall panels.

Wall 13

Wall No.	Days from casting	Loading Rate (per jack)	h	b (avg.)	t (avg.)	F		f_o
						Left	Right	
		kN/min	mm	mm	mm	kN	kN	N/mm^2
14	82	50	800	679.3	81.7	340.34	328.20	12.05

Table 4.15 – Failure stress under UDL for wall 13

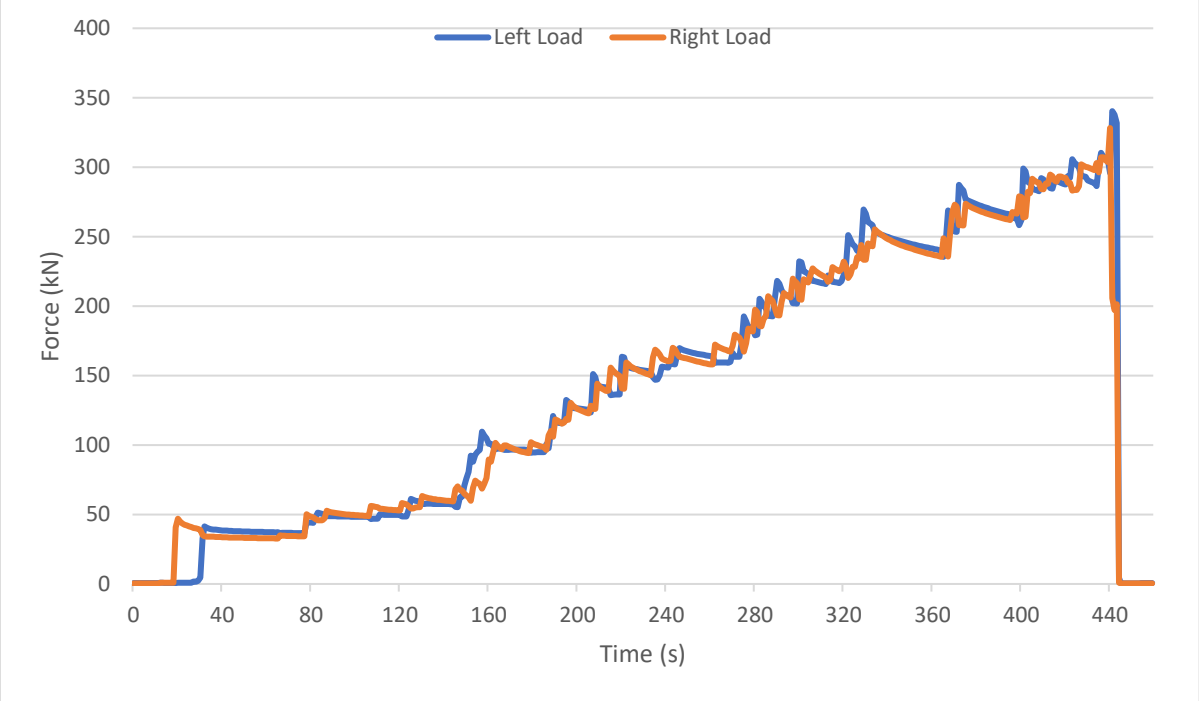

Figure 4.31 – Force vs time graph for wall 13

Figure 4.32 – Explosive wall failure

Wall 14

Wall No.	Days from casting	Loading Rate (per jack)	h	b (avg.)	t (avg.)	F		f_o
						Left	Right	
		kN/min	mm	mm	mm	kN	kN	N/mm^2
15	82	50	800	680	81.6	160.83	145.98	5.53

Table 4.16 – Failure stress under UDL for wall 14

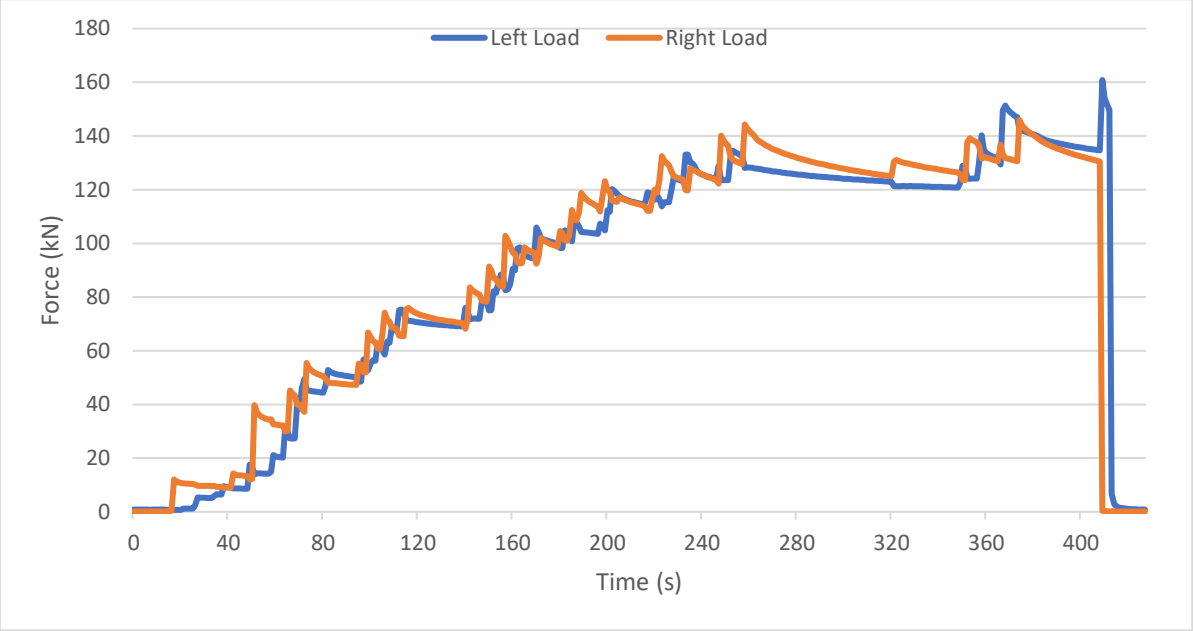

Figure 4.33 – Force vs time graph for wall 14

Figure 4.34 – *Left*, failure mode front elevation; *right*, failure mode back elevation

Wall 15

Wall No.	Days from casting	Loading Rate	h	a_1	t (average)	F_b	f_o
		kN/min	mm	mm	mm	kN	N/mm^2
13	83	20	800	136	81.6	201.678	18.17

Table 4.17 – Failure stress under CL for wall 15

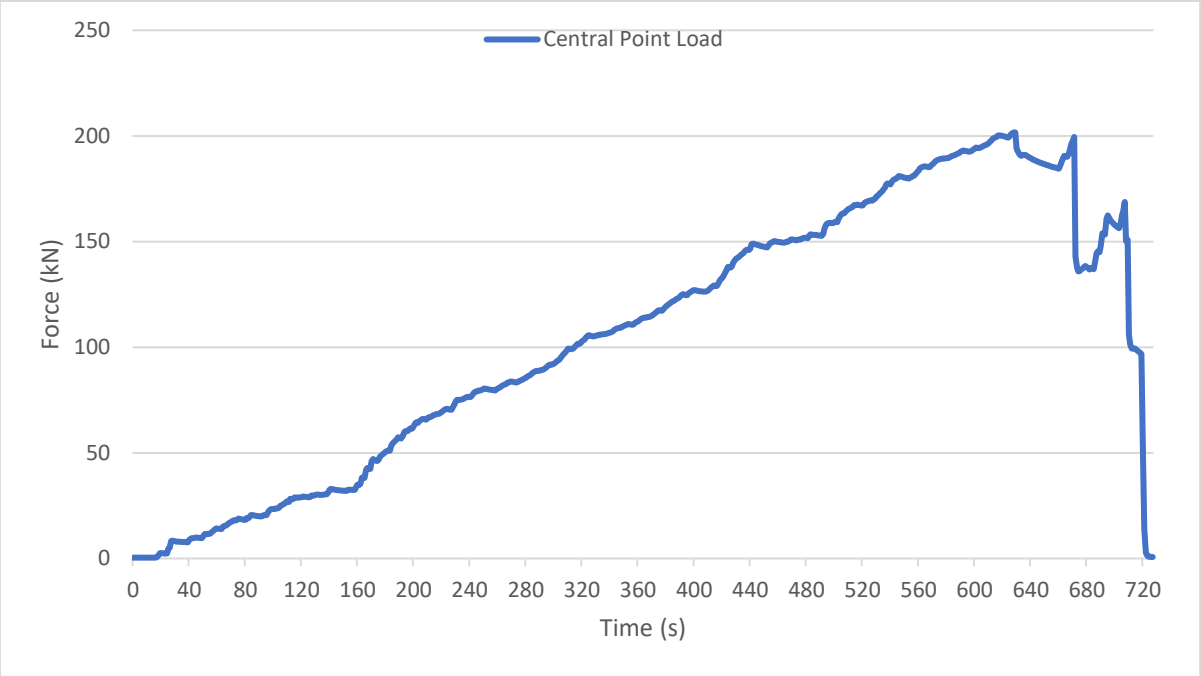

Figure 4.35 – Force vs time graph for wall 15

Figure 4.36 – Failure mode back elevation

Wall 16

Wall No.	Days from casting	Loading Rate	h	a_1	t (average)	F_b	f_o
		kN/min	mm	mm	mm	kN	N/mm^2
13	83	20	800	136	81.8	71.3331	6.41

Table 4.18 – Failure stress under CL for wall 16

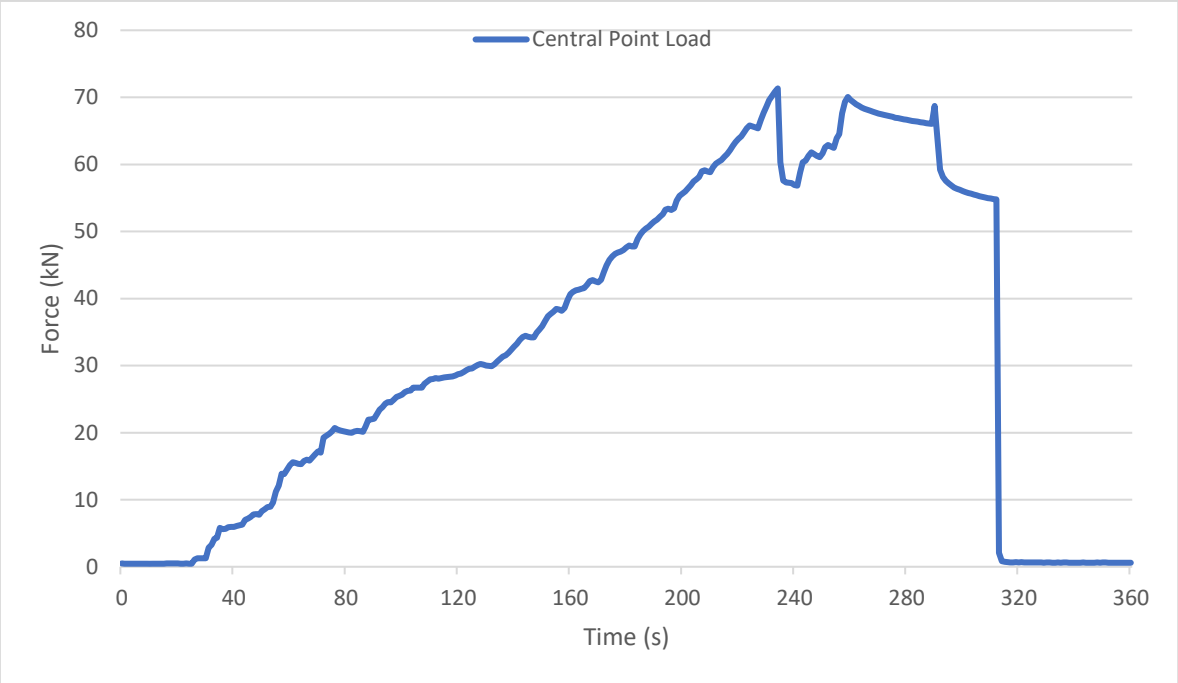

Figure 4.37 – Force vs time graph for wall 16

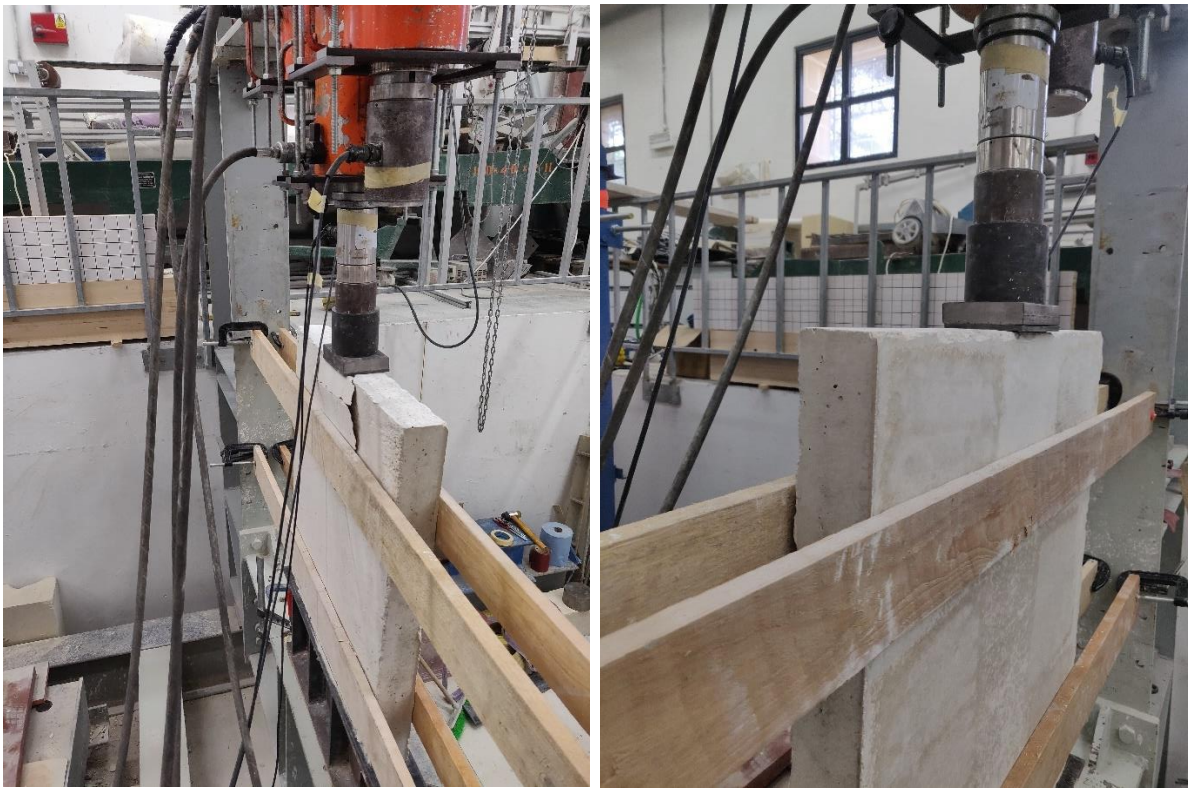

Figure 4.38 – *Left*, point load premature failure mode; *right*, loading setup

4.3.2 Grouted Wall Panels

Unfortunately, the results of the first 4 panels were very inconsistent. Although grinding the surfaces seemed to be an efficient way of levelling the wall panels, the results were not satisfactory. This required that the testing programme had to be amended to make the most out of the left 8 wall panels, which were then all grouted similar to the first testing programme.

4.3.2.1 UDL Tests

The first 2 tests were loaded uniformly to find and calculate the average bearing strength $f_{o,2}$, serving as a baseline for the following tests. The main failure mode of these 2 tests consisted of rotational failure, leading to crumbling and/or spalling of concrete pieces. For both tests the load was released prematurely as the concrete started to spall and rotate heavily, putting pressure on the lateral wooden strips, which could have led to explosive failure, similar to the previously tested wall 13.

Wall 17

Wall No.	Days from casting	Loading Rate (per jack)	h	b (avg.)	t (avg.)	F		f_o
						Left	Right	
		kN/min	mm	mm	mm	kN	kN	N/mm^2
17	87	50	820	680	81.5	248.79	230.47	8.65

Table 4.19 – Failure stress under UDL for wall 17

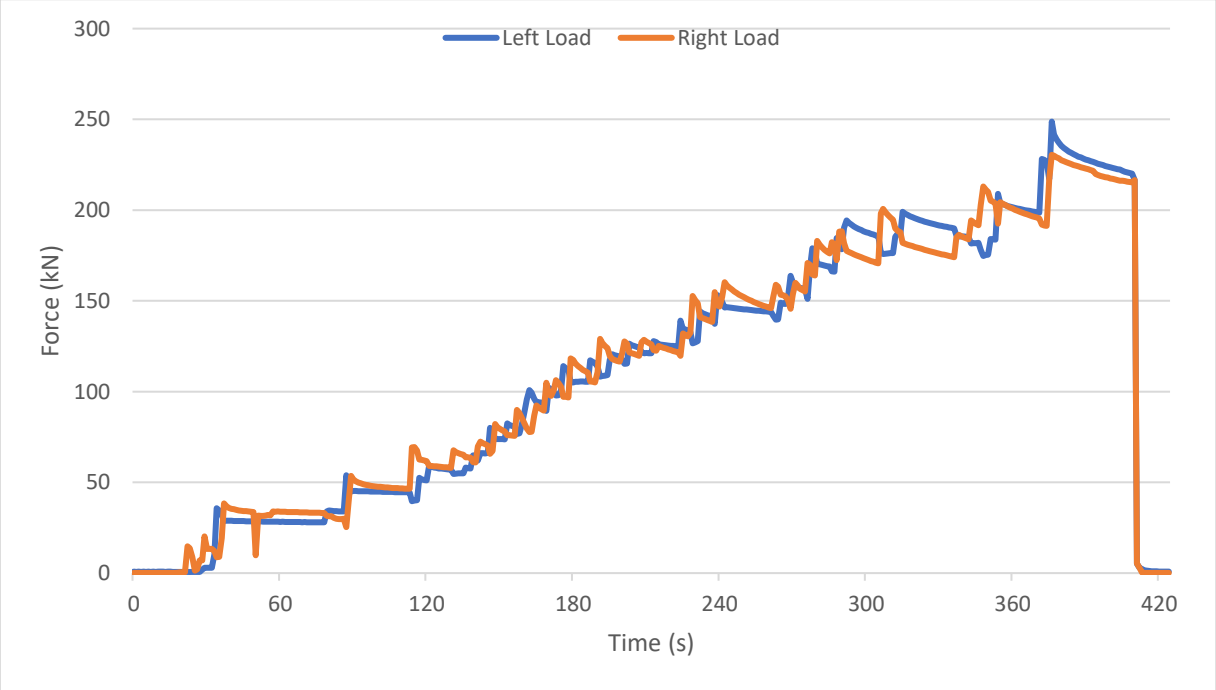

Figure 4.39 – Force vs time graph for wall 17

Figure 4.40 – Front elevation; spalling of concrete along the bottom edge

Figure 4.41 – Upper surface; brittle spalling of the concrete and grout layer

Wall 18

Wall No.	Days from casting	Loading Rate (per jack)	h	b (avg.)	t (avg.)	F		f_o
						Left	Right	
		kN/min	mm	mm	mm	kN	kN	N/mm^2
18	90	50	820	679.6	81.8	250.23	264.07	9.25

Table 4.20 – Failure stress under UDL for wall 18

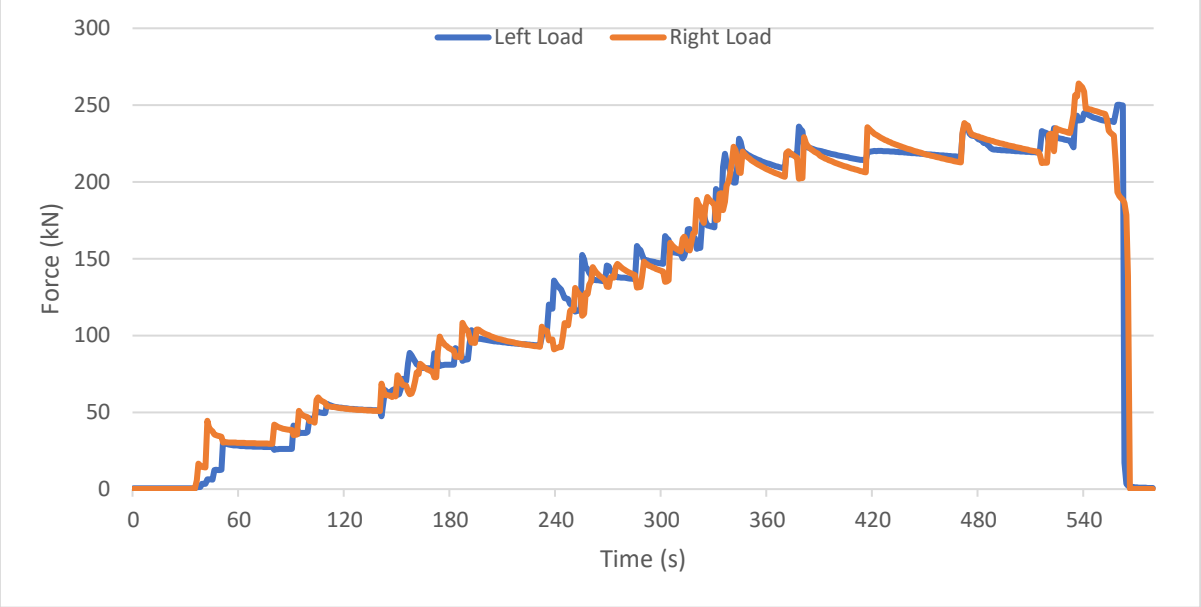

Figure 4.42 – Force vs time graph for wall 18

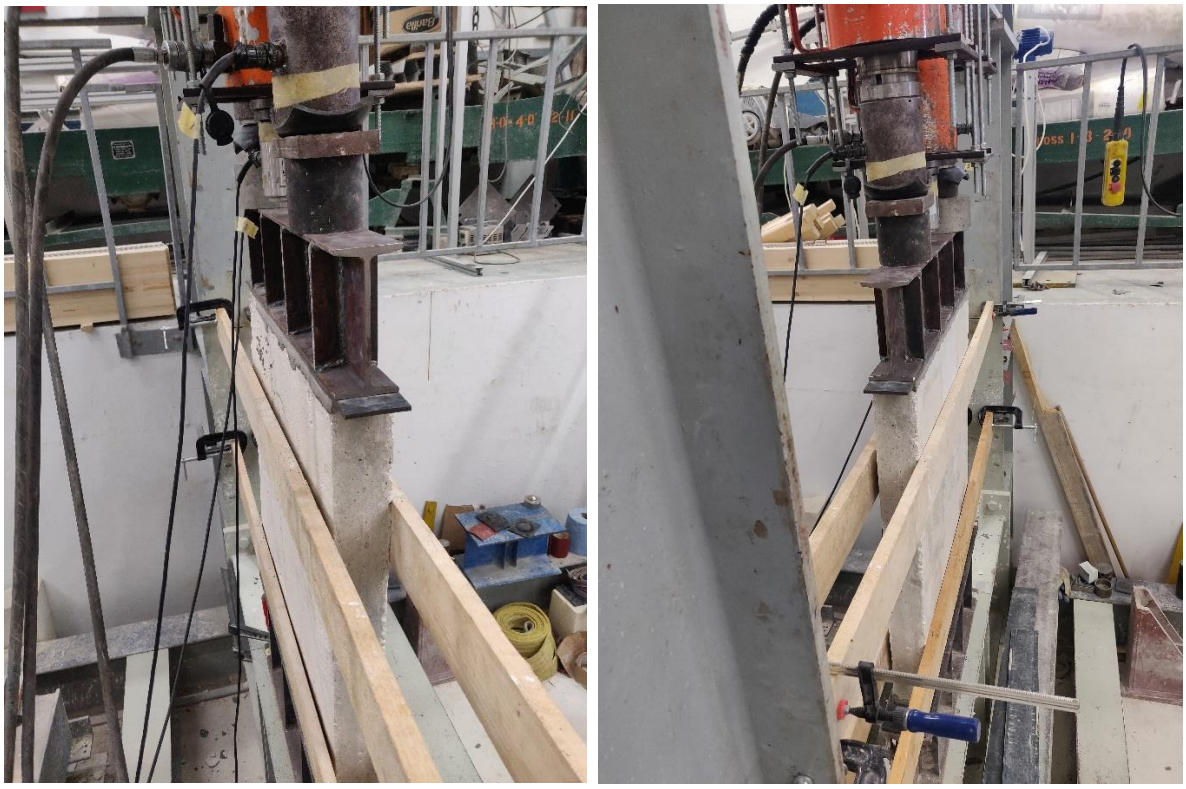

Figure 4.43 – Wall's rotational behaviour upon increasing the loads; applying pressure onto the lateral wooden strips

Figure 4.44 – *Left*, failure mode front elevation; *right*, failure mode back elevation

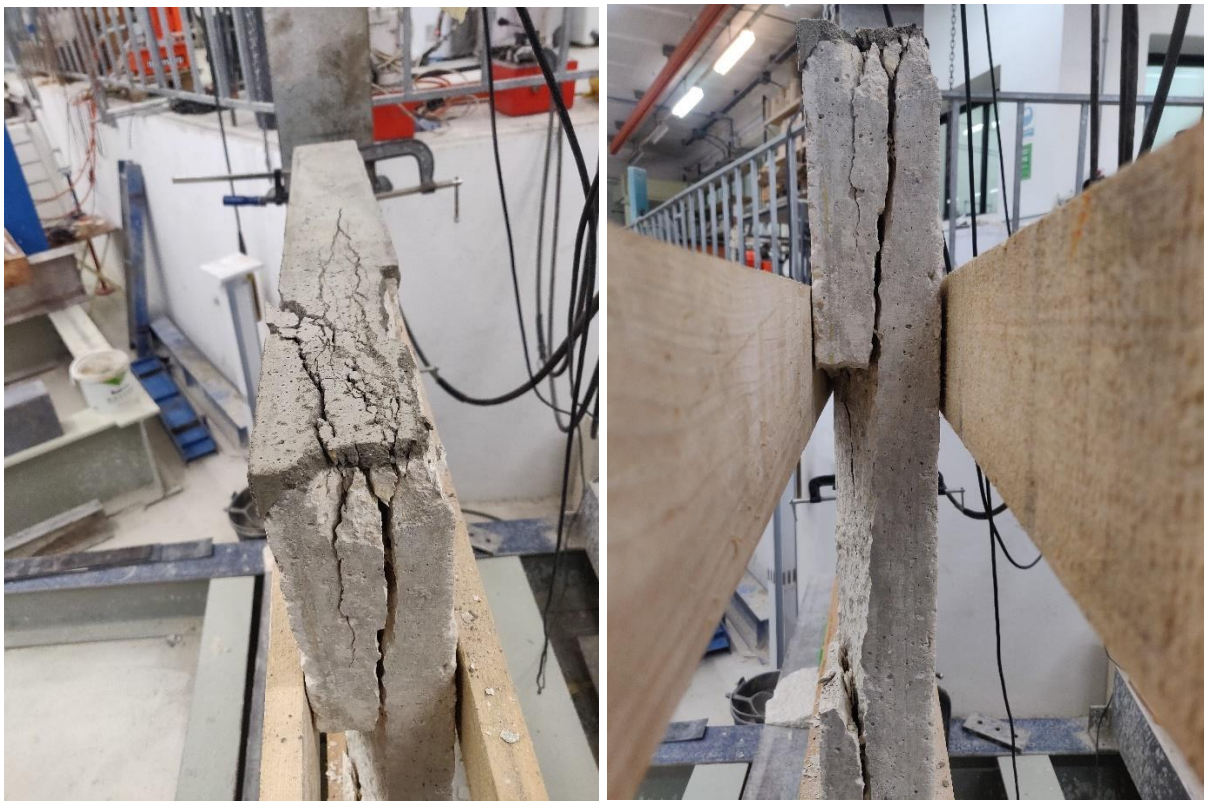

Figure 4.45 – Failure mode upon releasing the loads sequentially

Similar to wall 14 and 17, loaded under UDL conditions, wall 18 was not able to sustain large compressive loads due to the geometrical imperfections. The failure mode for wall 18 represented by Fig. 4.44 and 4.45 is due to the shearing stresses generated when the loads were released. Similar to the other walls, the UDL was applied using 2 loading jacks, which in this case, following a human error, were not released simultaneously. As one was released, the load from the other loading jack was still applying resistance, hence as the wall tried to retain back its original unrotated shape, the wall sheared and failed.

The results of the first two tests are summarised below in table 4.21.

Wall No.	Days from casting	Loading Rate (per jack)	h	b (average)	t (average)	F_p (total)	f_o
		kN/min	mm	mm	mm	kN	N/mm^2
17	87	50	820	680.0	81.5	479.25	8.65
18	90	50	820	679.6	81.8	514.29	9.25
						$f_{o,2}$ average =	8.95

Table 4.21 – Failure stress under UDL for the first 2 grouted walls

Analysing the failure modes under uniform loading for both the grouted and ungrouted wall panels, the closest failure mode to a compressive failure is that of wall 13. As a result, $f_{o,2}$ for the following concentrated load tests was taken to be 12.05N/mm^2, which is the failure stress of wall 13.

4.3.2.2 Concentrated Load Tests

Akin to the first testing set, these wall panels were tested using a constant loaded area ratio, which in this case was doubled to 0.2, hence a stiff bearing pad with a b_p of 136mm was used. Since the number of wall panels available at this point was less than expected, the precompressive stress ratios (δ) were not adjusted as initially planned as per section 3.2.2.

In general, the failure mode was similar to that of the first testing programme, consisting of a compressive vertical crack propagating from underneath the bearing plate down through the centre of the specimen. Also, as the precompressive stresses were increased, walls began to fail prior any central point load application, hence the precompressive increments were amended throughout the testing programme. As a consequence, no representative tests were performed for the higher precompressive stress ratios.

Wall 19

Wall No.	Days from casting	a_1	b_p	t	F_p (Avg.)	f_p	$\frac{f_p}{f_{o,2}}$	F_b	f_b	β
		mm	mm	mm	kN	N/mm²		kN	N/mm²	
19	90	272	136	81.9	/	/	/	196.49	17.64	1.46

Table 4.22 – Failure stress and strength enhancement factor for wall 19

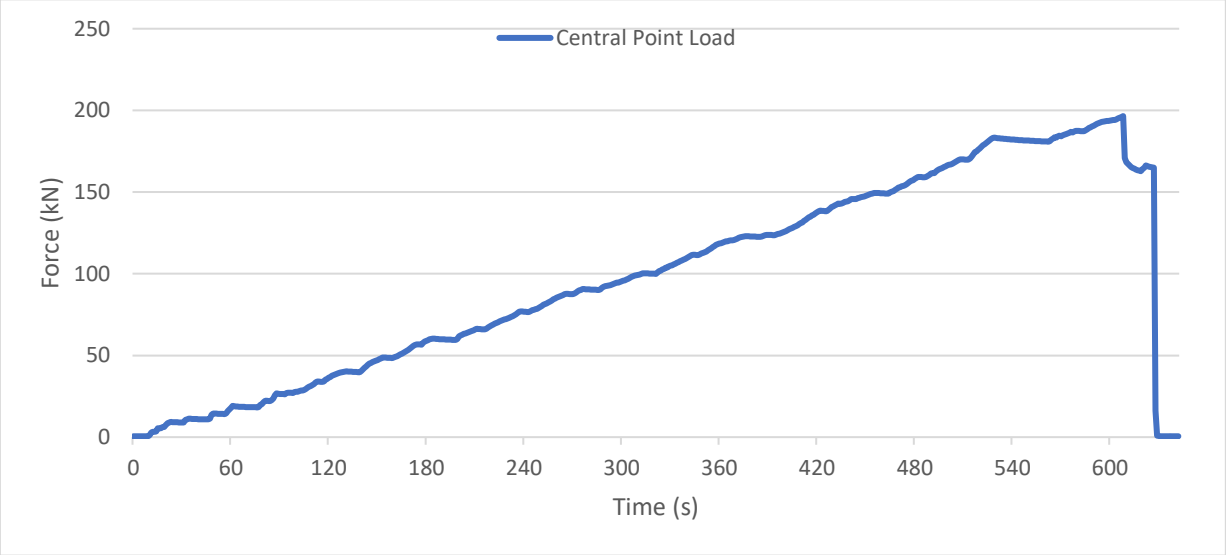

Figure 4.46 – Loading vs time graph for wall 19

Figure 4.47 – *Left*, failure mode front elevation; *right*, failure mode back elevation

Wall 20

Wall No.	Days from casting	a_1	b_p	t	F_p (Avg.)	f_p	$\frac{f_p}{f_{o,2}}$	F_b	f_b	β
		mm	mm	mm	kN	N/mm^2		kN	N/mm^2	
20	91	272	136	81.4	37.3	1.68	0.14	198.91	17.97	1.49

Table 4.23 – Precompressive stresses and strength enhancement factor for wall 20

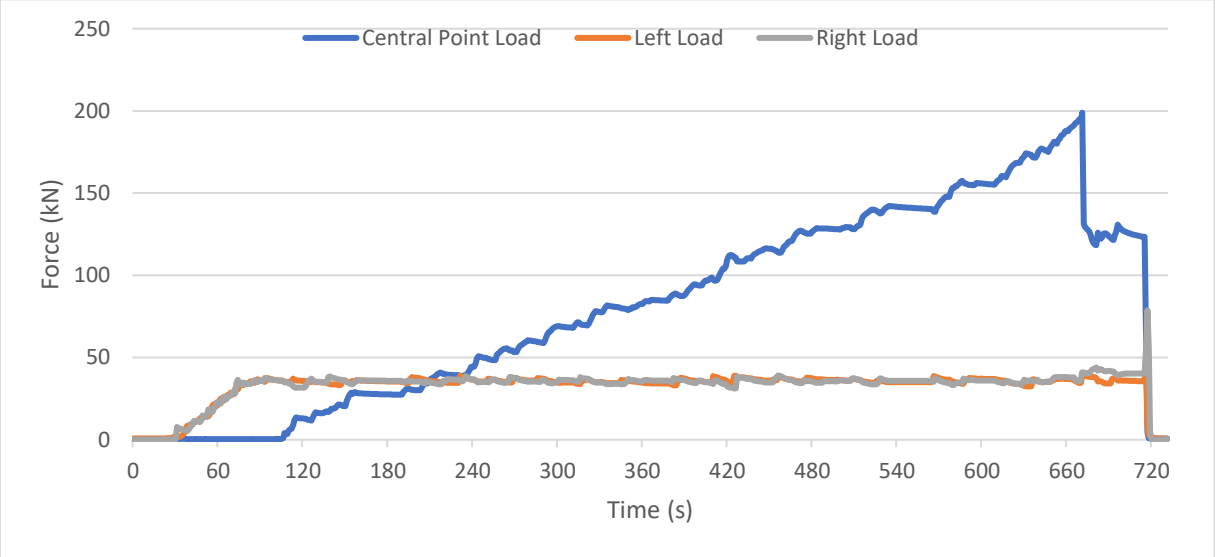

Figure 4.48 – Force vs time graph for wall 20

Figure 4.49 – *Left*, failure mode front elevation; *right*, failure mode back elevation

Wall 21

Wall No.	Days from casting	a_1	b_p	t	F_p (Avg.)	f_p	$\frac{f_p}{f_{o,2}}$	F_b	f_b	β
		mm	mm	mm	kN	N/mm^2		kN	N/mm^2	
21	91	272	136	82.1	74.3	3.32	0.28	225.92	20.34	1.68

Table 4.24 – Precompressive stresses and strength enhancement factor for wall 21

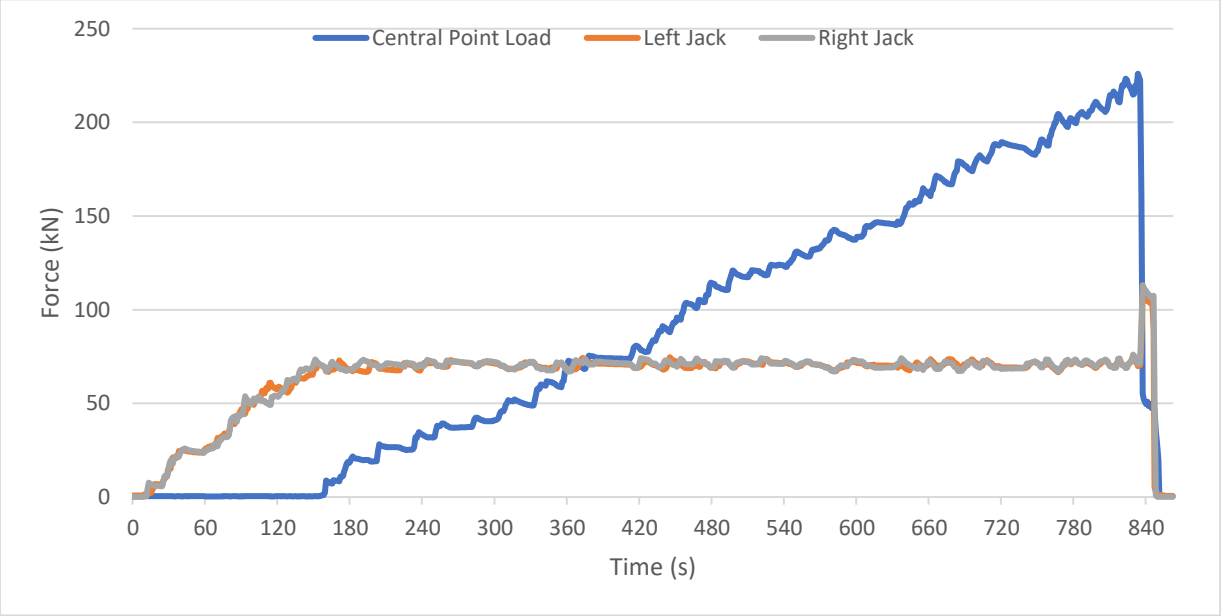

Figure 4.50 – Force vs time graph for wall 21

Figure 4.51 – *Left*, failure mode front elevation; *right*, failure mode back elevation

Wall 22

Wall No.	Days from casting	a_1	b_p	t	F_p (Avg.)	f_p	$\frac{f_p}{f_{o,2}}$	F_b	f_b	β
		mm	mm	mm	kN	N/mm²		kN	N/mm²	
22	92	272	136	81.7	112.8	5.07	0.42	189.7	17.07	1.42

Table 4.25 – Precompressive stresses and strength enhancement factor for wall 22

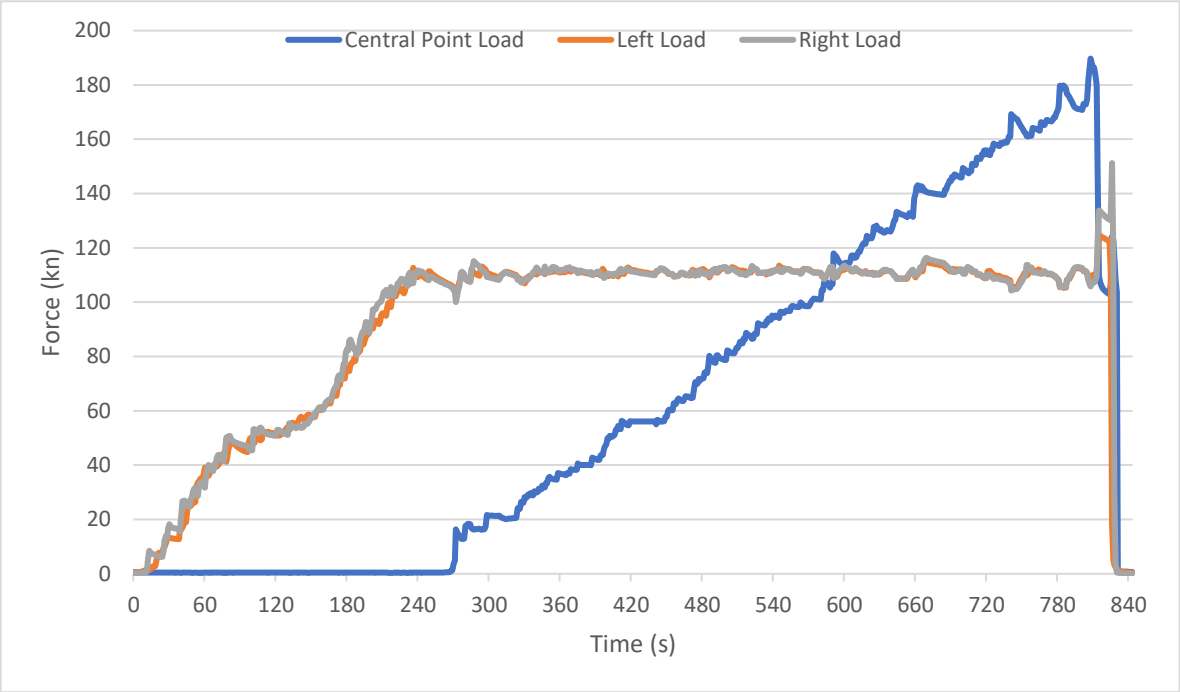

Figure 4.52 – Force vs time graph for wall 22

Figure 4.53 – *Left*, failure mode front elevation; *right*, failure mode back elevation

Wall 23

Wall No.	Days from casting	a_1	b_p	t	F_p (Avg.)	f_p	$\frac{f_p}{f_{o,2}}$	F_b	f_b	β
		mm	mm	mm	kN	N/mm²		kN	N/mm²	
23	94	272	136	81.5	152.09	6.86	0.57	/	/	/

Table 4.26 – Precompressive stresses for wall 23

During precompression, prior any central point load application, the wall failed via a vertical compression crack along the edge of the right distributing beam. Also, the wall seemed to have failed in compression underneath the left loading beam as shown in Fig. 4.55.

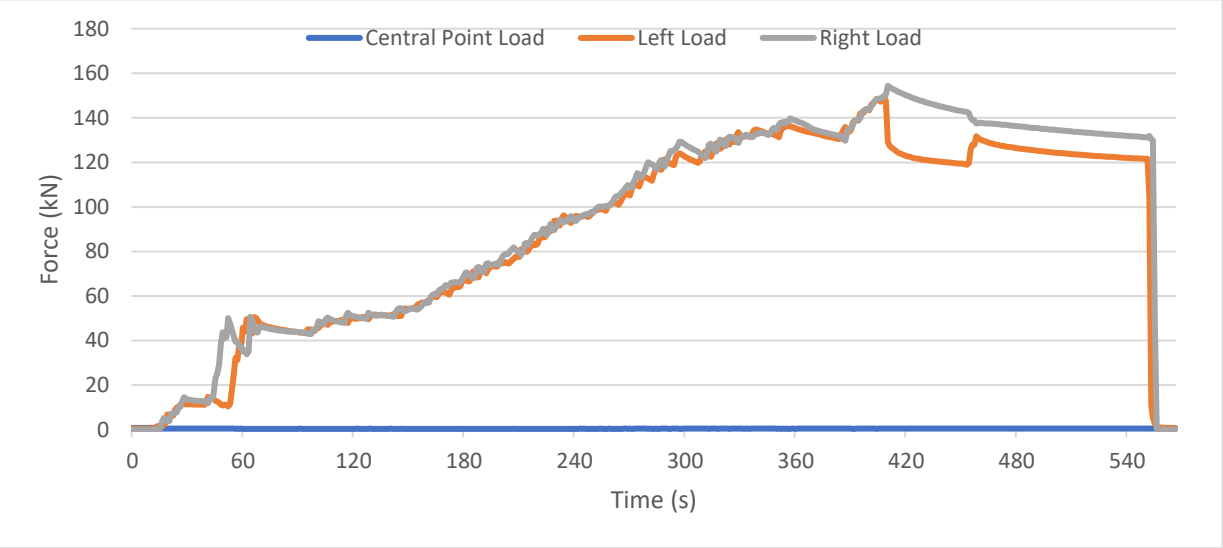

Figure 4.54 – Force vs time graph for wall 23

Figure 4.55 – *Left*, failure mode front elevation; *right*, failure mode underneath the left loading beam

Wall 24

Wall No.	Days from casting	a_1	b_p	t	F_p (Avg.)	f_p	$\frac{f_p}{f_{o,2}}$	F_b	f_b	β
		mm	mm	mm	kN	N/mm^2		kN	N/mm^2	
24	94	272	136	81.4	94.0	4.24	0.35	209.36	18.91	1.57

Table 4.27 – Precompressive stresses and strength enhancement factor for wall 24

Results from wall 23 suggested that applying an even higher precompressive stress ratio would have led to a similar failure. As a result, wall 24 was used to obtain an additional data point between the precompressive stress ratio of wall 21 and 22, providing a more indicative data for the lower f_p/f_o ratios.

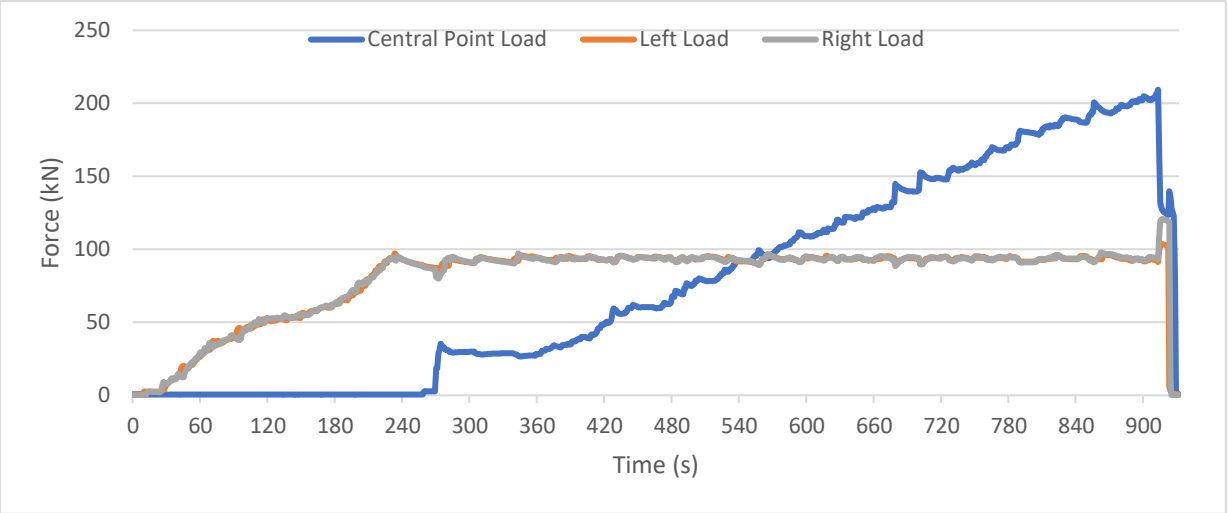

Figure 4.56 – Force vs time graph for wall 24

Figure 4.57 – *Left*, failure mode front elevation; *right*, failure mode back elevation

The concentrated load test results of the second experimental programme are summarised in table 4.28.

Wall No.	Days from casting	a_1	b_p	t	F			$f_{o,2}$	f_p	$\delta = \frac{f_p}{f_{o,2}}$	f_b	β
					Central	Left	Right					
		mm	mm	mm	kN	kN	kN	N/mm²	N/mm²	kN	N/mm²	
19	90	272	136	81.9	196.49	/	/	12.05	/	/	17.64	1.464
20	91	272	136	81.4	198.91	37.523	37.134	12.05	1.686	0.140	17.97	1.491
21	91	272	136	82.1	225.92	74.457	74.127	12.05	3.327	0.276	20.34	1.68
22	92	272	136	81.7	189.70	112.62	112.89	12.05	5.074	0.421	17.07	1.417
23	94	272	136	81.5	/	149.78	154.39	12.05	6.861	0.569	/	/
24	94	272	136	81.4	209.36	94.134	93.90	12.05	4..246	0.352	18.91	1.569

Table 4.28 – Summary of the precompressive stresses, failure stress and strength enhancement factor for the grouted wall panels of the second testing programme

Chapter 5: Analysis of Results

5.1 Introduction

In this chapter, results are analysed and re-organised to come up with discussions and conclusions, comparing the original hypothesis with the experimental results. The validity of the results and the variables are also highlighted, along with a new pattern which redirects the original assumptions, providing a new direction for further research.

5.2 Testing Validity and Variables

Throughout this study, measures were taken to reduce variables, however, one cannot exclude their possible occurrence which might hinder the validity of the experimental programme's results.

5.2.1 Materials Used

5.2.1.1 Concrete Mix

Although homogenous concrete wall panels were used to reduce irregularities between the wall specimens, one cannot rule out the presence of variables and local weaknesses which can be present throughout the wall panels. Considering that each batch was cast using the same mix, this should increase homogeneity between the different panels, however, one must also take into consideration that the property of the mix might alter slightly throughout the batch's volume.

Moreover, results from the second ungrouted wall panels can lead to the conclusion that the panels might be weaker along the upper facade due to segregation caused by casting and curing horizontally flat on the ground. The ungrouted wall panels (wall 13 to 16) all failed prematurely along the same façade, which might confirm the presence of strength variation along the walls' thickness.

Also, by the process of hydration, concrete gains strength with time. This might have led to strength differences between the wall panels of each respective batch. The rate of gain in strength is the greatest during the first few days after casting, decaying with time, which is still present beyond the arbitrary 28 days (Kosmatka et al., 2008). This rate of gain in strength is mostly dependant on the type of cement used, in this case being CEM II/A. LL 42.5R. However, considering the difference between the date of casting and that of the testing, as shown in table 5.1, the variation in strength between the first and last wall, although present, can be considered negligible.

Casting Batch	Date of Casting	First test		Last test	
		Date	Days from casting	Date	Days from casting
1	01/03	26/05	87	02/06	94
2	20/03	05/05	46	18/05	59

Table 5.1 – The difference between days of casting and testing

5.2.1.2 Grouting

The surfaces of each wall panel were grouted separately as per section 3.4.3, hence using a different grout mix for each wall. Although the same grout-to-water ratio was used, the properties of the mix might have been altered slightly from one batch to another. Moreover, as shown in appendix F, the days of grout curing was not constant for each test. However, enough time was allowed such that the wall panels always failed prior any grout failure, hence the slight difference in the grout's strength should have not affected the test results. The results of the tests performed to verify the grout's strength are presented in appendix E, which can confirm the relatively high compressive strength the grout can withstand within just a few days after casting.

5.2.2 Loading Jacks and Cells

For this experimental programme, 2 new loading jacks were ordered, however, these were not delivered on time. This meant that 2 identical Holmatro 100t hydraulic jacks had to be used for the application of the precompressive stresses. Unfortunately, the compatible load cells, although re-calibrated before testing, still were showing inconsistent readings, responding with a difference of 5-10% to the loading supplied by the calibrating compression machine. Considering that for the weaker mix, loading jacks with a capacity of 996.4kN were used to load within the range of 10 - 80kN, the lack of sensitivity for the relatively small loads could have hindered the results.

5.2.3 Concrete Comparative Analysis

The validity of using concrete wall panels to represent the enhancement factor phenomenon is analysed by comparing the factor β without any precompressive stresses to previous literature formulated for masonry works. As shown in table 5.2, the results compare favourably with Farrugia's and Malek and Hendry's work, verifying that this phenomenon is also present within concrete homogenous walls, and that these homogenous panels represent on a similar scale the behaviour of masonry works, as predicted in section 3.3.1.

Test Programme	$\frac{A^{eff}}{A^{b}}$	Strength Enhancement β_o (without precompression)			Delta (Δ) between Exp. Results and Avg. β
		Malek and Hendry $\beta = 0.701\left(\frac{A_{eff}}{A_b}\right)^{0.462}$	Farrugia $\beta = 0.57\left(\frac{A_{eff}}{A_b}\right)^{0.643}$	Experimental Results*	
1	10	2.03	2.51	2.368	+ 0.098
2.1**	5	1.47	1.61	1.51	- 0.030
2.2***	5	1.47	1.61	1.46	- 0.080

Table 5.2 – Comparison between existing literature as per section 2.3.2 and experimental results

* Values for the experimental enhancement factors are as per the following section 5.3

* Test programme 2 part 1: Ungrouted Wall panels (wall 15)

* Test programme 2 part 2: Grouted Wall panels (wall 19)

5.3 Results Analysis

5.3.1 Changes to the Precompressive Stresses

During testing, as the central point load was increasing, the precompressive stresses were continuously decreasing. With increase in loading, the overall material compresses, hence it slightly settles, relieving some of the stress which the side jacks are applying. This behaviour is not present in real-life scenarios, so these precompressive stresses were sequentially increased to maintain the predetermined precompression ratios constant.

5.3.2 Comparing UCS Tests and Uniformly Loaded Walls

UCS tests were performed as an indication of the expected uniform load bearing strength (f_o) of the respective wall panels. Results from the uniform axial loading of the first testing programme were slightly higher than the UCS tests, however, the differences are almost negligible such that UCS tests can be safely assumed to represent the expected behaviour of the weaker wall panels.

On the other hand, as described in section 4.3.2.1, the majority of the stronger panels did not fail primarily in compression under uniform loading, hence the same comparison could not be performed. Wall 13, being the strongest wall panel tested under UDL, reached a stress of around 0.7 of the UCS stress, which might suggest that as the panels get stronger, slenderness and eccentricity effects shifted the failure mode away from pure compression.

5.3.3 Testing Programme 1

After analysing the results from the first testing set, i.e., the weaker batch, it can be seen that wall 1 and 12, which were loaded twice, clearly showed to be weaker when compared to the rest of the panels. As the precompressive stresses for wall 12 were increased to a stress of around 2N/mm^2, the wall started showing premature bearing failure. This suggested that f_o for wall 12 should have been much smaller than the one predicted. Being also loaded twice, the bearing strength of wall 12 should be fairly similar to that of wall 1.

This implies that f_o from wall 1 should have been excluded from the calculation of $f_{o,1}$, leading to a lower $f_p/f_{o,1}$ ratio than the one originally desired. As a result, $f_{o,1}$ for walls 4 to 11 should have been taken as the average of the bearing strength of wall 2 and 3, as per equation 5.1, while for wall 12, one can assume to have the same bearing strength as wall 1.

$$f_{o,1} = \frac{3.80 + 3.62}{2} = 3.71 N/mm^2$$

Equation 5.1 – Average $f_{o,1}$ for wall 4 to 11

Amendments to the average bearing strength under uniform loading ($f_{o,1}$) results to changes both to the precompressive stresses δ (f_p/f_o) and to the enhancement factor β (f_b/f_o). Results of table 4.20 should be updated accordingly as represented by table 5.3, summarising all the results of the first testing programme.

5.3.4 Testing Programme 2

The results from the second testing programme are not as conclusive and representative as those of the first set. As indicated in section 4.3, since the walls were too strong, most often slenderness and eccentricity led to rotation generated by the uneven distribution of forces. Despite the fact that the vertical jacks were aligned to apply the load centrally, considering the walls' slender thickness of 82mm and the relatively large loads required to reach compressive failure, very slight load deviations and eccentricities led to premature failure due to the induced secondary effects.

As the walls started rotating, pressures and stresses are naturally concentrated towards one edge, hence exceeding the concrete's capacity, leading to brittle failure expressed in terms of crumbling and/or spalling of concrete pieces. This effect was more visible when the wall panels were loaded uniformly, resulting into an uncertain and a lower-than-expected bearing strength $f_{o,2}$. In the majority of the UDL tests, the loads were released prematurely as the wall's rotational behaviour resulted into lateral pressure on the perpendicular wooden strips. With increase in loads, this lateral pressure could have led to catastrophic collapse. Hence, the scale of the magnitude of the strength enhancement β, could be slightly decreased as f_o increases. A summary for the test results of the second testing programme is represented by Table 5.4.

Table 5.3 – Summary of the results for the first testing programme

Wall No.	Days from casting	Load Type	a_1	b_p	t	F			$f_{o,2}$	f_p	$\delta = \frac{f_p}{f_{o,1}}$	f_b	β
						Central	Left	Right					
			mm	mm	mm	kN	kN	kN	N/mm²	N/mm²		N/mm²	
1	44	UDL	/	/	82.5	149.000	/	/	/	2.66	/	/	/
2	46	UDL	/	/	84.0	217.743	/	/	/	3.80	/	/	/
3	49	UDL	/	/	83.5	206.205	/	/	/	3.62	/	/	/
4	52	CL	306	68	83.0	49.5792	/	/	/	3.71	/	8.784	2.368
5	53	CL + P.UDL	306	68	83.1	50.0324	6.6	6.2	0.252	3.71	0.068	8.854	2.387
6	56	CL + P.UDL	306	68	82.8	54.1243	16.8	17.4	0.675	3.71	0.182	9.613	2.591
7	57	CL + P.UDL	306	68	82.3	55.3454	25.5	24.9	1.001	3.71	0.270	9.889	2.665
8	57	CL + P.UDL	306	68	83.9	61.3268	34.1	33.7	1.320	3.71	0.356	10.749	2.897
9	58	CL + P.UDL	306	68	82.0	56.2901	42.5	43.1	1.706	3.71	0.460	10.095	2.721
10	58	CL + P.UDL	306	68	83.2	55.8661	50.9	51.4	2.009	3.71	0.542	9.875	2.662
11	59	CL + P.UDL	306	68	81.9	47.3086	59.4	58.7	2.356	3.71	0.635	8.495	2.290
12	59	CL + P.UDL	306	68	83.0	27.3271	53.2	52.8	2.087	2.66	0.785	4.842	1.820

Table 5.4 – Summary of the results for the second testing programme

Legend:		Bearing Strength ($f_{o,2}$) Baseline Test							Inconclusive Test Results				
Wall No.	**Days from casting**	**Grouted**	**Load Type**	**a_1**	**b_p**	**t**	**F**			**$f_{o,2}$**	**f_p**	**$\delta = \frac{f_p}{f_{o,2}}$**	**f_b**	**β**
		Yes/No					**Central**	**Left**	**Right**					
				mm	**mm**	**mm**	**kN**	**kN**	**kN**	**N/mm**	**N/mm**		**N/mm**	
13	82	No	UDL	/	/	81.7	/	340.34	328.19	12.05	/	/	/	/
14	82	No	UDL	/	/	81.6	/	160.83	145.98	5.529	/	/	/	/
15	83	No	CL	272	136	81.6	201.68	/	/	12.05	/	/	18.17	1.509
16	83	No	CL	272	136	81.8	71.333	/	/	12.05	/	/	6.41	0.532
17	87	Yes	UDL	/	/	81.5	/	248.79	230.47	8.654	/	/	/	/
18	90	Yes	UDL	/	/	81.8	/	250.23	264.07	9.251	/	/	/	/
19	90	Yes	CL	272	136	81.9	196.49	/	/	12.05	/	/	17.64	1.464
20	91	Yes	CL + P.UDL	272	136	81.4	198.91	37.523	37.134	12.05	1.686	0.140	17.97	1.491
21	91	Yes	CL + P.UDL	272	136	82.1	225.92	74.457	74.127	12.05	3.327	0.276	20.34	1.68
22	92	Yes	CL + P.UDL	272	136	81.7	189.70	112.62	112.89	12.05	5.074	0.421	17.07	1.417
23	94	Yes	P.UDL	272	136	81.5	/	149.78	154.39	12.05	6.861	0.569	/	/
24	94	Yes	CL + P.UDL	272	136	81.4	209.36	94.134	93.90	12.05	4.246	0.352	18.91	1.569

5.3.5 Hypothetical Scenarios Against Observed Trends

Assuming that the test results are fully representative, and that the prementioned variables in section 5.2 do not affect the outcome of the experimental tests, then the results can be used as a basis to formulate conclusions. As per chapter 2, from the limited previous studies, the inclusion of a modification reduction factor to the strength enhancement equation was suggested in order to factor into the effect of precompression (Malek, Mohammad H., 1987). It was assumed that as the precompressive stresses increases, the degree of unconfinement decreases, leading to a decrease in the enhancement factor. Also, theoretically the factor β should approach unity as the precompressive stresses (f_p) reaches the bearing strength under uniform loading (f_o). Following Hendry's and Malek's conclusion that the effect of precompression can be neglected for the smaller stressed ratios, then the expected behaviour can be graphically represented as shown in Fig. 5.1.

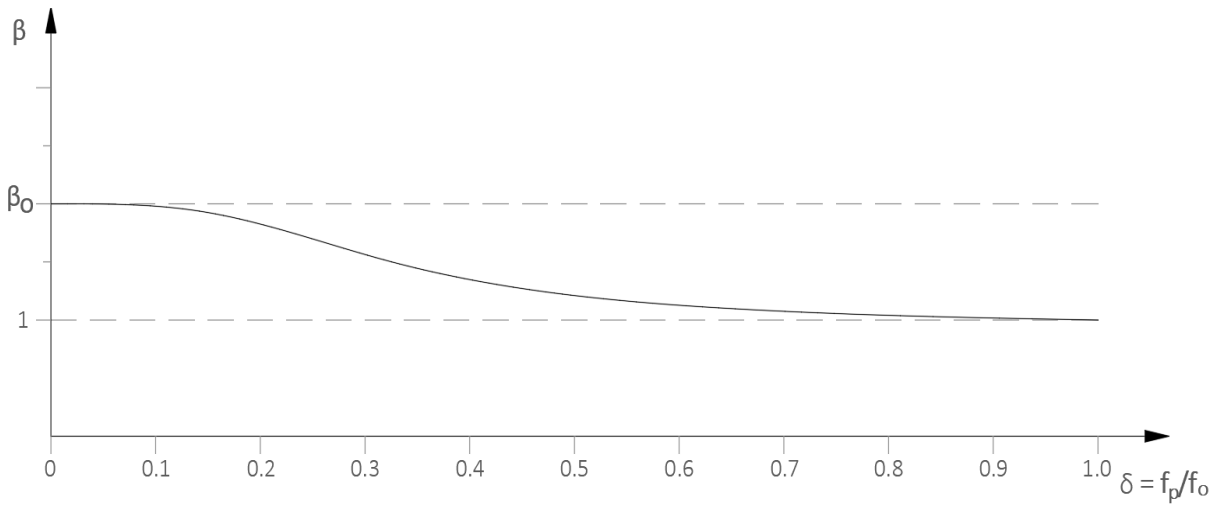

Figure 5.1 – Predicted behaviour for the enhancement factor β as δ reaches unity

From the first experimental testing programme, it was clearly shown that as the precompressive ratio δ was increased, there was an increase in the enhancement factor β, opposing the initial hypothetical behaviour. The maximum bearing strength under concentrated loads (f_b) was found to be at a δ ratio of around 0.4, beyond which β seemed to be reducing, as shown in Fig. 5.2. Unfortunately, the highest tested δ ratio was that of 0.785, as the last 2 walls were found to be cracked prior loading and could not be tested. However, one can logically assume that as the precompressive stresses approach the compressive bearing strength, the strength enhancement factor should approach unity, a trend which is also visible within the obtained results. Using these results one can amend the original hypothetical behaviour to the general behaviour as shown in Fig. 5.3.

The effect of friction between the bearing pad and the wall panels should increase confinement. This might lead to an apparent enhancement factor even in the case when the precompressive stress ratio approaches unity, hence;

$$\beta > 1.0 \text{ when } \delta = 1.0$$

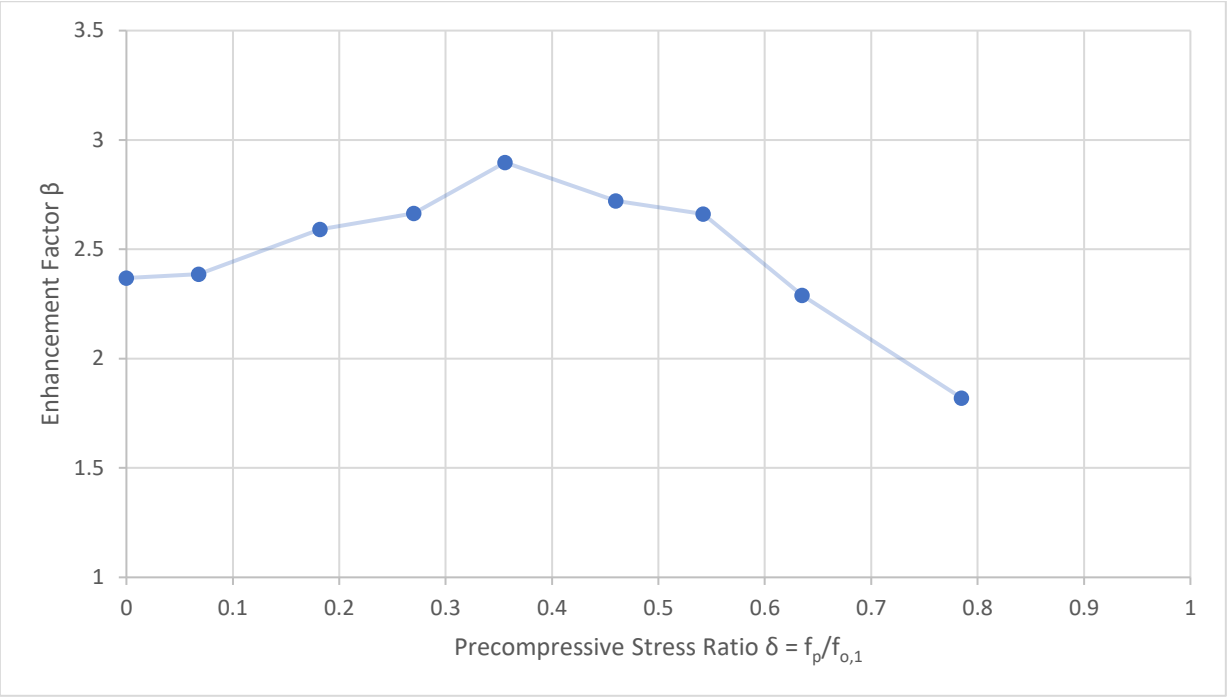

Figure 5.2 – Graph showing β vs f_p/f_o for the first testing programme

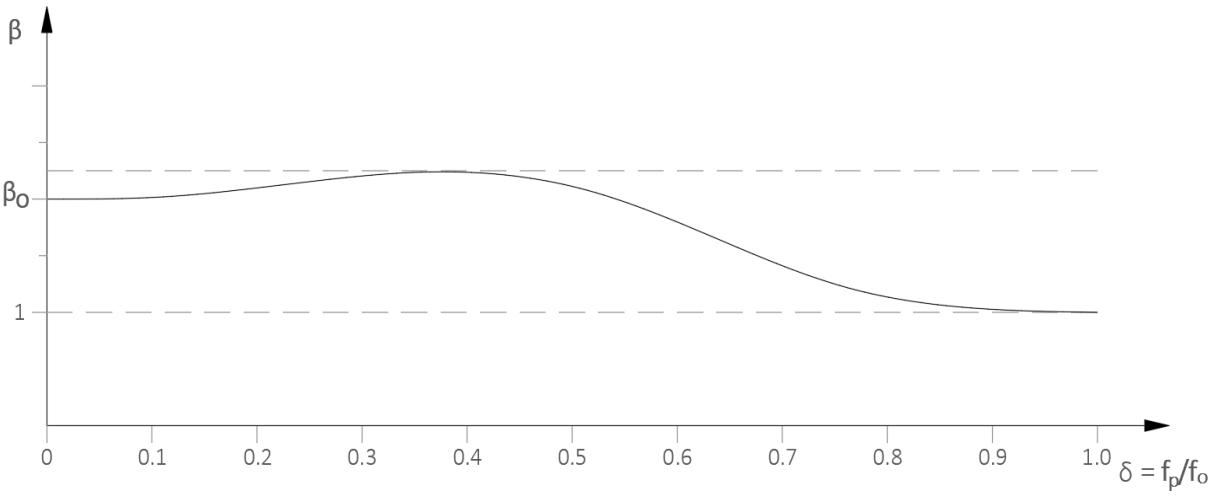

Figure 5.3 – Amended hypothetical behvaiour for enhancement factor β vs precompressive stress ratio δ

These results suggest for the introduction of a modification factor (ξ) which is to be multiplied to the existing provisions for finding β. This factor should follow the same trajectory as shown in Fig. 5.2, but on a different scale in the vertical axis, such that as;

$\delta = 0$, $\xi = 1$, hence no modification to the original enhancement factor β_o;

$\delta \approx 0.4$, ξ = maximum, hence maximum enhancement factor β;

$\delta = 1$, $\xi = \beta_o^{-1}$, such that effect of the enhancement factor β_o is neutralised;

as shown in Fig. 5.4, based on the results exclusively from the first experimental programme.

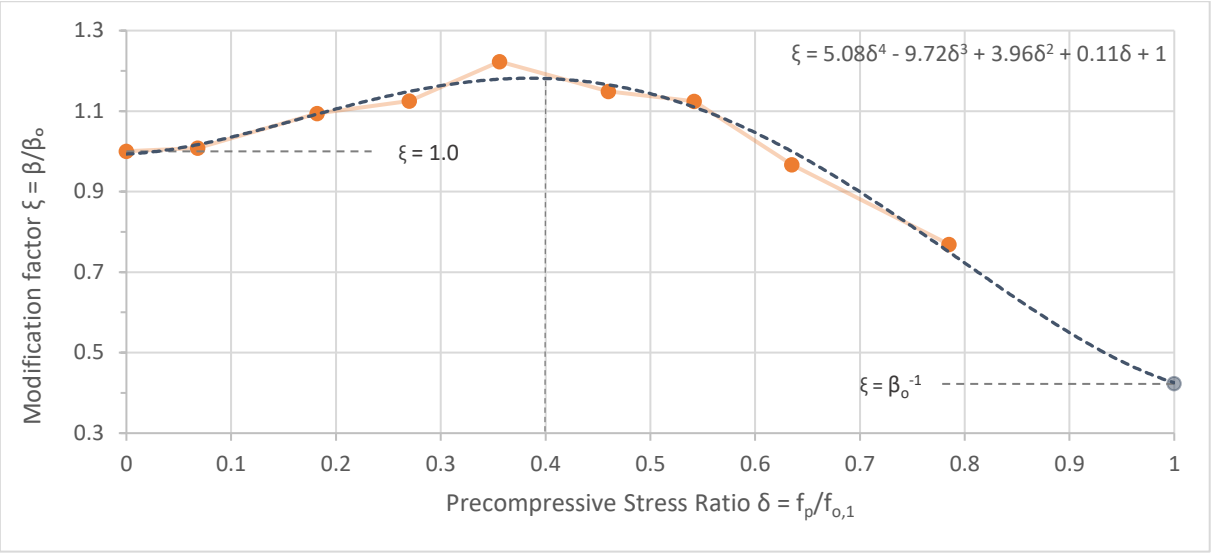

Figure 5.4 – Modification factor ξ vs precompressive stress ratios δ for the first testing programme

For the second testing programme, apart from having an uncertain baseline ($f_{o,2}$), there are less available data points onto which conclusions can be drawn. However, as shown in Fig. 5.5, a similar trend to that of the first testing programme was also noticeable. The enhancement factor seemed to be initially increasing, which however peaked at a smaller δ ratio. Similarly, beyond peaking, β seemed to be on the decline. Also, for the second testing programme, the scale of strength enhancement is drastically reduced, but, the ratio of β_{max} to β_o is quite similar, as presented by Table 5.5.

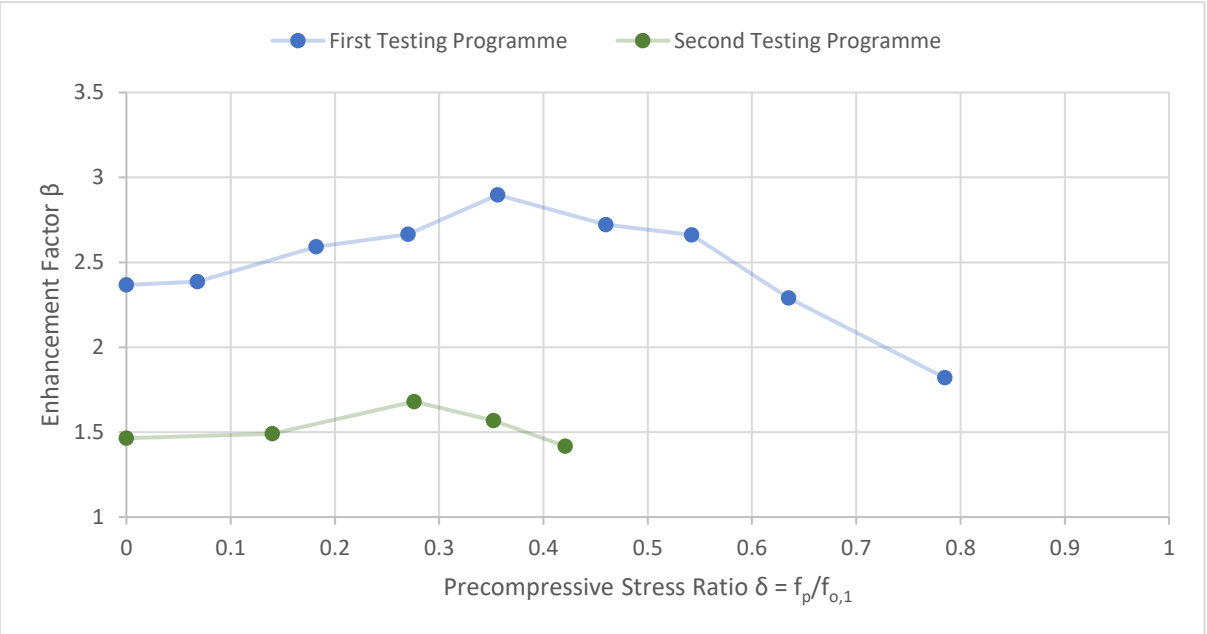

Figure 5.5 – Graph showing comparison between β vs f_p/f_o for the first and second testing set

Test Programme	β_o	β_{max}		β_{max}/β_o
		≈ β	At ≈ δ	
1	2.368	2.800	0.4	1.18
2	1.464	1.680	0.3	1.15

Table 5.5 – Comparison between βo and βmax of both testing programmes

Chapter 6: Comments and Conclusions

6.1 Conclusions

Despite being modest both in size and complexity, this testing programme turned out to be quite enlightening and interesting. It would have been of much greater value had the concrete design mix been cast as desired, as the results would have been more representative and handling would have not been an issue. Design mix 1 resulted to be too strong, such that slight eccentricities and imperfections would render the results unconclusive. Inversely, the second design mix was too weak, such that handling was quite challenging. Also, considering that the ordered jacks did not arrive on time, the available equipment lacked sensitivity for the relatively small loads, especially when it came to the first testing programme.

This experimental programme confirms the existence of an enhancement factor in homogenous concrete wall panels, which compare favourable to previous literature formulated for masonry works. Also, one can conclude that the strength enhancement phenomenon is still present with the introduction of confinement from the upper levels. However, as opposed to the initial hypothesis, which was developed from the limited previous studies, with an increase in the precompressive stresses, the test results showed an additional enhancement to the β_o factor, which seemed to peak at a particular precompressive ratio (δ). As the precompressive stresses were increased even further, the enhancement factor seemed to be reducing, hypothetically down to 1.0 as δ approaches unity.

Results from the first and second testing programme could not be directly compared as both the loaded area ratio and the properties of the design mix were varied. This implies that no conclusions could be drawn on which property led to a reduction and shift in the enhancement factor's peak when comparing the 1st to the 2nd data set, as shown in Fig. 5.5 and table 5.5. However, the results agree positively with Malek and Hendry's work, who suggested that the weaker the units are, the greater the strength enhancement is. Also, as per section 5.2.3, it was concluded that for the smaller A_{eff}/A_b (i.e., the second testing programme), there was a reduction in the enhancement factor, conforming with the previous studies. Moreover, as presented in table 5.2, comparing the delta of both tests, it can be seen that the for the second testing programme, the relative delta of the enhancement effect is slightly lower when compared to the delta of the first testing programme, which might prove the hypothesis that for the stronger panels, the strength enhancement effect is reduced. Logically this is understandable, because at infinite compressive strength there can be no additional strength enhancement.

As concluded from chapter 2, for economical and safety reasons, code drafters must re-examine the existing formulas used for the enhancement factor. The codes must be more holistic by taking into consideration more variables, leading to less conservative designs and hence reducing uncertainties while harmonising the provisions given by the different codes. As concluded from section 2.4, there is no existing code (to the author's knowledge), which

takes into consideration the effect of precompression, and neither gives provisions for the possibility of having a β factor which is less than 1.0. Previous literature, like for example the studies by Asteris et al. (2005), can be used to adopt a more representative design equation, which however must be modified by the proposed modification factor ξ, to factor into the effects of precompression;

$$\beta = \xi\,\theta\left(1.00 + \frac{2}{\alpha}\frac{\left(1-\frac{A_b}{A_{eff}}\right)}{\left(1+3\frac{A_b}{A_{eff}}\right)^4}\right)$$

Where;

$\theta = 1.00$ for the case of $0.20 \le \frac{a_1}{l} \le 0.50$

$\theta = 1.00 - 12\left(0.20 - \frac{a_1}{l}\right)^2$ for $0.00 \le \frac{a_1}{l} \le 0.20$

ξ = modification factor, to be formulated through further research

Equation 6.1 – Strength enhancement factor β, as proposed by Asteris et al., (2005), with the inclusion of a strength modification factor (by the author) to factor into the effects of the precompressive stresses

The number of tests performed was too modest to come up with a design equation for the modification factor ξ, however, results from the first testing programme suggest an equation to the fourth power, as shown by Fig. 5.4 and as represented by the below equation;

$$\xi = 5.08\delta^4 - 9.72\delta^3 + 3.96\delta^2 + 0.11\delta + 1$$

Equation 6.2 – Typical Modification factor equation; drawn out from the results of the first testing set

As per the calculations in Appendix B, taking a typical development scenario, the precompressive stress ratio δ was found to be within the range of 0.16 to 0.19. From the results of this test programme, one can conclude that for the majority of such cases, the effect of precompression does not seem to compromise the bearing strength underneath the applied concentrated loads. This slight confinement on the other hand should aid in resisting larger loads, resulting that adopting the β_o factor for such precompressive loads should be even more conservative than previously expected. However, considering the unpredictable nature of masonry works, bearing failure under UDL can be drastically less than the one calculated in appendix B, such that the precompressive ratio results to be much higher than predicted. This results into an effective smaller β factor, rendering the masonry codes unsafe to adopt.

Also, slight eccentric loads, which can be very common, might lead to premature failure. In such cases the walls are only able to withstand a fraction of the expected compressive strength. This trend was evident within the second testing set, which although attention was given to apply concentric loads, being slightly off centre, and considering the slender nature of the wall panels, resulted into premature rotational failures. On the other hand, this was not

noticeable within the first testing programme, as the walls being relatively weak in compression, resulted into compressive failure prior any rotational induced failure.

Another point to highlight from this experimental programme is the fragility of the wall panels which are encountered on site. As per appendix B, the unfactored characteristic strength of a typical HCB wall is 2.74N/mm^2, which is even less than the average bearing strength of the wall panels of the first testing programme. These panels resulted to be too fragile such that during handling the corners got easily crumbled away. Moreover, 2 of such panels cracked and failed during transportation and hence could not be tested. This gives an indication on the weak composite strengths of the wall panels which have to be handled on site.

6.2 Recommendations for Further work

Further testing should be carried out using masonry assemblies to take into consideration the effect of the vertical joints, altering the transverse stress distribution, and hence simulating a more realistic scenario. Also, as concluded from previous literature, there are numerous variables affecting the strength enhancement of concentrated loads, including:

- the loaded area ratio,
- the wall panel's aspect ratio,
- the strength of the masonry wall configuration, and
- the position of the load along the wall and its eccentricity.

These provisions, along with a larger number of test samples, would render it possible to come up with a design equation that can be adopted for the inclusion of a modification factor, represented by ξ. The complete spectrum of the precompressive stress ratio should be performed such that the newly formulated hypothesis is confirmed from $\delta = 0$, up to $\delta = 1.0$.

A different loading setup should be adopted such that the precompressive loads can be applied more uniformly, replicating more accurately real-life loading scenarios. The new setup should eliminate the need to load 2 separate jacks to generate the precompressive stresses, as it was quite challenging to maintain uniform loads, especially for the larger ones. Also, a better understanding would be obtained should a full-scale testing be carried out.

Alternative methods may be used to predict the effect of precompression to masonry structures when subject to concentrated loads: such methods include the use of Finite Element Analysis (FEA), obtaining a more accurate representation of the experimental tests performed in this study.

Also, considering that the use of HCB is quite common, a study can be based to analyse how the precompressive stresses effect the HCB walls. Moreover, it would also be interesting to research how double-leaf masonry walls respond to the application of such stresses alongside concentrated loads.

Bibliography

ACI, & MSJC. (2013). *Building Code Requirements and Specification for Masonry Structures, Containing Building Code Requirements for Masonry Structures (TMS 402-13/ACI 530-13/ASCE 5-13) & Specification for Masonry Structures (TMS 602-13/ACI 530.1-13/ASCE 6-13)*. American Concrete Institution.

Ali, S. S., & Page, A. W. (1988). *Finite Element Model for Masonry Subjected to Concentrated Loads*. American Society of Civil Engineers (ASCE). https://10.1061/(asce)0733-9445(1988)114:8(1761)

Arora, S. K. (1988). Performance of Masonry Walls Under Concentrated Load. *British Masonry Soc. Proc, 2*, 50-55.

Asteris, P. G., Asce, M., & Syrmakezis, C. A. (2005). *Strength of Unreinforced Masonry Walls under Concentrated Compression Loads.* https://10.1061/ASCE1084-0680200510:2133

Au, T., & Baird, D. L. (1960). Bearing capacity of concrete blocks. *Journal of the American Concrete Institute, 56(9)*, 869-879.

Australian Standard. (2011). *AS3700-2011, Masonry Code.*

Bezzina, I. (. (2017). *Assessment of the shear capacity of Maltese masonry wall assemblages through diagonal shear testing*. University of Malta; Faculty for the Built Environment. Department of Civil and Structural Engineering.

Bright, N., & Roberts, J. (2005). *The Treatment of Concentrated Loads in Masonry Design Codes.*

British Standards Institution. (2005). *Code of practice for the use of masonry - Part 1: Structural use of unreinforced masonry.*

Camilleri, D. H. (1988). Globigerina Limestone (Tal-Franka) As a Structural Material. *The Architect,* 17-25.

CSA. (2004). *S304.1-04 Design of Masonry Structures*. Canadian Standards Association.

Curtin, W. G., Shaw, G., & Davies, J. K. (1997). *Structural Masonry Designers' Manual* (3rd ed.). Chichester: John Wiley & Sons.

European Committee for Standardization. (2009a). EN 12390-2: Testing hardened Concrete - Part 2: Making and curing specimens for strength tests.

European Committee for Standardization. (2009b). EN 12390-3: Testing hardened Concrete - Part 3: Compressive strength of test specimens.

European Committee for Standardization. (2013). *Eurocode 6: Design of masonry structures - Part 1-1: General rules for reinforced and unreinforced masonry structures.*

European Committee for Standardization. (2016). *EN 196-1: Methods of testing cement — Part 1: Determination of strength.*

Farrugia, B. (1990). *Concentrated loads on masonry* (Bachelors Dissertation). https://https://www.um.edu.mt/library/oar/handle/123456789/80002

Gunkler, E., & Dashkhuu, O. (2014). On the loadbearing capacity of masonry walls subjected to concentrated end strip loads. *Mauerwerk, 18*(3-4), 213-221. https://api.istex.fr/ark:/67375/WNG-3V2PDWKW-X/fulltext.pdf

Hawkins, N. M. (1968). The bearing strength of concrete loaded through rigid plates. *Magazine of Concrete Research, 20(62)*, 31-40.

Hendry, A. W. (1981). *Concentrated Loading on Brick Masonry with Precompression*. University of Edinburgh. https://10.1007/978-1-349-81439-8_8

Hendry, A. W. (1990). *Structural Masonry*. Macimllan Education Ltd.

Kosmatka, S. H., Kerkhoff, B., & Panarese, W. C. (2008). *Design and Control of Concrete Mixtures* (14th ed.). Portland Cement Association.

Kozielova, M., Mynarzova, L., & Mynarcik, P. (2020). *Experimental Testing of Masonry Subjected to Concentrated Load in Direction of Bed Joints*. MDPI AG. https://10.3390/su12229474

Laird, M. G., Drysdale, R. G., Stubbs, D. W., & Sturgeon, G. R. (2005). The New CSA S304.1-04 "Design of Masonry Structures". https://10.1306/74D71F69-2B21-11D7-8648000102C1865D

Malek, M. H., & Hendry, A. W. (1988). Compressive Strength of Brickwork Masonry Under Concentrated Loading. *British Masonry Soc. Proc, 2*

Malek, M. H. (1987). *Compressive Strength of Brickwork Masonry with Special Reference to Concentrated Loads*. Department of Civil Engineering and Building Science, University of Edinburgh.

Mann, W., & Pfeifer, M. (1985). *Investigations on the Stresses in Masonry Walls Subjected to Concentrated Loads*. Technische Hochschule.

Page, A. W., & Hendry, A. W. (1988). Design Rules for Concentrated Loads on Masonry. *The Structural Engineer 66, 17.*

Page, A. W., & Shrive, N. G. (1990). Failure of Hollow Masonry Subjected to Concentrated Loads. *Canadian Journal of Civil Engineering, 17*(3), 479-490. https://10.1139/l90-047

Sayed-Ahmed, E. Y., & Shrive, N. G. (1995). Numerical analysis of face-shell bedded hollow masonry walls subject to concentrated loads. *Canadian Journal of Civil Engineering, 22*(4), 802-818. https://10.1139/l95-090

Shrive, N. G., & Sayed-Ahmed, E. Y. (1997). Design recommendations for hollow concrete masonry walls subject to concentrated loads, based on a test program. *Canadian Journal of Civil Engineering.* https://10.1139/cjce-24-3-380

Torpiano, A. (1988). Do We Know Our Limestone? *The Architect*, 27-29.

Vella, E. (. (2018). *Repair and strengthening of hollow concrete block masonry walls using textile-reinforced mortar (TRM)*. University of Malta; Faculty for the Built Environment. Department of Civil and Structural Engineering.

Yi, J., & Shrive, N. G. (2003). Design rules for hollow concrete masonry walls subjected to concentrated loads. *Canadian Journal of Civil Engineering, 30*(1), 203-211. https://10.1139/l02-104

Zavalis, M. (2020). Analysis of Behaviour of Calcium Silicate Hollow Blocks Masonry Subjected to the Concentrated Loads. *Engineering Structures and Technologies, 12*(2), 39-45. https://10.3846/est.2020.14041

Zhenfang, Y., & Bin, L. (2001). *A Brief Introduction to a Newly Revised Version of the Chinese Code for Design of Masonry Structures (GB50003-2001).*

Appendices

Appendix A - Full-scale Preliminary Calculations

Assuming the adoption of a full-scale model having the dimensions of 2700 x 1500 x 230mm, being within the parameters provided by the British Standard Institution as shown in Fig.A.1.

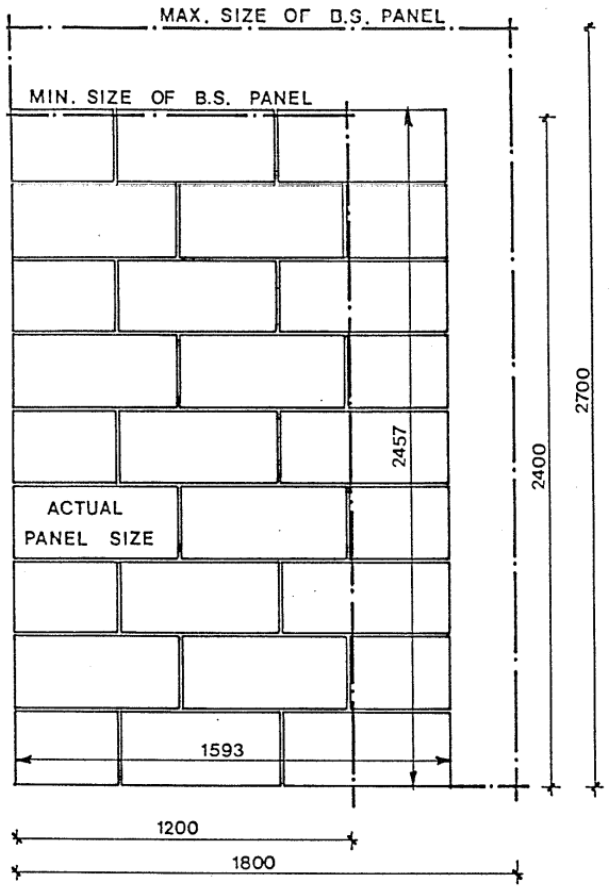

Figure A.1 – British Standard wall panel sizing limits (Farrugia, 1990)

The required load capacity, assuming a concrete strength of 10 N/mm² (as per section 3.3.2):

$$\text{Expected Failure Load} = 10N/mm^2 \times 230mm \times 1500mm$$

$$= 3450000\ \text{N} = 3450\ \text{kN}$$

There were no available jacks and testing rig that could withstand these loads.

Weight and Size considerations:

$$\text{Weight} = 2400\ {}^{kg}/_{m^3} \times 0.230m \times 1.5m \times 2.7m$$

$$= 2235.60\ \text{kg}.$$

The physical limitation of the available rigs did not allow these dimensions to fit within, and the overhead crane's maximum load capacity was not enough to handle such weight.

Appendix B - Typical Loadings in Malta

B.1 Finding the Characteristic Compressive Strength Using Eurocode 6 (EN1996-1-1)

$$f_k = K\, {f_b}^{0.7} {f_m}^{0.3}$$

Equation B.1 – EN 1996-1-1 Equation 3.2, The characteristic compressive strength of masonry (European Committee for Standardization, 2013)

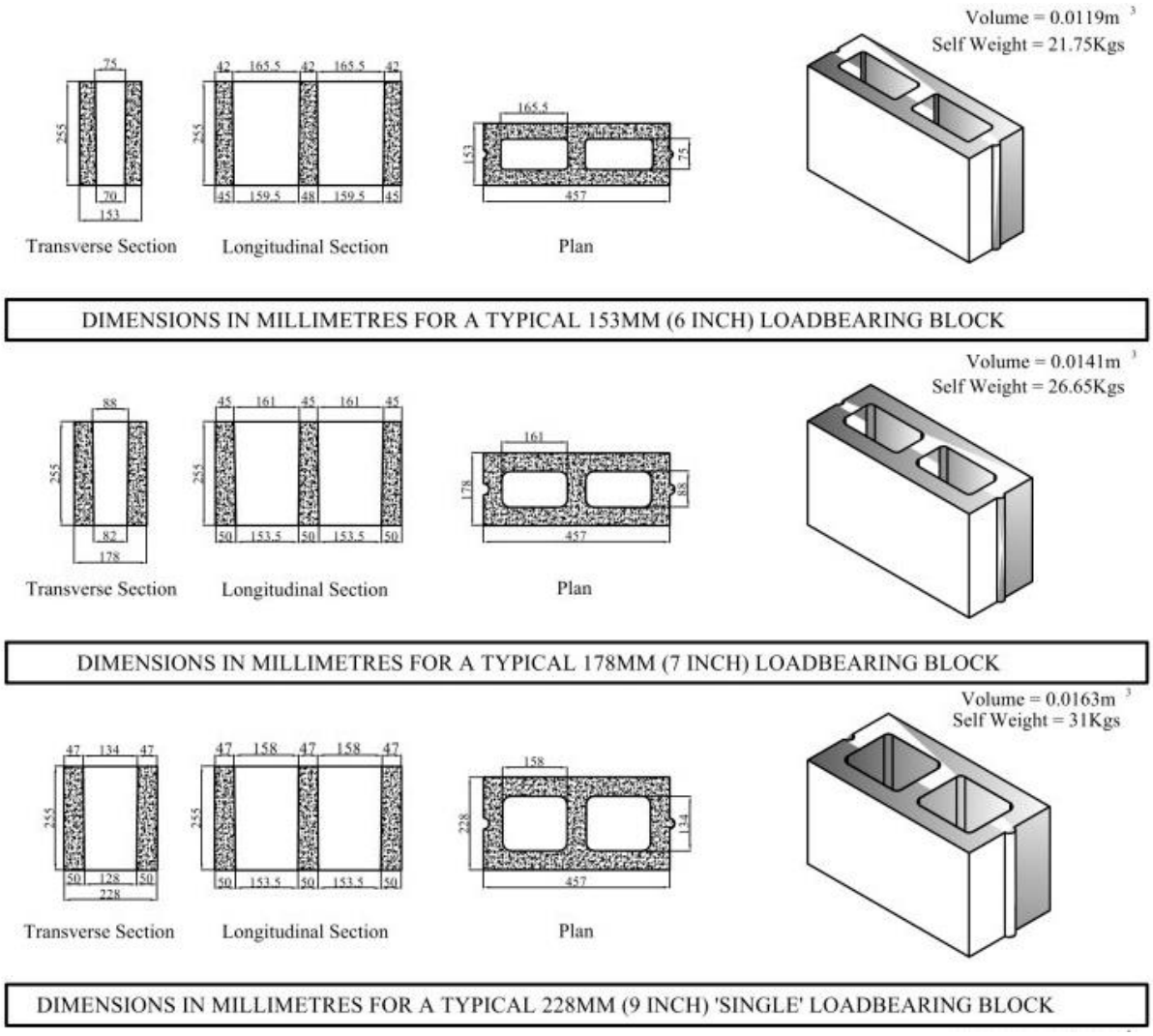

Figure B.1 – Dimensions in mm for a typical 6”,7”, and single 9” Loadbearing Brick (By Ballut Blocks Ltd.)

Wall Type		Height	Length	Width	Void Length	Void Width	Void Percent	Cross-Section Area
t	type							
mm		mm	mm	mm	mm	mm	%	mm^2
153	Stone	255	457	153	0	0	0.00	69921.00
178	Stone	255	457	178	0	0	0.00	81346.00
228	Stone	255	457	228	0	0	0.00	104196.00
153	HCB	255	457	153	165.5	75	35.50	45096.00
178	HCB	255	457	178	163	88	35.27	52658.00
228	Single HCB	255	457	228	158	134	40.64	61852.00

Table B.1 – Typical Stone and HCB masonry units properties

Masonry Unit		General purpose mortar	Thin layer mortar (bed joint ≥ 0,5 mm and ≤ 3 mm)	Lightweight mortar of density	
				$600 \leq \rho_d \leq 800$ kg/m^3	$800 < \rho_d \leq 1\,300$kg/m^3
Clay	Group 1	0,55	0,75	0,30	0,40
	Group 2	0,45	0,70	0,25	0,30
	Group 3	0,35	0,50	0,20	0,25
	Group 4	0,35	0,35	0,20	0,25
Calcium Silicate	Group 1	0,55	0,80	‡	‡
	Group 2	0,45	0,65	‡	‡
Aggregate Concrete	Group 1	0,55	0,80	0,45	0,45
	Group 2	0,45	0,65	0,45	0,45
	Group 3	0,40	0,50	‡	‡
	Group 4	0,35	‡	‡	‡
Autoclaved Aerated Concrete	Group 1	0,55	0,80	0,45	0,45
Manufactured Stone	Group 1	0,45	0,75	‡	‡
Dimensioned Natural Stone	Group 1	0,45	‡	‡	‡
‡ Combination of mortar/unit not normally used, so no value given.					

Table B.2 – EN 1996-1-1 Table 3.3, Values of K for use with general purpose, thin layer and lightweight mortars (European Committee for Standardization, 2013)

For solid "Franka" stone;

K = 0.45 (Table 3.3 EN 1996-1-1) – Dimensioned Natural Stone – Group 1

F_b = 20 N/mm^2

F_m = 4 N/mm^2 (Class M4 Mortar)

Hence,

$$f_k = 0.45 \times 20^{0.7} \times 4^{0.3} = 5.55\ N/mm^2$$

Excluding the effects of eccentricity and slenderness, the characteristic load bearing capacity is:

A. Assuming a **153mm solid stone wall**;

UDL failure load = 5.55 x 153 = 849.15 N/mm = 849.15 kN/m

B. Assuming a **178mm solid stone wall**;

UDL failure load = 5.55 x 178 = 987.9 N/mm = 978.9 kN/m

C. Assuming a **228mm solid stone wall**;

UDL failure load = 5.55 x 228 = 1,265.4 N/mm = 1,265.4 kN/m

For HCB Loadbearing brick;

K = 0.45 (Table 3.3 EN 1996-1-1) – Dimensioned Natural Stone – Group 2

F_b = 7.3 N/mm^2

F_m = 4 N/mm^2 (Class M4 Mortar)

Hence,

$$f_k = 0.45 \times 7.3^{0.7} \times 4^{0.3} = 2.74\ N/mm^2$$

Excluding the effects of eccentricity, slenderness, and the reduction in compressive strength due to having a gross cross-sectional area < 0.1m^2 (EN 1996-1-1 Clause 6.1.2.1 (3)), the characteristic load bearing capacity is:

D. Assuming a **153mm HCB wall**;

UDL failure load = 2.74 x 153 = 419.22 N/mm = 419.22 kN/m

E. Assuming a **178mm HCB wall**;

UDL failure load = 2.74 x 178 = 487.72 N/mm = 487.72 kN/m

F. Assuming a **228mm single HCB stone wall**;

UDL failure load = 2.74 x 228 = 624.72 N/mm = 624.72 kN/m

B.2 Finding the Typical Precompressive Stresses

Taking a typical case study where an existing 2 storey traditional terraced house building will be developed. This development includes the removal of a dividing wall at ground and first floor level, hence the introduction of 2 beams as marked in red in Fig. B.2, along with the building of additional 3 floors, splitting the original 2 storey house into 5 separate units.

Assumptions made:

- The terraced house's back façade is built out of a 228mm stone masonry wall, plastered along both sides.
- Typical floor slab is 250mm thick and roof floor slab is 300mm thick.
- Self-weight of the floor and roof tiling finishes and screed is 100kg/m^2.
- The roof is assumed to have a 1m parapet wall, and floor height (finish-to-finish) is assumed to be 3.2m
- Existing slabs are assumed to span on the existing divider wall (to be removed), hence only a 1m contribution is assumed to be directly induced on the back façade wall.
- The floor slabs of the newly constructed floors span directly on the back façade, hence assuming a contribution of 3m being induced on the back façade wall.
- Loadings are taken unfactored, and live loads are taken as:
    - 2.5kN/m^2 for the typical floor slab
    - 5kN/m^2 for the roof services slab

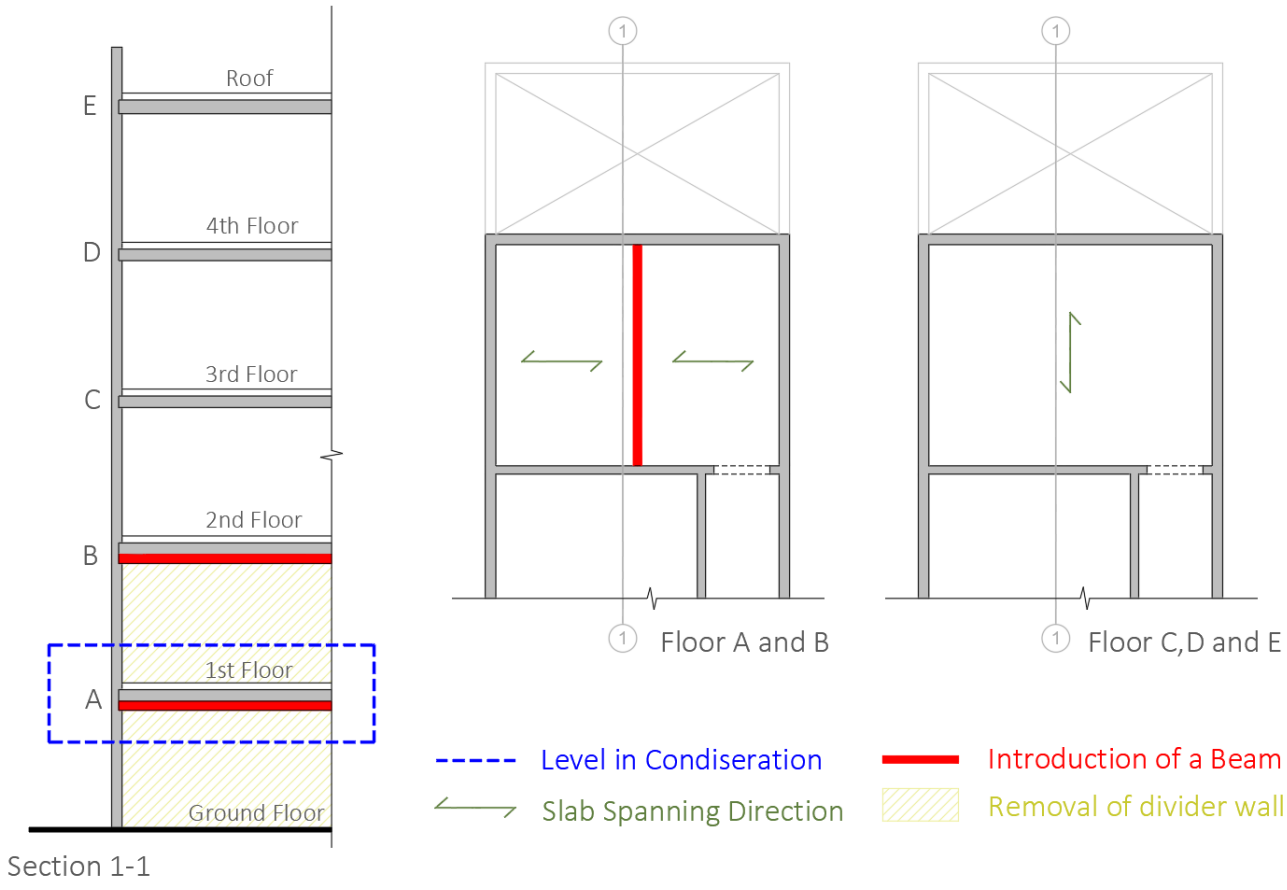

Figure B.2 – Typical Development showing a section and the respective structural floor plans

Finding the Self-weight:

Density of Concrete: = 2400 kg/m^3

$= \frac{2400\ x\ 9.81}{1000}$ =23.54 kN/m^3

Self-weight of floor slab: = 23.54 x 0.250 = 5.89 kN/m^2

Self-weight of roof slab: = 23.54 x 0.300 = 7.06 kN/m^2

Self-weight of the floor and roof tiling finishes and screeds:

= 100.00 kg/m^2

$= \frac{100\ x\ 9.81}{1000} = 0.98$ kN/m^2

Live Load Typical Floor: = 2.50 kN/m^2

Live Load Roof Service Floor: = 5.00 kN/m^2

Total Unfactored Loads:

Floor A - D: = 9.37 kN/m^2

Floor E: = 13.04 kN/m^2

Self-weight of 228mm thick stone masonry wall:

= 2500 kg/m^3

$= \frac{2500\ x\ 9.81\ x\ 0.228}{1000} = 5.59$ kN/m^2

Self-weight of wall plastering (12mm)

= 2100 kg/m^3

$= \frac{2100\ x\ 9.81\ x\ 0.012}{1000} = 0.25$ kN/m^2

Self-weight of back façade wall:

228mm stone masonry + plaster on both sides

= 6.09 kN/m^2

Finding the Precompression above slab A:

As assumed;

floor A & B has 1m slab contribution

UDL from Slab A and B = 9.37 kN/m

floor C, D & E has 3m contribution

UDL from Slab C and D = 28.10 kN/m

UDL from Slab E = 39.13 kN/m

Total Height above slab A: $= (3.2\ x\ 4) + 1 = 13.8$m

Self-weight of Back façade wall above slab A:

= 84.042 kN/m

Hence Total Precompression above Slab A = 198.11 kN/m

Comparing this load to the characteristic compressive strength found in B.1;

The UDL characteristic failure load of a 228mm Stone masonry wall = 1,265.4 kN/m

Hence, the precompressive stress ratio δ = $\frac{198.11}{1265.4}$ = 0.16

However, EN 1996-1-1 Clause 6.1.2.2 also includes a Φ factor, taking into account slenderness and eccentricity. This factor reduces the UDL compressive strength capacity, hence $f_k\ x\ \Phi$ should represent f_o from this testing programme.

(i) At the top or bottom of the wall (Φ_i)

$$\Phi_i = 1 - 2\frac{e_i}{t} \qquad (6.4)$$

where

e_i is the eccentricity at the top or the bottom of the wall, as appropriate, calculated using the equation (6.5):

$$e_i = \frac{M_{id}}{N_{id}} + e_{he} + e_{init} \geq 0{,}05\ t \qquad (6.5)$$

M_{id} is the design value of the bending moment at the top or the bottom of the wall resulting from the eccentricity of the floor load at the support, analysed according to 5.5.1 (see figure 6.1);

N_{id} is the design value of the vertical load at the top or bottom of the wall;

e_{he} is the eccentricity at the top or bottom of the wall, if any, resulting from horizontal loads (for example, wind);

e_{init} is the initial eccentricity with a sign that increases the absolute value of e_i (see 5.5.1.1);

t is the thickness of the wall.

Figure B.3 – Eccentricity and slenderness reduction factor at top/bottom of the wall (EN 1996-1-1 Clause 6.1.2.2)

(ii) In the middle of the wall height (Φ_m)

By using a simplification of the general principles given in 6.1.1, the reduction factor within the middle height of the wall Φ_m, may be determined [AC] *deleted text* [AC] using e_{mk}, where:

e_{mk} is the eccentricity at the middle height of the wall, calculated using equations (6.6) and (6.7):

$$e_{mk} = e_m + e_k \geq 0{,}05\ t \qquad (6.6)$$

[AC] $$e_m = \frac{M_{md}}{N_{md}} + e_{hm} + e_{init}$$ [AC] (6.7)

e_m is the eccentricity due to loads;

M_{md} is the design value of the greatest moment at the middle of the height of the wall resulting from the moments at the top and bottom of the wall (see figure 6.1), including any load applied eccentrically to the face of the wall (e. g. brackets);

N_{md} is the design value of the vertical load at the middle height of the wall, including any load applied eccentrically to the face of the wall (e. g. brackets);

e_{hm} is the eccentricity at mid-height resulting from horizontal loads (for example, wind);

NOTE The inclusion of e_{hm} depends on the load combination being used for the verification; its sign relative to that of M_{md}/N_{md} should be taken into account.

Figure B.4 – Eccentricity and slenderness reduction factor at middle height of the wall (EN 1996-1-1 Clause 6.1.2.2)

(10) The effective height of a wall should be taken as:

$$h_{ef} = \rho_n\ h \qquad (5.2)$$

where

h_{ef} is the effective height of the wall;

h is the clear storey height of the wall;

ρ_n is a reduction factor where n = 2, 3 or 4 depending on the edge restraint or stiffening of the wall.

(11) The reduction factor, ρ_n, may be assumed to be:

(i) For walls restrained at the top and bottom by reinforced concrete floors or roofs spanning from both sides at the same level or by a reinforced concrete floor spanning from one side only and having a bearing of at least 2/3 of the thickness of the wall:

$$\rho_2 = 0{,}75 \qquad (5.3)$$

Figure B.5 – Effective height of the wall (EN 1996-1-1 Clause 6.1.2.2)

Hence;

$P_n = 0.75$

$H_{ef} = 0.75 \times 3.2 = 2.4m$

Eccentricity at Top/Bottom of wall (Φ_i):

Design Value of the bending moment	M_{id}	=	0	kNm
Design value of the vertical load	N_{id}	=	198.11	kN per m strip
Eccentricity resulting from horizontal loads	e_{he}	=	0	m
Initial eccentricity for construction imperfections	e_{init}	=	0.005	m
thickness of wall	t	=	0.228	m
Top/Bottom Eccentricity	e_i	=	0.005	m
	e_i	=	0.011	m
	e_i	=	11.4	mm

Hence, Φ_i = 0.900 *(using equation 6.4 from Fig. B.3)*

Eccentricity at mid-height of wall (Φ_m):

Design Value of the bending moment	M_{md}	=	0	kNm
Design value of the vertical load	N_{md}	=	198.11	kN per m strip
	e_k	=	0	m
Initial eccentricity for construction imperfections	e_{init}	=	0.005	m
Eccentricity resulting from horizontal loads	e_{hm}	=	0	m
thickness of wall	t	=	0.228	m
Mid-height Eccentricity	e_m	=	0.005	m
	e_{mk}	=	0.005	m
	e_{mk}	=	0.011	m
	e_{mk}	=	11.4	mm
		=	0.05	t

Hence, Φ_m = 0.830 *(using Fig. B.6)*

Applying minimum of Φ_i & Φ_m to f_k, and hence to the precompressive stress ratio δ should be:

$$\delta = \frac{198.11}{1265.4\ x\ 0.830} = 0.19$$

For this typical loading scenario, the unfactored precompressive stress ratio δ ranges between 0.16 and 0.19. The variable nature and level of workmanship on site might reduce the compressive failure load at uniform stress, explaining the relatively large factor of safety which is usually applied as shown in Fig. B.7.

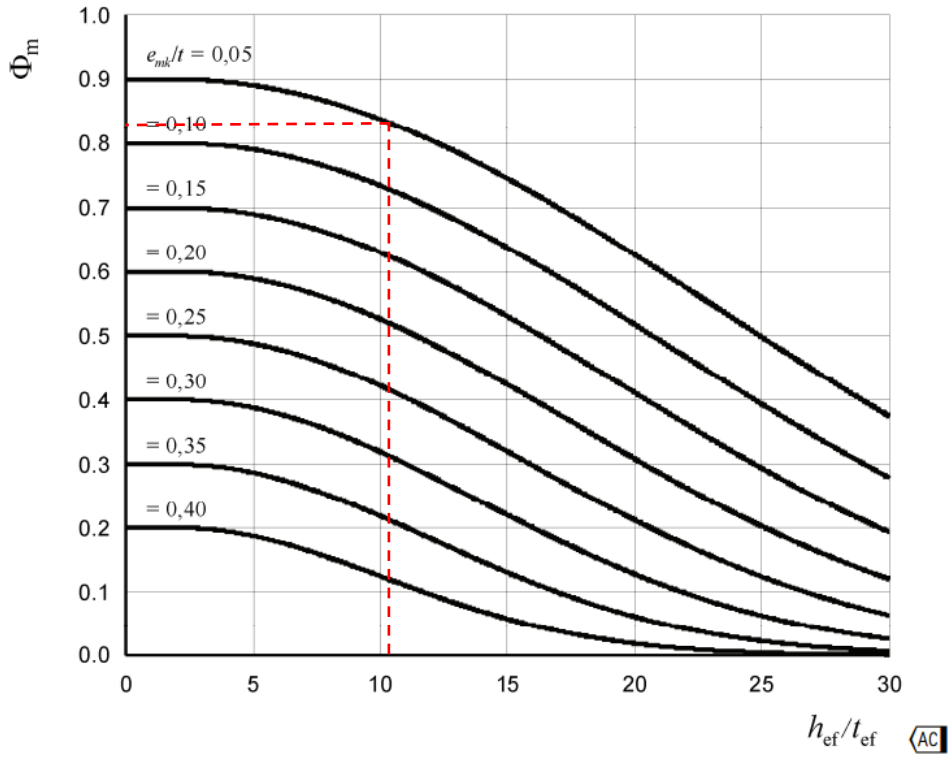

Figure B.6 – Φ_m graphical estimation (EN 1996-1-1, Appendix G, Figure G.1)

	Material	γ_M				
		Class				
		1	2	3	4	5
	Masonry made with:					
A	Units of Category I, designed mortar[a]	1,5	1,7	2,0	2,2	2,5
B	Units of Category I, prescribed mortar[b]	1,7	2,0	2,2	2,5	2,7
C	Units of Category II, any mortar[a, b, e]	2,0	2,2	2,5	2,7	3,0
D	Anchorage of reinforcing steel	1,7	2,0	2,2	2,5	2,7
E	Reinforcing steel and prestressing steel	1,15				
F	Ancillary components[c, d]	1,7	2,0	2,2	2,5	2,7
G	Lintels according to EN 845-2	1,5 to 2,5				

a Requirements for designed mortars are given in EN 998-2 and EN 1996-2.

b Requirements for prescribed mortars are given in EN 998-2 and EN 1996-2.

c Declared values are mean values.

d Damp proof courses are assumed to be covered by masonry γ_M.

e When the coefficient of variation for Category II units is not greater than 25 %.

Figure B.7 – Partial factor for masonry materials γ_M (EN 1996-1-1 Clause 2.4.3)

Appendix C - Loading Rate Calculations

Converting loading rates from stress (N/mm^2 per min) to load required (kN per min):

For the first testing set, the final loading rate is that of 0.45N/mm^2 per minute, which considering the wall having an average thickness of 82mm, this converts into a load rate of 36.9kN/m per minute.

For UDL loading, supplied solely by the middle jack, the load required would be that of approximately 25kN per minute;

$$\frac{0.45\ x\ 82\ x\ 680}{1000} \approx 25kN\ per\ minute$$

For the concentrated load, considering a loaded area ratio of 0.1, the jack has to distribute the load over a width of 68mm, resulting into a load of 2.5kN per minute;

$$\frac{0.45\ x\ 82\ x\ 68}{1000} \approx 2.5kN\ per\ minute$$

For the precompressive stresses, each side jack has to distribute the load over a width of;

$$\frac{680 - 68}{2} = 306mm$$

Hence, the loading rate required is;

$$\frac{0.45\ x\ 82\ x\ 306}{1000} \approx 11.5kN\ per\ minute$$

For the second testing set, using a load rate of 1.79 N/mm^2 per minute, and assuming the same width and thickness, results into a load of 100kN per minute for the UDL loading;

$$\frac{1.79\ x\ 82\ x\ 680}{1000} \approx 100kN\ per\ minute$$

However, considering that this load is to be supplied by 2 separate jacks, then each jack has to supply a load of 50kN per minute.

For the concentrated load, considering a loaded area ratio of 0.2, the jack has to distribute the load over a width of 136mm, resulting into a load of 20kN per minute;

$$\frac{1.79\ x\ 82\ x\ 136}{1000} \approx 20kN\ per\ minute$$

For the precompressive stresses, each side jack has to distribute the load over a width of;

$$\frac{680 - 136}{2} = 272mm$$

Hence, the loading rate required is;

$$\frac{1.79\ x\ 82\ x\ 272}{1000} \approx 40kN\ per\ minute$$

Appendix D - UCS Cube Strength Tests

For the first batch, cast on 01/03/2023, the 7-day UCS tests were performed by Ballut Blocks Ltd. The blocks were tested using the standard loading rate of 0.6Mpa/s, and the results are tabulated below:

Truck No:	PAS 113	Mould Size: 150mm³		Cond. of Sample:	Dry	
Pump Mix:	Na	No. of Samples: 4		Method of Curing:	Covered	
Qty (units³):	1 Yards	No. of Layers: 2	No. of Strokes: 30	Surface Condition	Dry	

Sampling Time:	16:30	Sample No.1 of 4	Sample No.2 of 4	Sample No.3 of 4	Sample No.4 of 4	
Sampling Date:		01/03/2023	01/03/2023	31/12/1902	01/03/2023	
Date Tested:		08/03/2023	08/03/2023	28/01/1903	12/04/2023	
Age Days:		7 DAYS	7 DAYS	28 DAYS	42 DAYS	
Height	h	mm.	150	150		
Width	w	mm.	150	150		
Breadth	b	mm.	150	150		
Volume	v	mm³	3375000	3375000		
Weight (grams):			6940	7150		
Density (Kg/m³):			2056	2119		
Failure Load (KN):			347	338		
Comp Strength (N/mm²):			**15.40**	**15.02**		

Comments:	Duration on site: Na
Tested By:	YD - The concrete samples were taken at the BBL plant.
Prepared By:	LB

Table D.1 – 7-day test for the first casting batch, performed by Ballut Blocks Ltd.

As the 7-day tests were much stronger than expected, the third cube was later tested using a slower loading rate, similar to the one predicted for the wall panels, factoring in the effect of creep. The cube was prestressed overnight, as shown in Fig. D.1, and then loaded to failure on the following day, with a loading rate of 0.020Mpa/s.

Figure D.1 – Prestressing the cube overnight using a Holmatro hydraulic loading jack

Figure D.2 – UCS cube failure mode for; *Left*, cube 3; *right*, cube 4

Using the results from the previous UCS tests, the fourth cube was tested at a later stage using a loading rate of 0.03Mpa/s, corresponding to a rate of 100kN per minute for the corresponding UDL wall tests. This test was performed just before the respective UDL wall tests to provide an indication on the expected compressive strength of a typical concrete wall panel.

Both results are tabulated below:

Cube No.	Days from casting	Loading Rate	m	l	b	h	v	ρ	F	f_c
		Mpa/s	g	mm	mm	mm	mm^3	kg/m^3	kN	N/mm^2
3	20	0.02	7234	150.46	150.76	150.54	3414751.4	2118	338.7	14.93
4	79	0.03	7196	150.33	150.37	152.3	3442760.8	2090	394.6	17.46

Table D.2 – UCS test results for the 2 remaining 2 cubes of concrete batch 1

The third cube tested on the 20th day from casting resulted in a compressive failure stress of 14.93Mpa, while the initial 7-day tests, averaged a stress of 15.21Mpa. The former, although tested at a more hardened stage, still resulted to be relatively weaker since it was loaded using a slower rate. However, this stress was still relatively high, meaning that large forces were needed for compressive wall failure, resulting into the testing rig having an undesirable small factor of safety. This led to alterations within the design mix for the second batch, as shown in chapter 3, table 3.3.

For the second batch, cast on 20/03/2023, a sample was also tested by Ballut Blocks Ltd. at the 7th day from casting, using the standard loading rate of 0.6Mpa/s. Result is tabulated below:

Truck No:	BBL 003	Mould Size: 150mm³		Cond. of Sample:	Dry	
Pump Mix:	Na	No. of Samples: 4		Method of Curing:	Covered	
Qty (units³):	1.5 Yards	No. of Layers: 2	No. of Strokes: 30	Surface Condition	Dry	

Sampling Time: 11:00			Sample No.1 of 4	Sample No.2 of 4	Sample No.3 of 4	Sample No.4 of 4
Sampling Date:			20/03/2023	20/03/2023	31/07/1904	20/03/2023
Date Tested:			27/03/2023	17/04/2023	28/08/1904	01/05/2023
Age Days:			7 DAYS	28 DAYS	28 DAYS	42 DAYS
Height	h	mm.	150			
Width	w	mm.	150			
Breadth	b	mm.	150			
Volume	v	mm³	3375000			
Weight (grams):			7220			
Density (Kg/m³):			2139			
Failure Load (KN):			71			
Comp Strength (N/mm²):			**3.16**			

Comments:	Duration on site: Na
Tested By:	YD - The concrete samples were taken at the BBL plant.
Prepared By:	LB

Table D.3 – 7-day test for the second concrete batch, performed by Ballut Blocks Ltd.

The number of days from casting varied from one cube to another since a cube was separately tested prior testing the first three walls. When it comes to loading, the first cube was tested using a rate of $1N/mm^2$ per minute which corresponds approximately to 0.017Mpa/s. When the same rate was applied to the wall, considering its weak nature, it would have resulted to

immediate failure. Hence for the following cubes, the rate was halved, as shown in table D.4. The walls were always loaded using the same loading rate such that comparison can be made between the UCS and the UDL failure stress, f_o.

Cube No.	Days from casting	Loading Rate	m	l	b	h	v	ρ	F	f_c
		Mpa/s	g	mm	mm	mm	mm^3	kg/m^3	kN	N/mm^2
2	39	0.017	7227	150.98	150.69	150.67	3427919.7	2108	79.8	3.51
3	46	0.008	7201	150.25	150.34	150.81	3406584.5	2114	77.2	3.42
4	49	0.008	7134	150.14	150.27	150.93	3405212.9	2095	77.2	3.42

Table D.4 – UCS test results for the 3 remaining cubes of concrete batch 2

Figure D.3 – Typical Concrete cube from the second batch being tested

Figure D.4 – Typical Failure Mode for a concrete cube sample of batch 2

Appendix E - Grouting Tests

Results from the grouting prisms, as shown in table E.1 and E.2, were convincing enough to ensure that the walls were always going to fail prior any grout failure. Conservatively the wall grouting was at least allowed to harden for 2 whole days before testing.

Prism No.	Days from casting	Loading Rate	l	b	h	F	R_f
		N/s	mm	mm	mm	kN	N/mm²
1	1	50	160.25	40.15	42.15	1.58	3.70
2	2	50	160.39	40.09	41.17	2.339	5.48
3	3	50	160.64	40.05	41.28	3.325	7.79
4	3	50	160.49	40.07	41.1	3.037	7.12
5	4	50	160.75	39.98	40.08	3.67	8.60
6	7	50	160.34	41.69	40.14	4.247	9.95

Table E.1 – Flexural Tests as per BS EN 196-1:2016

Cube No.	Days from casting	Loading Rate	l	b	h	F	f_c
		N/s	mm	mm	mm	kN	N/mm²
1.1	1	2400	40.00	40.15	42.15	31.29	19.56
1.2	1	2400	40.00	40.15	42.15	33.23	20.77
2.1	2	2400	40.00	40.09	41.17	60.61	37.88
2.2	2	2400	40.00	40.09	41.17	62.56	39.1
3.1	3	2400	40.00	40.05	41.28	74.99	46.87
3.2	3	2400	40.00	40.05	41.28	71.92	44.95
4.1	3	2400	40.00	40.07	41.1	78.05	48.78
4.2	3	2400	40.00	40.07	41.1	75.15	46.97
5.1	4	2400	40.00	39.98	40.08	95.65	59.78
5.2	4	2400	40.00	39.98	40.08	102	63.75
6.1	7	2400	40.00	41.69	40.14	109.16	68.225
6.2	7	2400	40.00	41.69	40.14	113.24	70.775

Table E.2 – Compressive Tests as per BS EN 196-1:2016

Figure E.1 – Testing grout sample in; *left*, flexure; *right*, compression

Appendix F - Wall Testing Timelines and Photos

Wall 1:

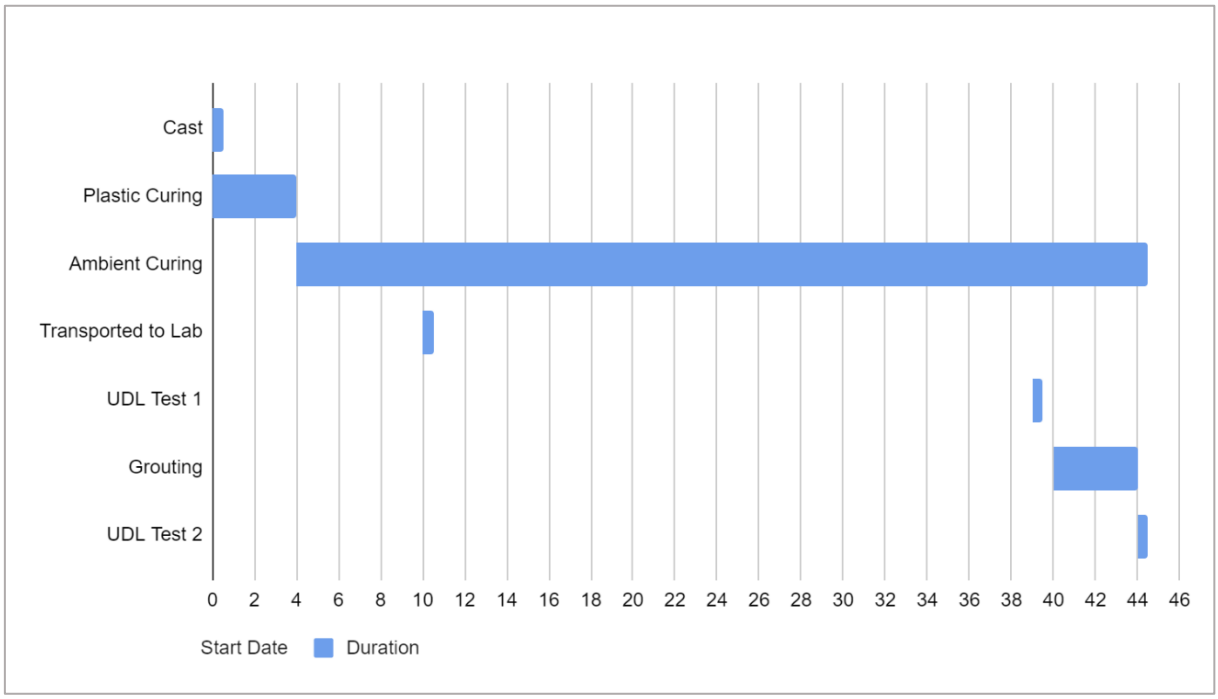

Figure F.1 – Wall 1 gannt chart

Figure F.2 – Setup 1 for the initial test

Figure F.3 – Using fine sands to level the loading surface

Figure F.4 – Diagonal crack failure mode for wall 1, setup 2

Wall 2:

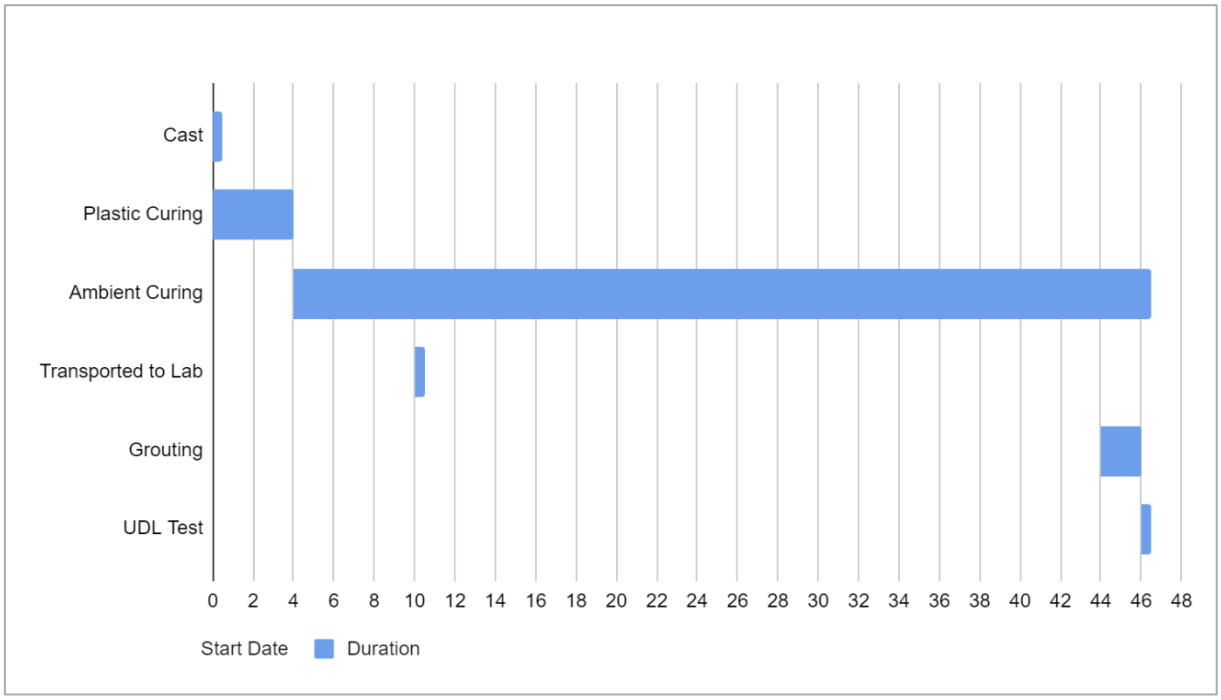

Figure F.5 – Wall 2 gannt chart

Figure F.6 – *Left*, failure mode back elevation; *right*, diagonal cracking failure through the top surface

Wall 3:

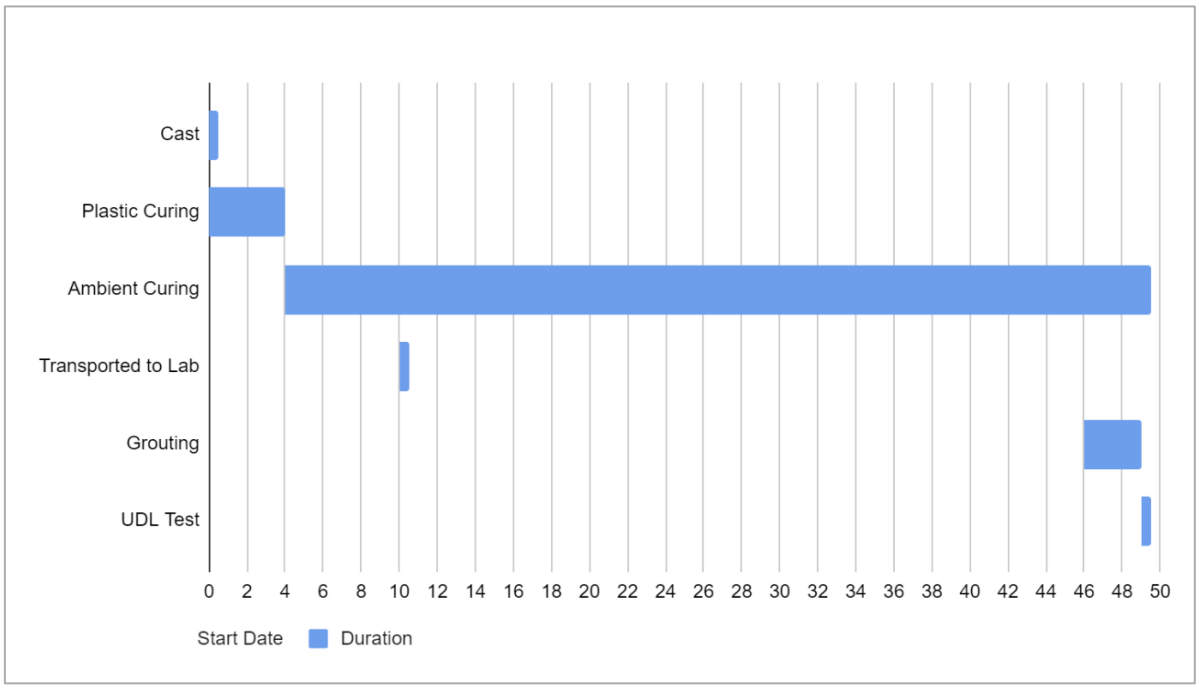

Figure F.7 – Wall 3 gannt chart

Wall 4:

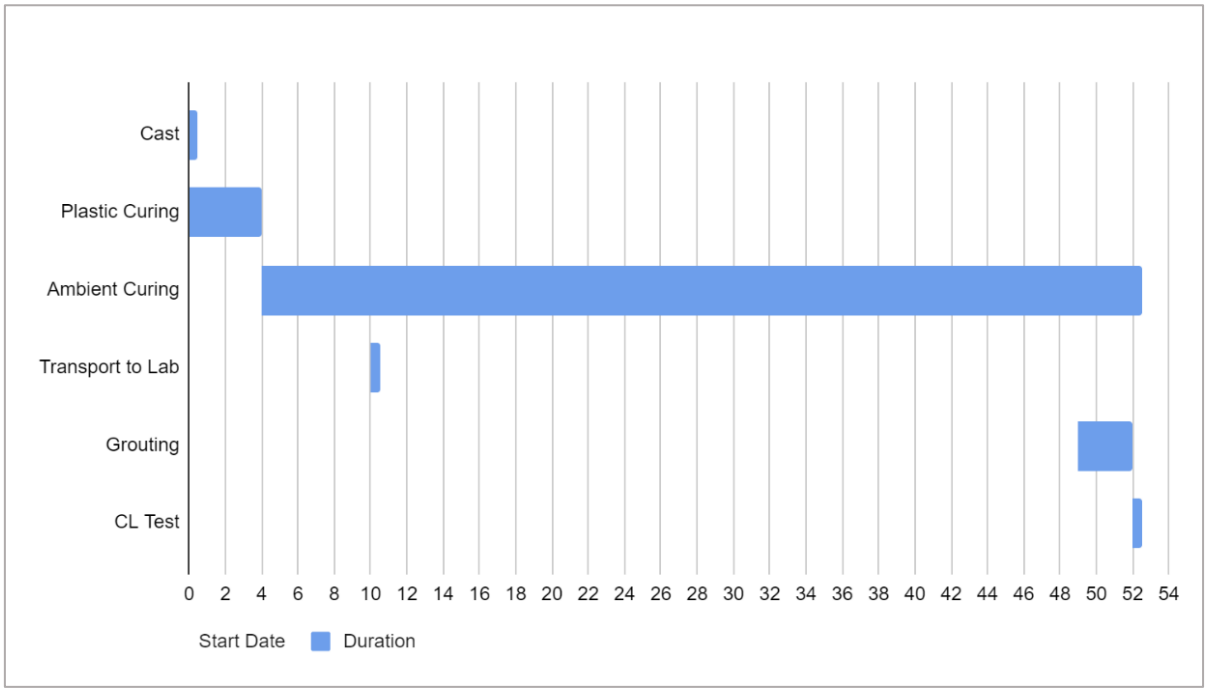

Figure F.8 – Wall 4 gannt chart

Figure F.9 – Failure mode back elevation

Figure F.10 – Wedge cone failure mode

Wall 5:

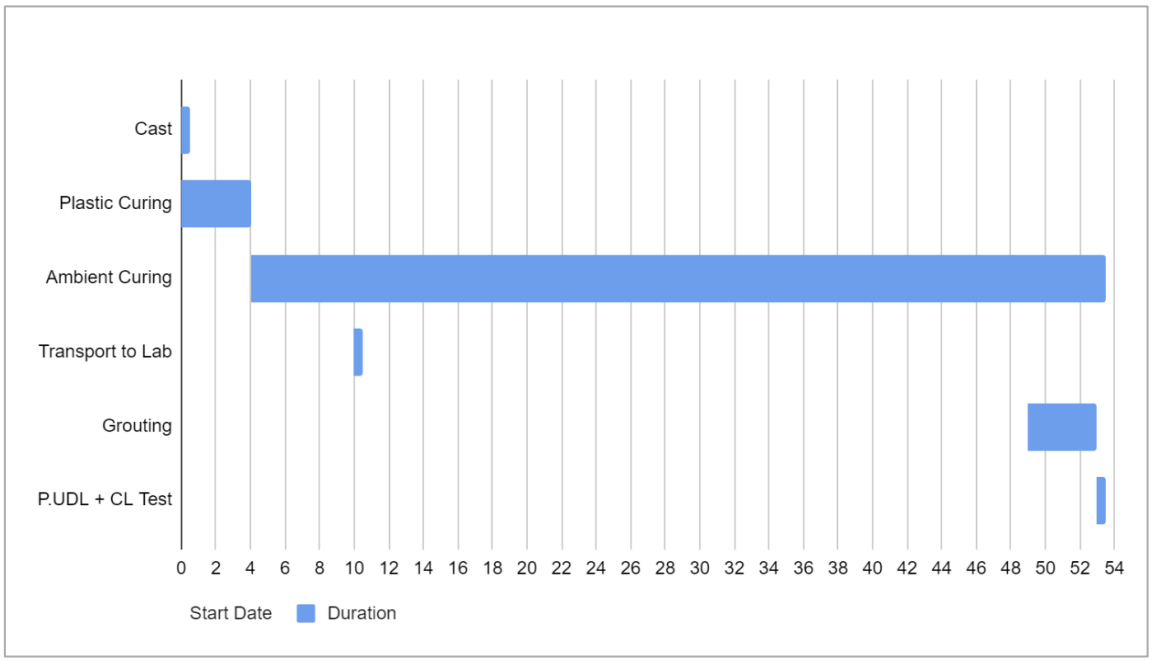

Figure F.11 – Wall 5 gannt chart

Figure F.12 – *Left*, failure mode front elevation; *right*, wedge cone failure

Wall 6:

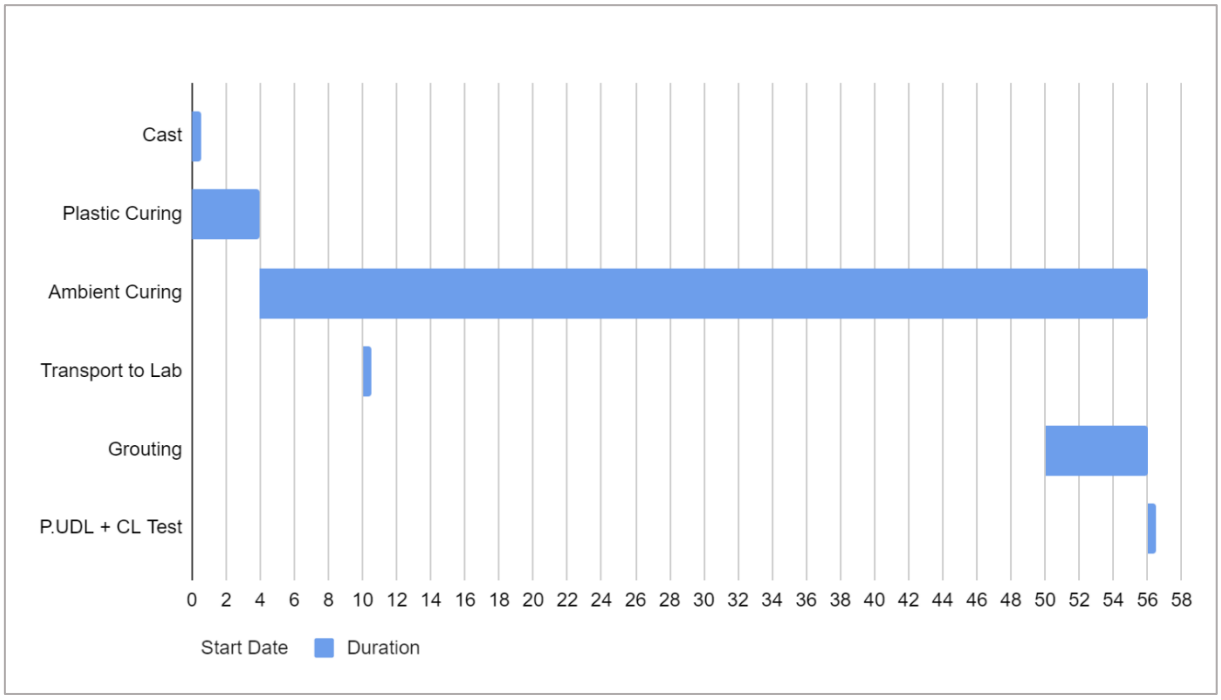

Figure F.13 – Wall 6 gannt chart

Figure F.14 – *Left*, failure mode front elevation; *right*, wedge cone failure

Wall 7:

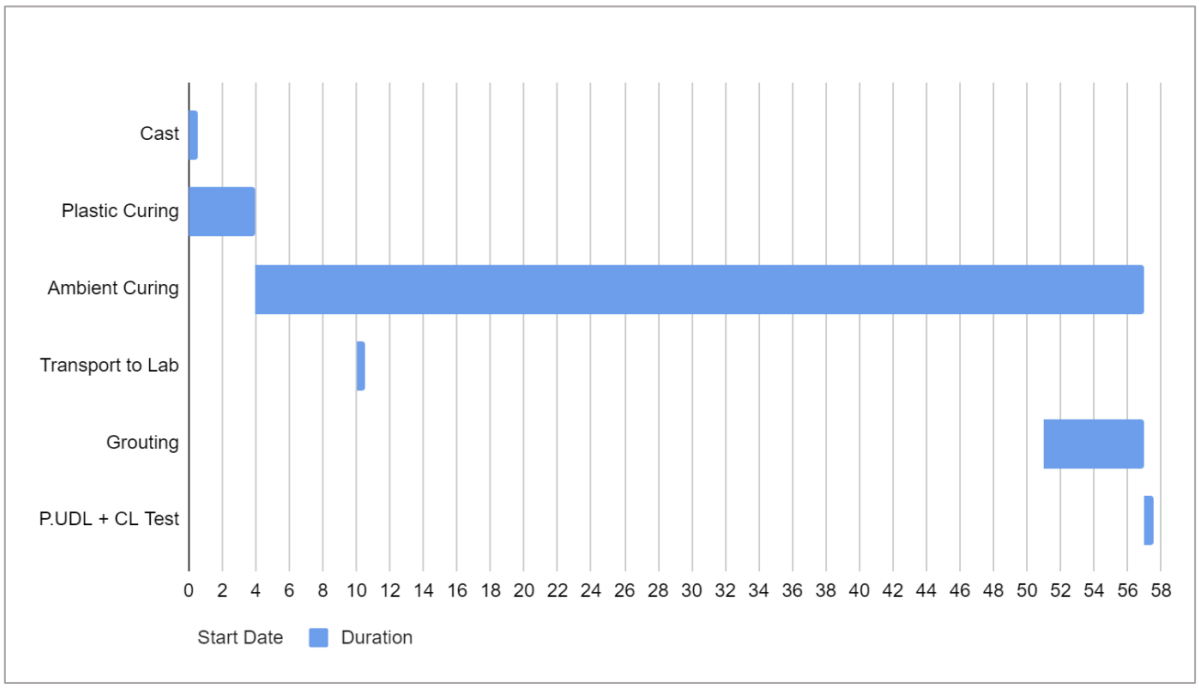

Figure F.15 – Wall 7 gannt chart

Figure F.16 – *Left*, failure mode front elevation; *right*, wedge cone failure

Wall 8:

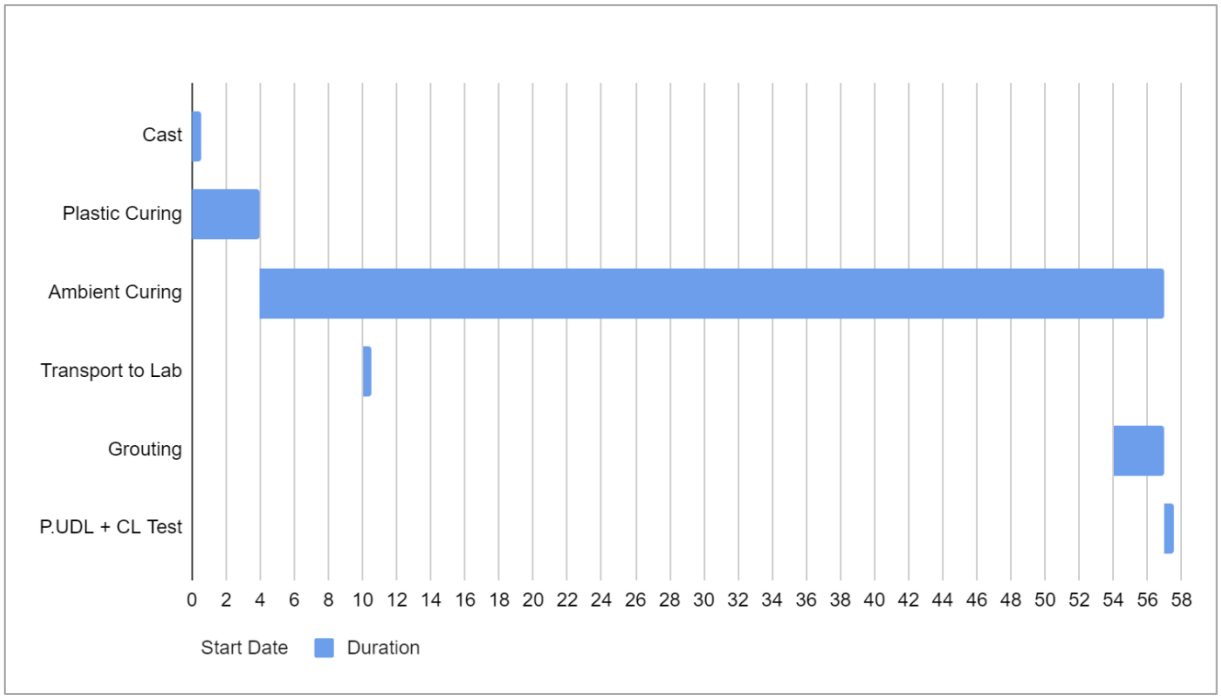

Figure F.17 – Wall 8 gannt chart

Figure F.18 – Failure mode wedge cone failure

Wall 9:

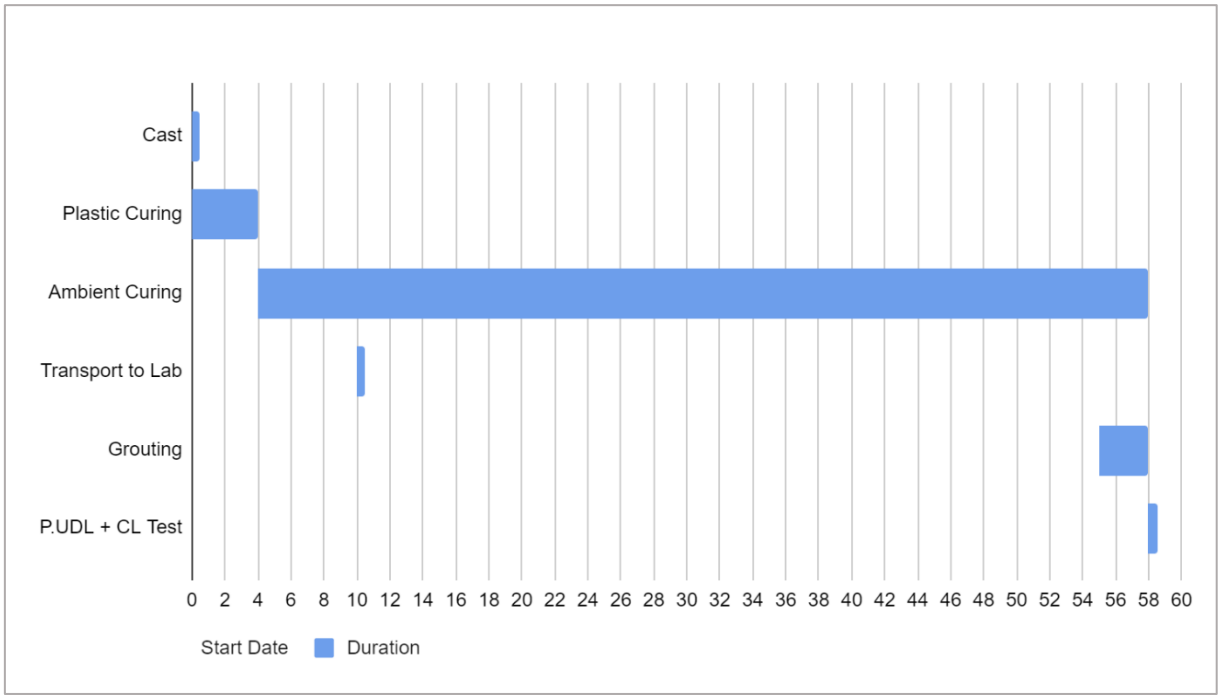

Figure F.19 – Wall 9 gannt chart

Figure F.20 – *Left*, failure mode front elevation; *right*, wedge cone failure

Wall 10:

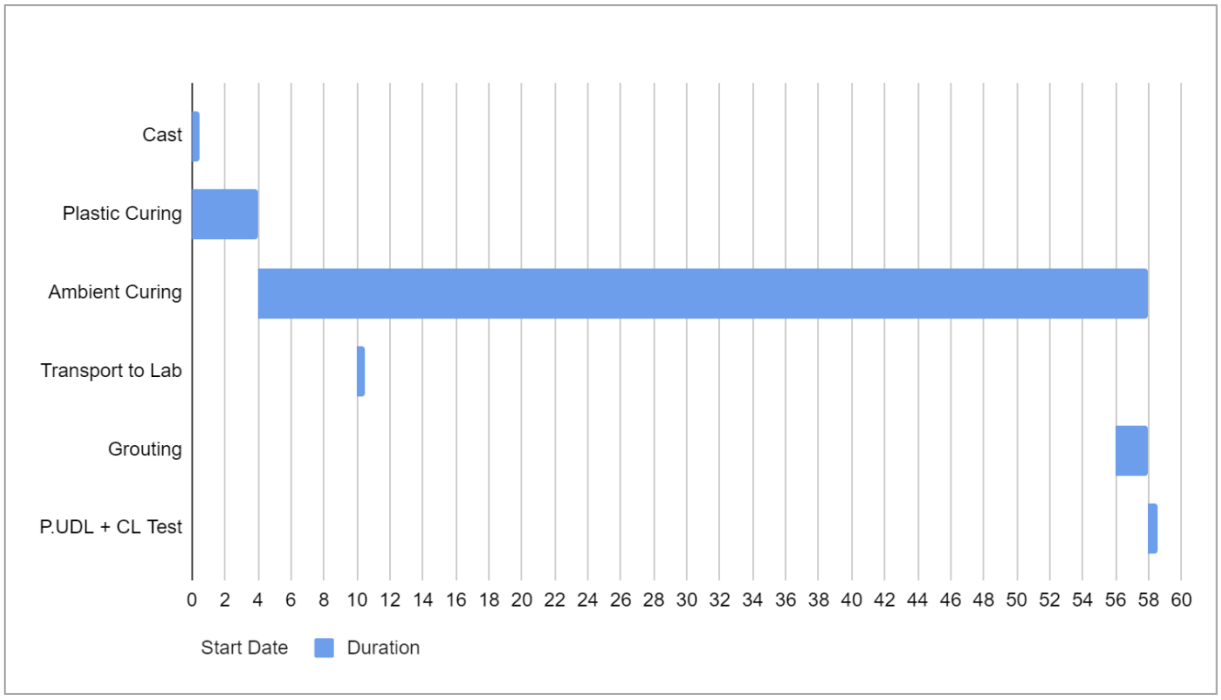

Figure F.21 – Wall 10 gannt chart

Figure F.22 – Failure mode wedge cone failure

Wall 11:

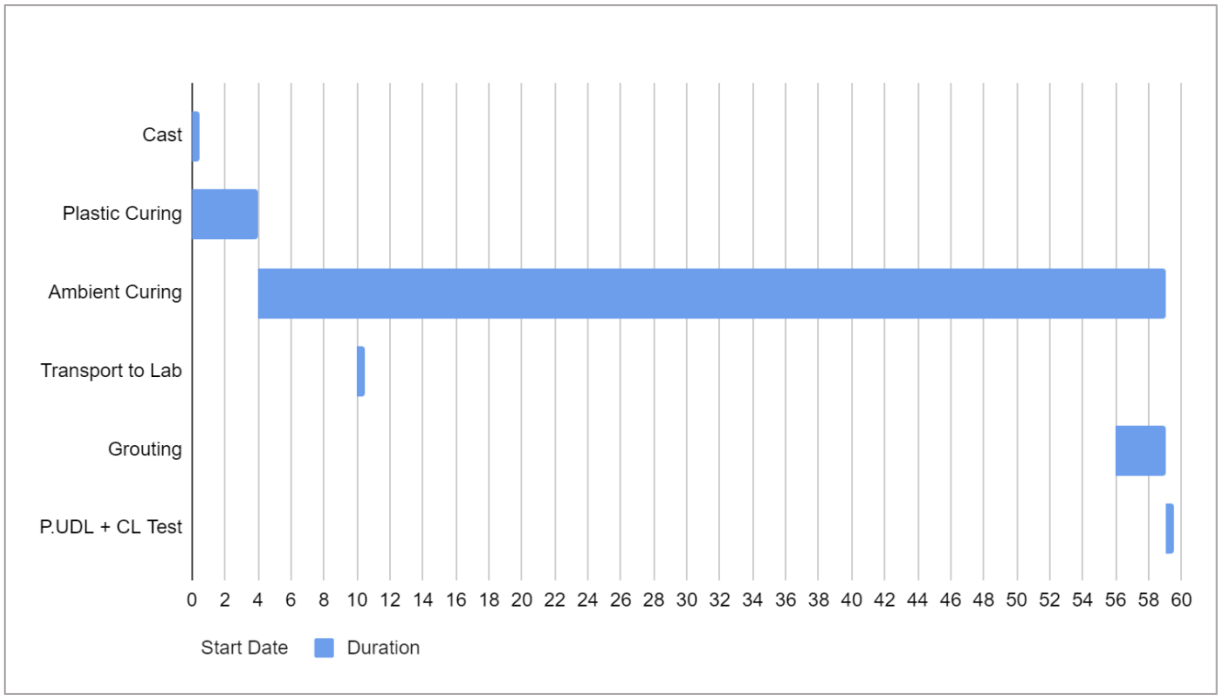

Figure F.23 – Wall 11 gannt chart

Figure F.24 – Failure mode wedge cone failure

Wall 12:

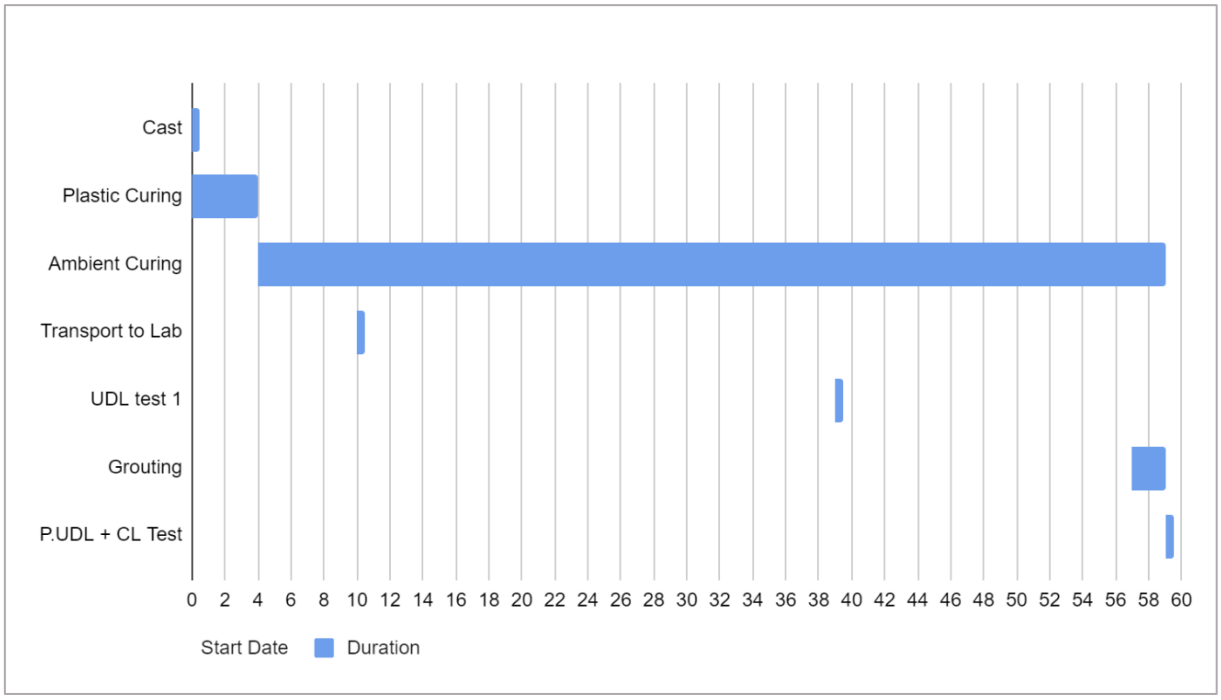

Figure F.25 – Wall 12 gannt chart

Figure F.26 – Crushing failure along the pre-damaged surface

Wall 13:

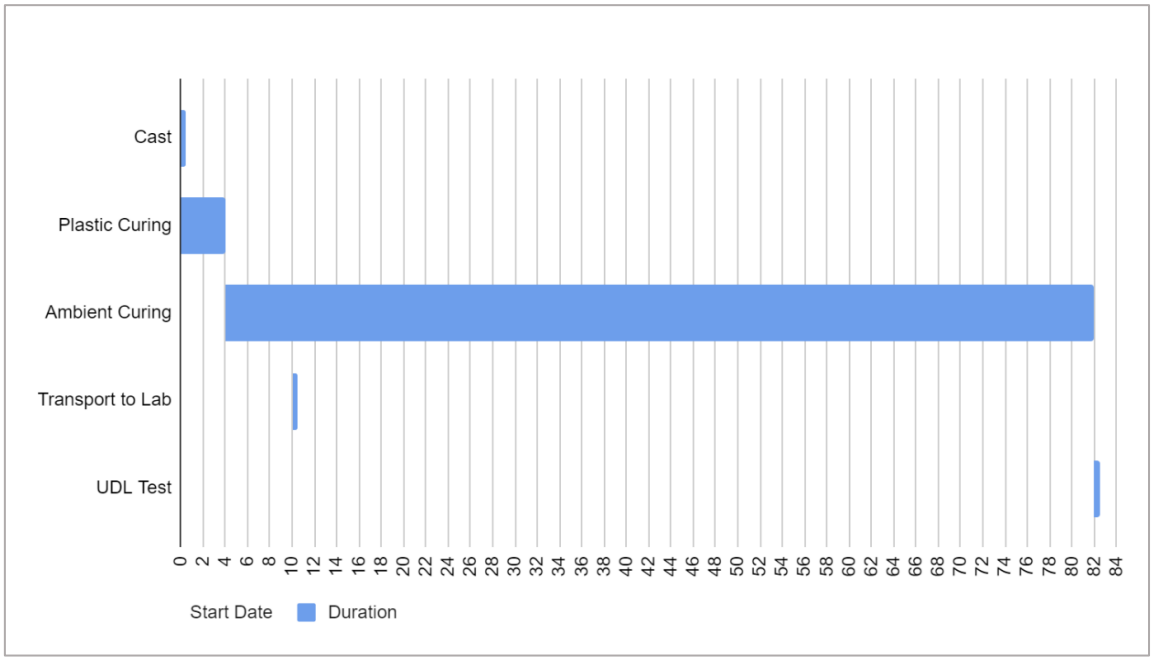

Figure F.27 – Wall 13 gannt chart

Figure F.28 – Failure mode under UDL loading

Figure F.29 – *Left*, left over pieces from the explosive failure; *right*, main vertical crack

Wall 14:

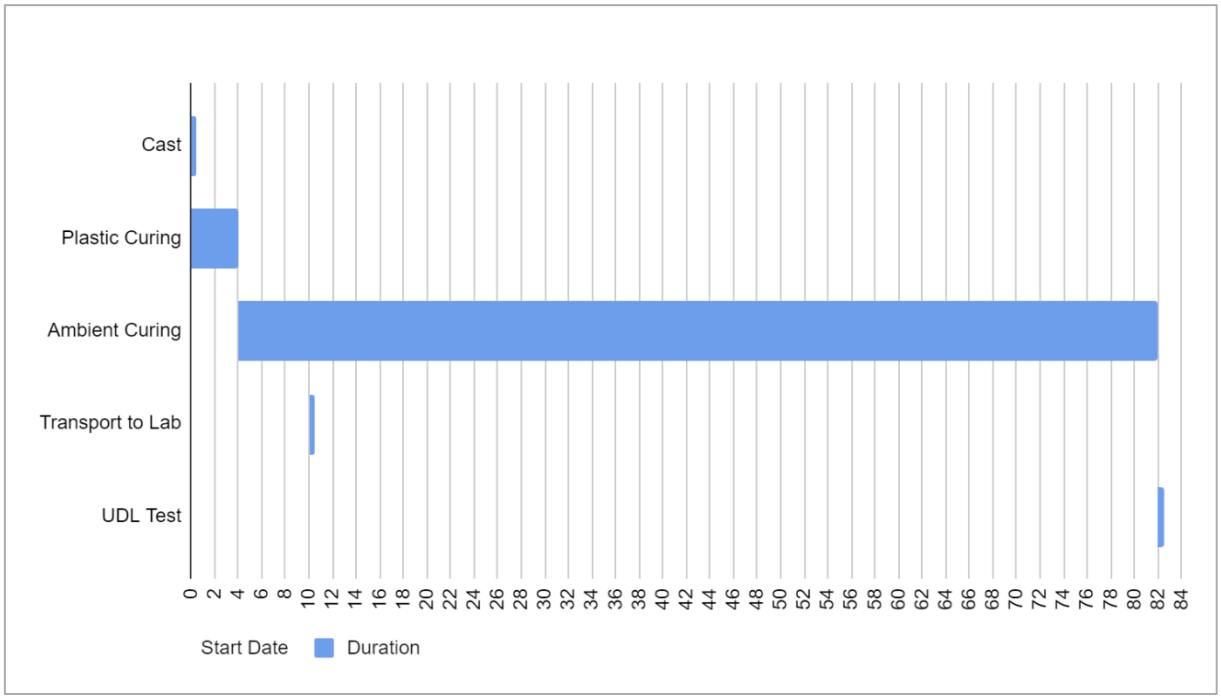

Figure F.30 – Wall 14 gannt chart

Wall 15:

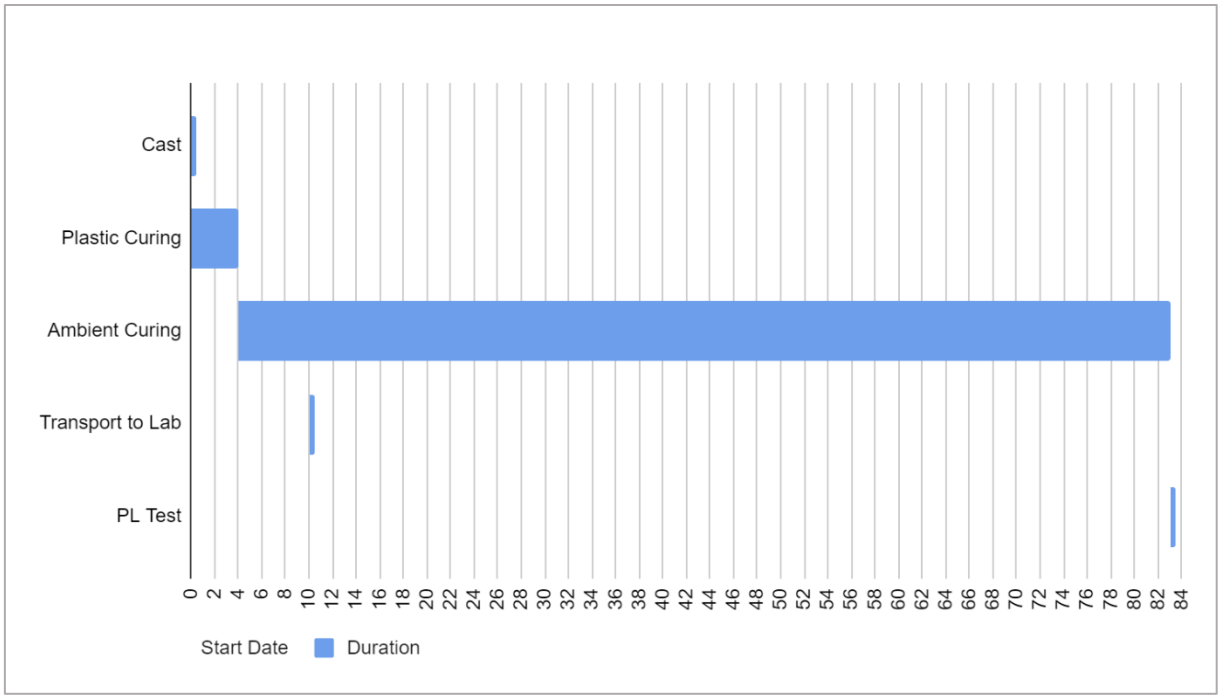

Figure F.31 – Wall 15 gannt chart

Figure F.32 – *Left*, front elevation showing no signs of failure; *right*, failure along the back elevation

Figure F.33 – Concentrated load failure mode through the grout layer

Wall 16:

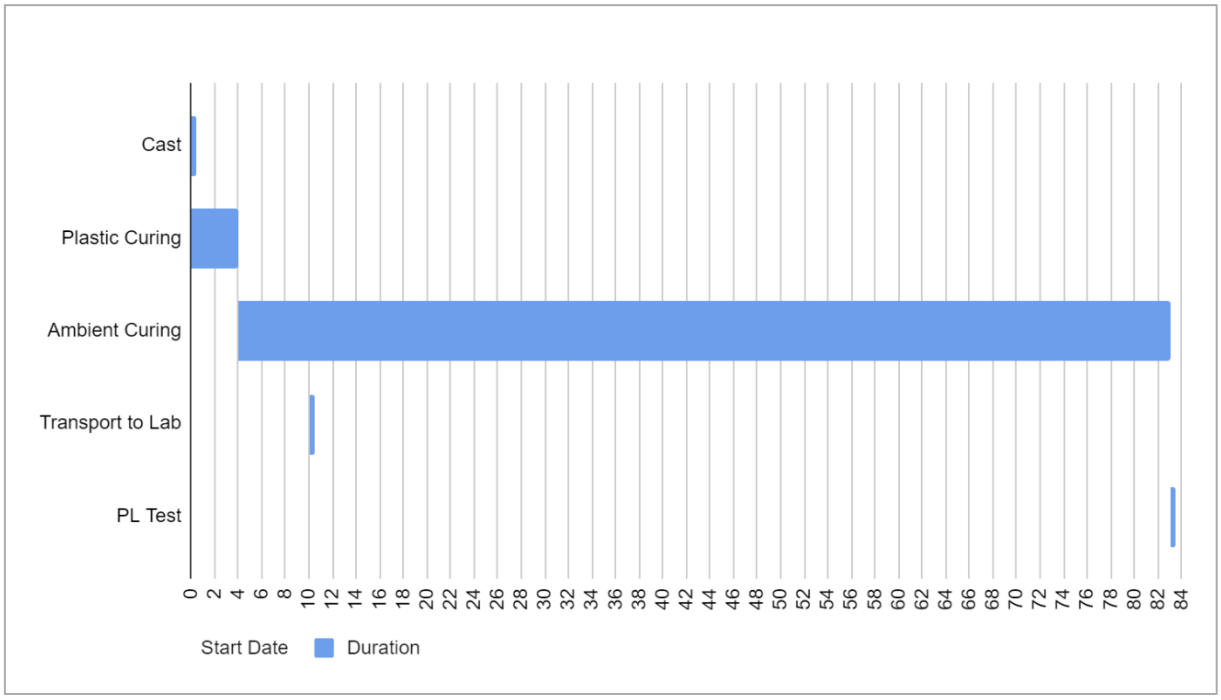

Figure F.34 – Wall 16 gannt chart

Figure F.35 – Failure along the back elevation; pressure along one particular side

Wall 17:

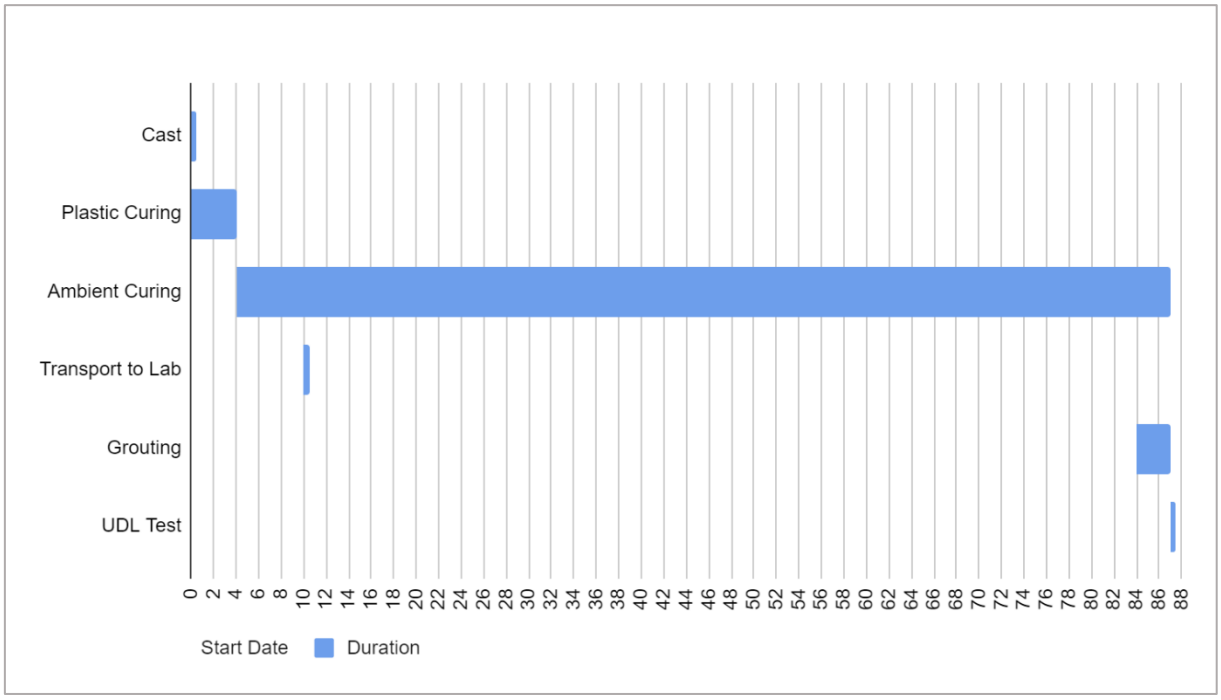

Figure F.36 – Wall 17 gannt chart

Wall 18:

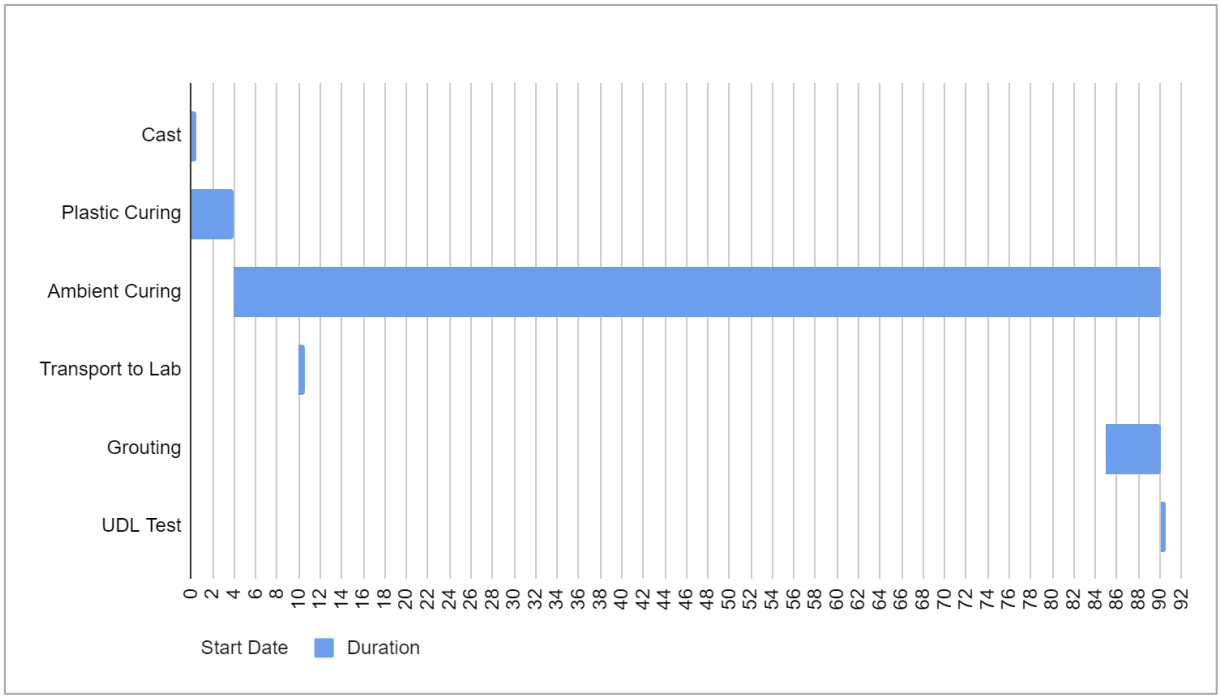

Figure F.37 – Wall 18 gannt chart

Wall 19:

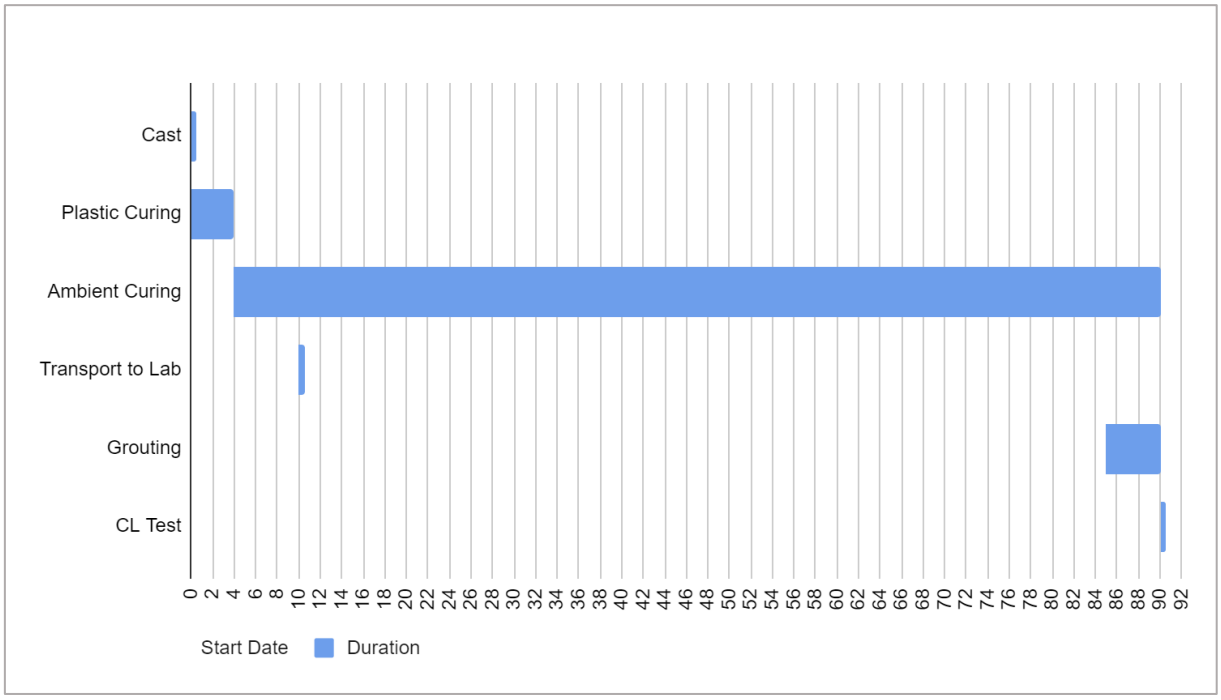

Figure F.38 – Wall 19 gannt chart

Figure F.39 – Failure through the grout layer

Wall 20:

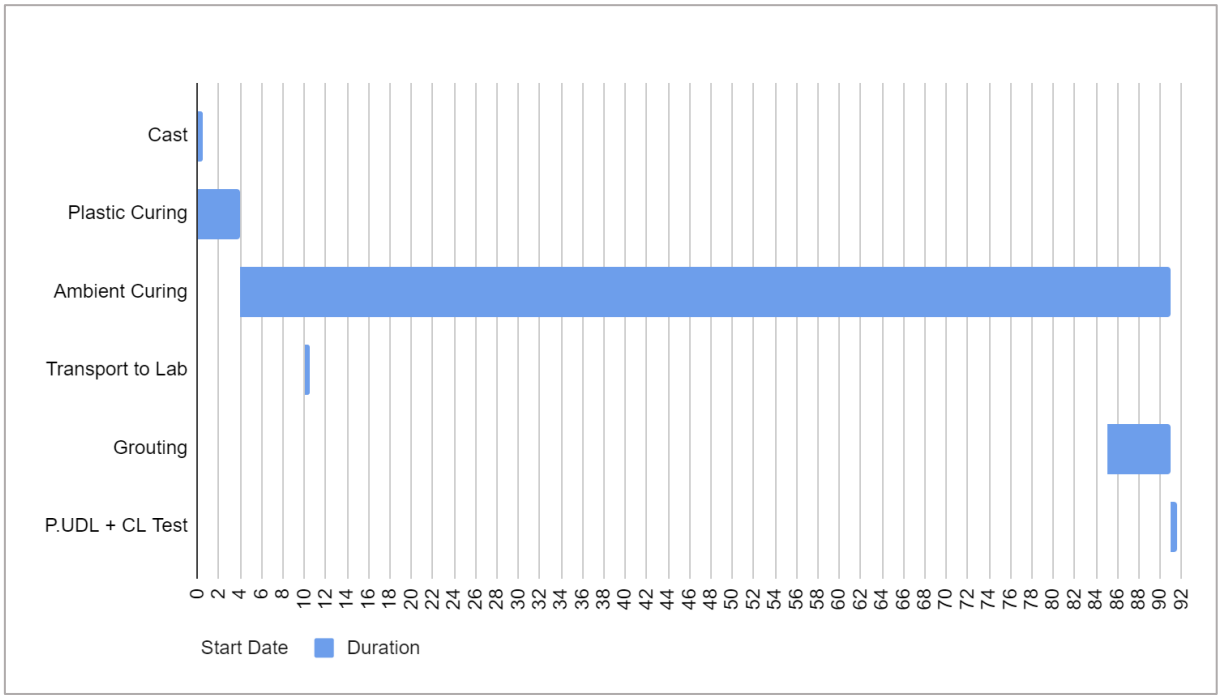

Figure F.40 – Wall 20 gannt chart

Figure F.41 – Concentrated load failure mode through the grout layer

Wall 21:

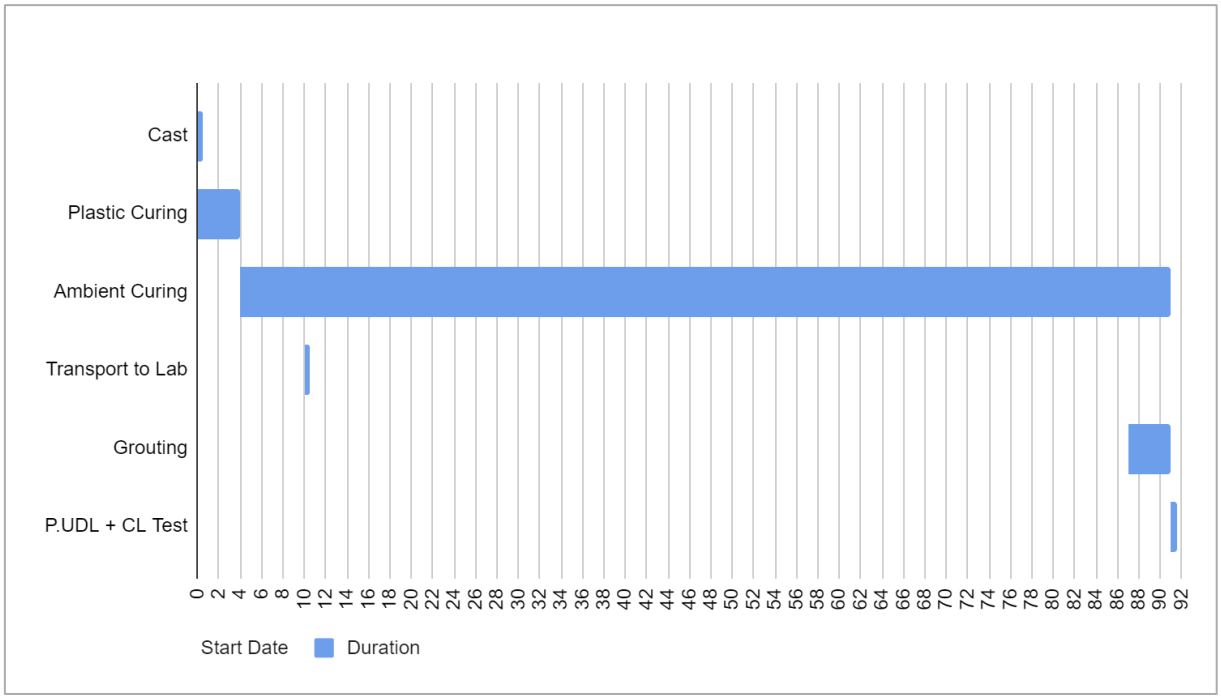

Figure F.42 – Wall 21 gannt chart

Figure F.43 – Concentrated load failure mode through the grout layer, forming a cone/wedge

Wall 22:

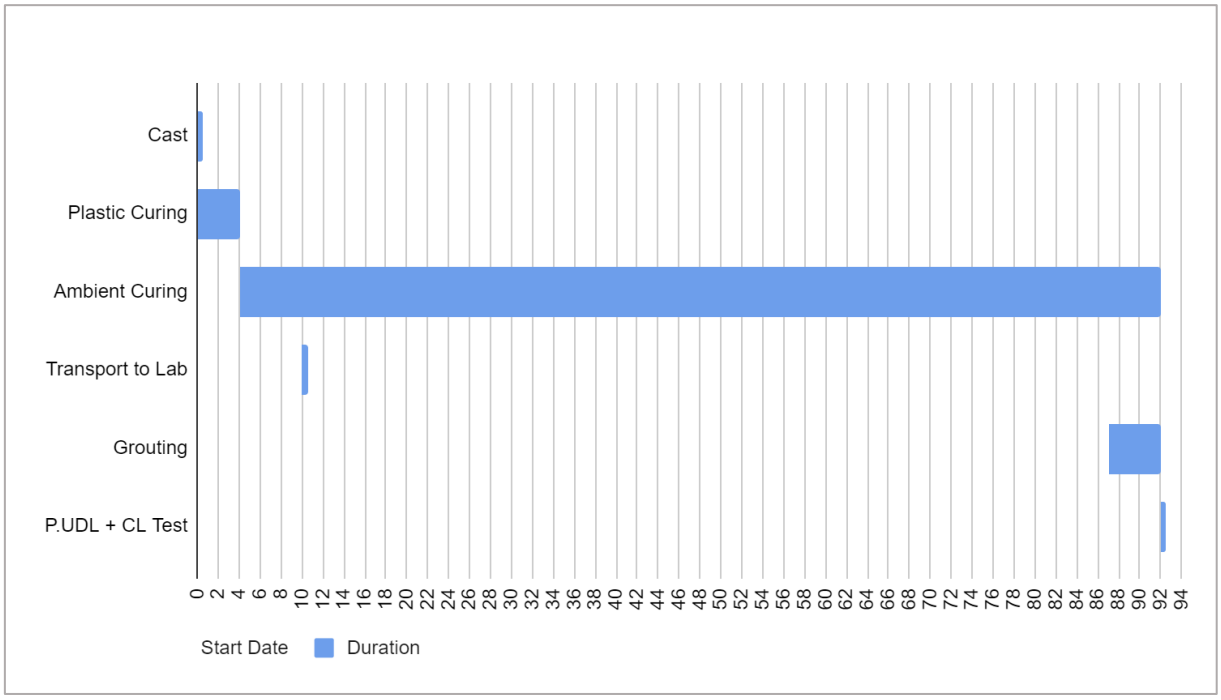

Figure F.44 – Wall 22 gannt chart

Figure F.45 – Concentrated load failure mode through the grout layer, forming a cone/wedge

Wall 23:

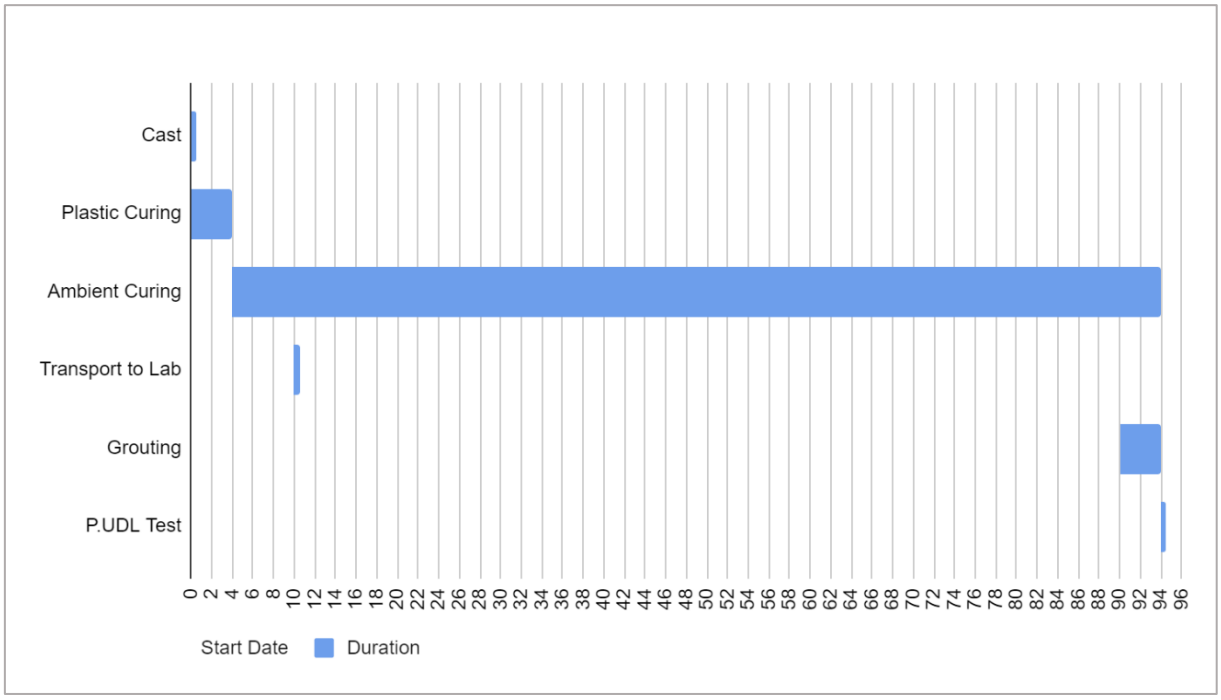

Figure F.46 – Wall 23 gannt chart

Figure F.47 – Failure mode back elevation

Wall 24:

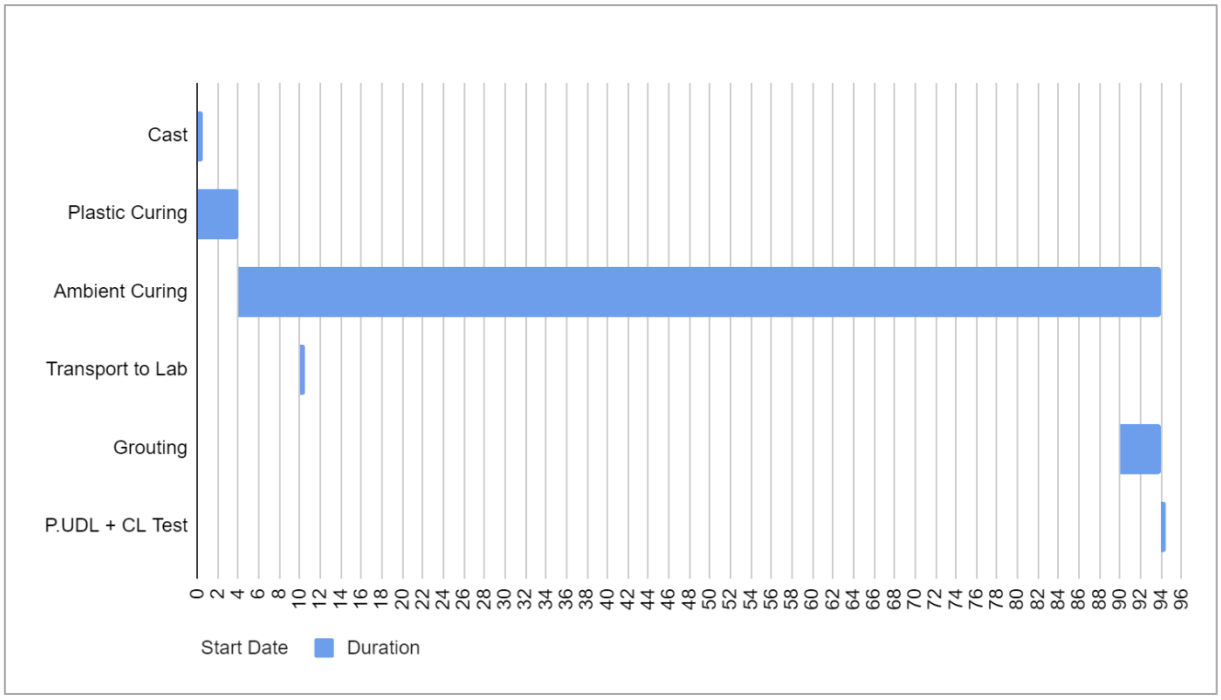

Figure F.48 – Wall 24 gannt chart

Figure F.49 – Concentrated load failure mode through the grout layer

Appendix G - Miscellaneous Figures and Photos

Figure G.1 – Manufacturing of the steel beams used for distributing the point loads

Figure G.2 – Grouting of the walls' loading surfaces

Figure G.3 – Grouting surface finish post curing

Figure G.4 – Pressing back the hydraulic single acting jack using a hand operated jack.

Figure G.5 – Majority of the wall panels post loading from the first testing programme